MATHEMATICAL MODELING OF NO_x EMISSIONS IN BUBBLING FLUIDIZED BED COMBUSTORS

A THESIS SUBMITTED TO
THE GRADUATE SCHOOL OF NATURAL AND APPLIED SCIENCES
OF
MIDDLE EAST TECHNICAL UNIVERSITY

BY

M. ONUR AFACAN

IN PARTIAL FULFILLMENT OF THE REQUIREMENTS
FOR
THE DEGREE OF MASTER OF SCIENCE
IN
CHEMICAL ENGINEERING

AUGUST 2005

Approval of the Graduate School of Natural and Applied Sciences.

Prof. Dr. Canan Özgen
Director

I certify that this thesis satisfies all the requirements as a thesis for the degree of Master of Science.

Prof. Dr. Nurcan Baç
Head of Department

This is to certify that we have read this thesis and that in our opinion it is fully adequate, in scope and quality, as a thesis and for the degree of Master of Science.

Dr. Olcay Oymak
Co-Supervisor

Prof. Dr. Nevin Selçuk
Supervisor

Examining Committee Members

Prof. Dr. Deniz Üner (METU, CHE) _____

Prof. Dr. Nevin Selçuk (METU, CHE) _____

Dr. Olcay Oymak (MSET) _____

Prof. Dr. Faruk Arınç (METU, ME) _____

Asst. Prof. Görkem Kırbaş (METU, CHE) _____

I hereby declare that all information in this document has been obtained and presented in accordance with academic rules and ethical conduct. I also declare that, as required by these rules and conduct, I have fully cited and referenced all material and results that are not original to this work.

Name, Last name : M. Onur AFACAN

Signature :

ABSTRACT

MATHEMATICAL MODELING OF NO_x EMISSIONS IN BUBBLING FLUIDIZED BED COMBUSTORS

Afacan, M. Onur
M.S., Department of Chemical Engineering
Supervisor: Prof. Dr. Nevin Selçuk
Co-Supervisor: Dr. Olcay Oymak

August 2005, 99 Pages

A comprehensive model, previously developed and tested for prediction of behavior of continuous fluidized bed combustors is extended to incorporate NO_x formation and reduction reactions and applied to the simulation of METU 0.3 MW_t Atmospheric Bubbling Fluidized Bed Combustor (ABFBC) burning lignites with high volatile matter in their own ashes.

The predictive accuracy of the model was assessed by comparing its predictions with measurements taken previously on the same rig. Favorable comparisons are obtained between the predicted and measured temperatures and concentrations of gaseous species along the combustor. Results show that determination of partitioning of coal nitrogen into char nitrogen and volatile nitrogen, and release of volatile nitrogen along the combustor are found to be the most important parameters that affect NO_x formation and reduction in bubbling fluidized bed combustors. The system model proposed in this study proves to be a useful tool in qualitatively and quantitatively simulating the processes taking place in an atmospheric fluidized bed combustor.

Keywords: NO_x emissions, NO_x formation and reduction, fluidized bed combustion, mathematical modeling and lignite.

ÖZ

AKIŞKAN YATAKLI YAKICILARDA NO_x EMİSYONLARININ MODELLENMESİ

Afacan, M. Onur
Yüksek Lisans, Kimya Mühendisliği Bölümü
Tez Yöneticisi: Prof. Dr. Nevin Selçuk
Yardımcı Tez Yöneticisi: Dr. Olcay Oymak

Ağustos 2005, 99 Sayfa

Bu çalışmada, akışkan yataklı yakıcıların performansını öngörmek için daha önce geliştirilmiş ve doğruluğu saptanmış kapsamlı bir matematik model, NO_x oluşum ve indirgenme tepkimelerini kapsayacak şekilde genişletilmiştir.

Model öngörülerinin doğruluğu kendi külü içinde linyit yakan ODTÜ 0.3 MW_t atmosferik kabarcıklı akışkan yataklı yakıcı test ünitesinin davranışının belirlenmesine uygulanmış ve aynı test ünitesi üzerinden alınan ölçümlerle yapılan karşılaştırma ile değerlendirilmiştir. Karşılaştırma sonucu, yakıcı boyunca, sıcaklık ve gaz derişimleri öngörülerinin deneysel verilerle uyum içerisinde olduğu görülmüştür. Kabarcıklı akışkan yataklı yakıcılarda NO_x oluşumu ve indirgenmesini etkileyen en önemli parametrelerin kömür azotunun kok azotu ve uçucu azotuna bölünmesinin belirlenmesi ve uçucu azotun yakıcı boyunca dağılımı olduğu bulunmuştur. Geliştirilen sistem modelinin akışkan yataklı yakıcıda gerşekleşen olayların nicel ve nitel temsilinde yararlı olduğu görülmüştür.

Anahtar kelimeler: NO_x emisyonu, NO_x oluşumu ve indirgenmesi, akışkan yataklı yakıcı, matematiksel modelleme ve linyit.

to *My Family*

ACKNOWLEDGEMENTS

I would like to express my deepest gratitude to my supervisor, Prof. Dr. Nevin Selçuk for many insightful conversations during the development of this thesis, and for helpful comments on the text.

I would like to show my appreciation to my co-supervisor Dr. Olcay Oymak, for his precious suggestions and support.

I also thank to the AFBC research team members for their friendship and support during my study; Ertan Karaismail, Fatma Nihan Çayan, Mehmet Kürkçü, Yusuf Göğebakan, Işıl Ayrancı, Ahmet Bilge Uygur, Tanıl Tarhan and Hakan Altındağ.

My Special thanks go to my family for their great support, encouragement and unshakable faith in me.

TABLE OF CONTENTS

LIST OF TABLES

LIST OF FIGURES

LIST OF SYMBOLS

a	Decay constant, cm^{-1}
A	Cross-sectional area, cm^2
c_p	Specific heat capacity, $cal\ g^{-1}\ K^{-1}$
C	Concentration, $mol\ cm^{-3}$
d	Diameter, cm
D	Diffusivity of oxygen in nitrogen, $cm^2\ s^{-1}$
E	Activation energy, $cal\ mol^{-1}$
$E(r)$	Elutriation rate constant, s^{-1}
$f(E)$	Activation energy distribution function for devolatilization, $mol\ cal^{-1}$
F	Char flow rate, $g\ s^{-1}$
F_z	Upward flow rate of entrained particles at any height z in freeboard, $g\ s^{-1}$
g	Gravitational acceleration, $cm\ s^{-2}$
h	Individual heat transfer coefficient, $cal\ cm^{-2}\ s^{-1}\ K^{-1}$
H	Height, cm
ΔH^0	Heat of reaction at standard state, $cal\ mol^{-1}$
k	Overall sulfation rate constant, cm/s; thermal conductivity, $cal\ cm^{-1}\ s^{-1}\ K^{-1}$
$k(E)$	First-order reaction rate constant for devolatilization, s^{-1}
k_C	Reaction rate constant for char combustion, $cm\ s^{-1}$
k_{CO}	Reaction rate constant for CO oxidation, $(cm^3\ mol^{-1})^{0.8}\ s^{-1}$
k_f	Film mass transfer coefficient, $cm\ s^{-1}$
k_s	First order surface reaction rate constant for char combustion, $cm\ s^{-1}$
K	Coal nitrogen partitioning factor
K_{be}	Interphase mass transfer coefficient, s^{-1}
$K^*_{i\infty}$	Dispersed non-cluster flux of entrained particles in size i, $g\ cm^{-2}\ s^{-1}$

K_{ih}^{*}	Cluster flux of entrained particles in size *i*, $g\ cm^{-2}\ s^{-1}$
K_{i}^{*}	Total flux of entrained particles in size *i*, $g\ cm^{-2}\ s^{-1}$
L	Length, *cm*
m	Mass flow rate, $g\ s^{-1}$
M	Molecular or atomic weight, $g\ mol^{-1}$; hold-up in the bed, *g*
n	Index of the dimension; molar flow rate, $mol\ s^{-1}$
n_C	Carbon consumption rate, $mol\ cm^{-3}\ s^{-1}$
n_N	Char nitrogen oxidation rate, $mol\ cm^{-3}\ s^{-1}$
N_r	Number of cycles of recycled sorbent and ash particles
$P(r)$	Size distribution function, cm^{-1}
$P_z(r)$	Size distribution of entrained particles at any height *z* in freeboard, cm^{-1}
Q	Volumetric flow rate, $cm^3\ s^{-1}$; energy generation/loss rate, $cal\ s^{-1}$
r	Spatial independent variable, *cm*
r_C	Carbon consumption rate on the surface of char particle, $mol\ cm^{-2}\ s^{-1}$
r_N	Char nitrogen oxidation rate on the surface of char particle, $mol\ cm^{-2}\ s^{-1}$
r_{CO}	Rate of CO combustion, $mol\ cm^{-3}\ s^{-1}$
r_{SO_2}	Rate of sulfation reaction, $mol\ s^{-1}$
r_{NO}	Rate of heterogeneous reaction over single particle of size r, $mol\ g^{-1}s^{-1}$
$r_{N,het}$	Rate of heterogeneous reaction, $mol\ s^{-1}$
$r_{N,hom}$	Rate of homogeneous reaction, R10: $mol\ cm^{-3}\ s^{-1}$; R11: $mol\ s^{-1}$
R	Ideal gas constant, $cal\ mol^{-1}\ K^{-1}$; radius, *cm*
$\boldsymbol{R}$	Energy generation/loss rate in freeboard, $cal\ cm^{-3}\ s^{-1}$
$\Re$	Species generation/depletion rate, $mol\ cm^{-3}\ s^{-1}$
$\Re(r)$	Shrinkage rate of char particles, $cm\ s^{-1}$
Re_p	Particle Reynolds number, -
R_w	Thermal resistance across the freeboard wall, $cal\ cm^{-2}\ s^{-1}\ K^{-1}$
S	External sorbent surface area, cm^2
t	Time, *s*
T	Temperature, *K*
u_0	Superficial velocity in the bed, $cm\ s^{-1}$
u_b	Superficial bubble phase velocity, $cm\ s^{-1}$

u_e	Superficial velocity in emulsion phase, $cm\ s^{-1}$
u_{mf}	Superficial minimum fluidization velocity, $cm\ s^{-1}$
u_t	Terminal velocity of the particles, $cm\ s^{-1}$
u_{tf}	Superficial throughflow velocity in bubbles, $m\ s^{-1}$
U	Overall heat transfer coefficient, $cal\ cm^{-2}\ s^{-1}\ K^{-1}$
U_f	Unit filter function
V	Volume, cm^3
W_N	Mass of char nitrogen, g
X_{NH_3}	Molar ratio of NH_3 in the volatile nitrogen
x	Mass fraction (dry basis); spatial independent variable, cm
x_{vl}	Fraction of volatiles released in the bed
y	Mole fraction
z	Spatial independent variable, cm

Greek Letters

α	Thermal diffusivity, $cm^2\ s^{-1}$
δ	Bubble phase volume fraction
ε	Voidage; emissivity; convergence criterion
ε_f	Voidage at fluidization conditions
ε_{mf}	Voidage at minimum fluidization conditions
ε_s	Solids volume fraction
η	Contact efficiency
λ^0	Latent heat of vaporization at standard state, $cal\ g^{-1}$
μ	Viscosity, $g\ cm^{-1}\ s^{-1}$
ρ	Density, $g\ cm^3$
σ	Standard deviation of activation energy distribution, $J\ mol^{-1}$; Stephan-Boltzman constant, $cal\ cm^{-2}\ s^{-1}\ K^{-4}$; Fractional sorbent surface area
v	Volatiles released, %
v_∞	Ultimate yield of volatiles released, %
ϕ	Sphericity, -

Subscripts

32	Surface/volume mean
a	Air; ash; attrition
avg	Average
b	Bubble
bd	Bed drain
bed	Bed
bw	Bed wall
c	Combustion
C	Carbon
co	Carryover
cw	Cooling water
d	Char
e	Emulsion
elut	Elutriation
f	Freeboard; fine; feed coal
fc	Fixed carbon
fw	Freeboard wall
G	Gas
H	Hydrogen
het	heterogeneous
hom	homogeneous
I	Inert; inner
J	Species index
lst	Limestone
max	Maximum
maxe	Maximum elutriated
min	Minimum
o	Feed; outer; at the bed surface; initial
p	Particle

r	Radiation; reference
recy	Recycle
rxn	Reaction
S	Sulfur
s	Surface; solid
T	Tube
vm	Volatile matter
w	Wall; water

Abbreviations

d.a.f.	dry ash free
ABFBC	Atmospheric Bubbling Fluidized Bed Combustor
AFBC	Atmospheric Fluidized Bed Combustor
FBC	Fluidized Bed Combustion
FC	Fixed Carbon
FTIR	Fourier Transform Infrared
GC	Gas Chromotography
OHTC	Overall Heat Transfer Coefficient
TGA	Thermogravimetric Analyzer
VM	Volatile Matter
XANES	X-ray Absorption Near Edge Spectroscopy
XPS	X-ray Photoelectron Spectroscopy

CHAPTER 1

INTRODUCTION

Applications of fluidized bed combustion (FBC) technology developed for burning coal with high efficiency and within acceptable levels of gaseous pollutant emissions have been steadily increasing in both capacity and number over the past decade. However, gradual introduction of increasingly restrictive legislations on emissions from combustion sources has been keeping the topic attractive for further research.

Lignite is not only the world's most abundant fossil fuel, but also one of the two major indigenous sources of energy in Turkey with an estimated quantity of 9.3 billion tons of reserves. Major proportion of this quantity is characterized by high volatile matter and ash contents. It is indeed this high volatile matter content that leads to further reduction of NO_x emissions from fluidized bed combustion of lignites.

Nitrogen oxides consist of nitric oxide (NO), nitrogen dioxide (NO_2), and nitrous oxide (N_2O). NO and NO_2 are collectively referred to as NO_x, and NO makes up for the major proportion of NO_x. In fluidized bed coal combustion, the source of NO_x emissions is the organic nitrogen present in the coal owing to uniform and low combustion temperatures.

A considerable number of studies has been carried out in the past to investigate NO_x emissions from FBCs. Although this technology is regarded as a mature technology with its well-known low NO_x emission, dependence on local coal properties and

ever demanding environmental regulations may point to further research. Furthermore, any slight improvement in NO_x emission reduction would make FBCs more favorable amongst other competing clean coal technologies.

During devolatilization in fluidized bed combustion of coal, fuel nitrogen is partitioned into volatile nitrogen and char nitrogen. The extent of split is depended on coal type, and influences the NO_x emission behaviour in fluidized bed combustors, significantly. With regard to this and the complexity of the mechanism of NO formation and reduction including both homogeneous and heterogeneous reactions, investigation of NO_x emission from FBCs necessitates mathematical modeling studies. There exists a significant number of models in the literature. However, the modeling studies [1-14] on NO_x emission performance of FBCs so far focused on low volatile matter and ash content coals.

Therefore, in this study, a previously developed comprehensive system model, originally proposed by Selçuk and Sivrioğlu [15] and later improved, extended and validated against experimental data by Selçuk and her colleagues [16, 17], is chosen as a basis for incorporation of a sufficiently detailed NO formation and reduction reactions. Coal nitrogen split into char and volatiles, which is unique to coal type, is determined by pyrolysis experiments. The predictive performance of the model is tested by comparing the model predictions with on-line concentration measurements of O_2, CO_2, CO, NO_x along the 0.3 MW_t Atmospheric Bubbling Fluidized Bed Combustor (ABFBC), where typical Turkish lignite with high volatile matter and ash content is burned in its own ash.

CHAPTER 2

NO FORMATION AND REDUCTION IN FBCs

Conversion of coal nitrogen into nitric oxide is not straightforward. The process comprises of evolution of nitrogenous products during devolatilization and char combustion, and concurrent reactions among these species either in gas phase or solid phase over catalytic surfaces like char, ash and calcined limestone. An overall reaction scheme illustrating main formation and reduction paths adapted from Johnsson [18] is given in Figure 2.1.

During devolatilization, coal nitrogen is partitioned into char nitrogen and volatile nitrogen with a factor that depends on maximum temperature of pyrolysis, heating rate, and coal type. Char nitrogen is oxidized to *NO* and N_2O and partly oxidized to N_2. On the other hand, nitrogen in tar, *HCN* and NH_3 make up for the volatile nitrogen [18]. Pyrolysis studies show that, for low rank coals, N_2 is the major nitrogenous product [19, 20] and NH_3/*HCN* ratio is greater than that of high rank coals [18, 21].

There is a general agreement that *HCN* is an important precursor of N_2O formation, whereas NH_3 takes place in both homogeneous formation and reduction of *NO* at fluidized bed combustion temperatures. Heterogeneous reactions play an important role in *NO* formation and reduction due to high solid loading in fluidized bed combustors. Reduction of *NO* is mainly achieved by solid catalytic reactions in the presence of reducing agents like *CO* and H_2. Oxidation and decomposition of volatile nitrogenous products over solid surfaces also contribute to *NO* formation as shown in Figure 2.1.

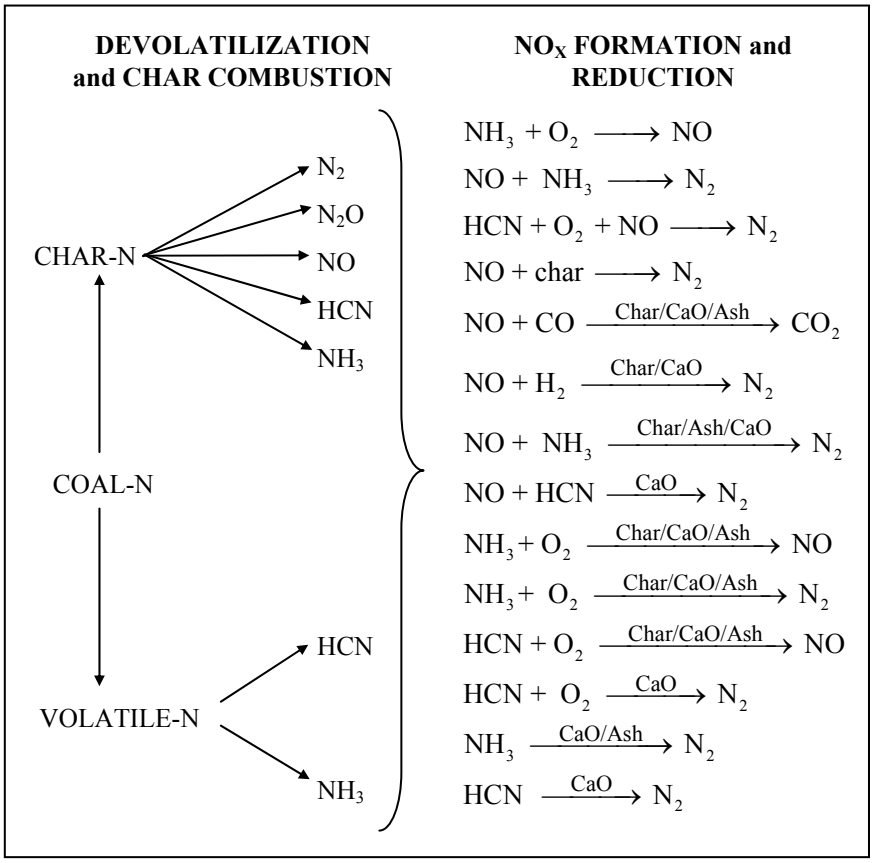

Figure 2.1. Reaction scheme for NO_x formation and reduction

In this chapter, chemical structure of nitrogen in coal, release of nitrogen from coal during devolatilization process, reactions leading to formation and reduction of *NO* will be explained in detail. This chapter reviews the available information in the literature by taking fluidized bed combustion conditions and lignite as the coal type into consideration. Furthermore, effect of operating conditions on NO_x emissions will be discussed and mathematical models for NO_x emissions from fluidized bed combustors published so far will be reviewed in detail.

2.1 Nitrogen in Coal

Coal is formed from plant residues in a process that requires high pressure, heat and very long time [21, 22]. Ranks of coal, from lignite to anthracite, increases during coalification process as oxygen and hydrogen contents decrease [18]. Nitrogen in

coal is the organic nitrogen that is fixed in biochemical (peat) stage of coalification [23]. The nitrogen content of coal is not strongly dependent on coal rank but it tends to increase in coals containing up to 85 wt% carbon (d.a.f) and decrease at higher ranks. The nitrogen content typically ranges from 1-2.5 wt% (d.a.f.) [23, 24].

Nitrogen functionality has been investigated as there might be a relation between functional forms of nitrogen and conversion into nitrogenous products during devolatilization and combustion. However, detailed information is not available as no reliable methods for the identification of the groups are present. In earlier studies, destructive methods like pyrolysis and extraction were used, where changes might occur to the functional forms of nitrogen. Later, non-destructive methods like X-ray photoelectron spectroscopy (XPS) and X-ray absorption near edge spectroscopy (XANES) were utilized. XPS is surface sensitive having limited penetration depth, whereas bulk properties are analyzed by XANES. Yet, both methods require curve resolution to estimate the nitrogen functionalities as bands from specific groups overlap [21, 23, 24].

These studies showed that nitrogen in coal is present in the forms of pyridinic (6-ring), pyrrolic (5-ring) and quaternary (*N*-oxide of pyridinic-*N* or protonated pyridinic-*N*) functional groups [22]. XPS studies also indicated that these functional groups make up 0-40%, 50-100%, and 0-30% of the total nitrogen, respectively [21]. In addition, small amounts of amino groups (0-10%) were found in low rank coals [22, 24].

Although it was postulated that relative amount of functional forms of nitrogen in coal could control the rate of nitrogen release [25], the scatter in the literature data shows that no significant relation between amount of pyridinic and pyrrolic nitrogen and coal type can be proposed. Yet, there is a general acceptance that amount of quaternary nitrogen increase with decreasing rank [21, 23, 24].Kambara et al. [26] pyrolyzed 20 different coals and analyzed the pyrolysis gases by Gas Chromatography (GC) and the remaining chars by XPS. All quaternary nitrogen

was found converted to NH_3 and the residual pyridine and pyrrolic nitrogen converted to HCN and N_2.

Consequently, investigating functional forms of nitrogen present in coal is a very difficult study due to insufficiency of quantitative methods used and wide range of coal properties. Given the vast number of different type of coals, these studies can only estimate the relation between functional forms of nitrogen and their conversion to a certain extent. Therefore, the knowledge of nitrogen functionality is not of prior importance in understanding transformation of coal nitrogen.

2.2 Coal Devolatilization

Thermal decomposition of coal is called devolatilization. The extent of volatiles release depends on fuel type, temperature of the medium and heating rate.

2.2.1 Partitioning of Coal Nitrogen

Coal nitrogen is partitioned into volatile nitrogen and char nitrogen during devolatilization. Volatile nitrogen can be found in the forms of tar nitrogen and light gases like, NH_3 and HCN. Formation of N_2 is also observed [21, 22]. The knowledge of volatile nitrogen composition and amount is crucial to estimate the NO formation in the combustor.

The rank dependence of volatile nitrogen release was demonstrated by Bassilakis et al [27]. As the oxygen content of the parent fuel increases, i.e. with decreasing rank, volatile nitrogen release increases, due to secondary reactions of tars taking place to a great extent especially in low rank coals [28].

The release of tars which have similar nitrogen (pyrrolic and pyridinic) contents to that of the coal occurs at the primary devolatilization taking place at lower temperatures. At higher temperatures or long residence times, the secondary

devolatilization takes place, where gases such as methane and hydrogen are released and char *N*/*C* ratio increases. Then, release of *HCN* and NH_3 start as the pyrolysis temperature is increased further, leading to decrease in *N*/*C* ratio [21, 23, 25].

For low rank coals, volatile nitrogen is released in minor amounts in the primary devolatilization both as tar nitrogen and as light gas species. The major proportion of volatile nitrogen releases during the secondary devolatilization of the char residue [22, 27].

2.2.2 Volatile Nitrogen Species

It was extensively reviewed in the literature that release of NH_3 from lignites is larger than *HCN* [18, 22, 27, 29]. NH_3 release was observed to be higher for coals with higher *O*/*N* ratio, i.e. decreasing rank as mentioned in the section 2.2.1. [30]. It was suggested that evolution of *HCN* precedes that of NH_3 [27, 29]. Bassilakis et al. [27] performed pyrolysis experiments in a thermo balance at a heating rate of 30 $^{o}C/min$ at fluidized bed combustion temperatures and analyzed the pyrolysis gases with Fourier Transform Infrared (FTIR). It was found that apart from the formation of NH_3 by direct cleavage of amino groups or amides, NH_3 is also produced in a secondary reaction involving *HCN* gas through a heterogeneous reaction. The conversion is mainly determined by the residence time of gas in the pores of char. Reactions inside the particle is favored especially for low rank coals due to their porous structure [30]. It was proposed that conversion of *HCN* to NH_3 by secondary reaction is favored in fluidized beds due to longer gas-coal contact time.

In recent pyrolysis studies, significant amounts of N_2 was measured during pyrolysis of lignite with different heating rates, from 10 *K*/*min* to 1400 *K*/*min*. Almost half of the fuel nitrogen was released as N_2 above the temperatures of 800^{o}C. Besides, NH_3 was the main volatile nitrogen product by 10 wt% of the total nitrogen in the coal. Tar nitrogen and *HCN* were measured to be 4 wt% and 2 wt% of the total nitrogen content, respectively [19, 20]. The influence of heating rate was found to be insignificant but it was found out that mineral content of coal ash

(calcium and iron) promotes the formation of N_2 and NH_3, and suppresses HCN formation [20, 31, 32].

Apart from the pyrolysis studies, dense bed measurements from FBCs show that NH_3 is the dominant volatile nitrogen product [33-35]. In a recent study, it was also shown that the highest NH_3 concentrations were obtained under reducing conditions at severe air-staging and the lowest at no air-staging [36].

2.3 NO Formation and Reduction Reactions

During coal combustion *NO* may be produced from the oxidation of molecular nitrogen present in the combustion air (Thermal *NO*), reaction between hydrocarbon fragments and molecular nitrogen in the flame (Prompt *NO*), and oxidation of organic nitrogen present in the coal (Fuel *NO*). In fluidized bed combustors, the source of *NO* emissions is Fuel *NO* due to low combustion temperatures. *NO* is produced by char nitrogen and volatile nitrogen through homogeneous and heterogeneous reactions.

2.3.1 Homogeneous Gas Phase Reactions

The homogeneous reactions are governed by radicals, and due to high solid loading in the dense phase of an FBC radical recombination may occur on the surface of solids [21, 37]. However, the importance of homogeneous reactions arise in a freeboard of bubbling FBC or riser of a circulating FBC where the solids concentration is lower. A detailed reaction mechanism was originally proposed by Miller and Bowman [37] including reactions of hydrocarbons. In the following, overall reaction mechanism of volatile nitrogen species is briefly reviewed.

2.3.1.1 Reactions of HCN

HCN is an important precursor for the formation of N_2O at typical FBC temperatures. *HCN* forms *NCO* which reacts to give N_2O or N_2 by the following reactions:

$$NCO + NO \rightleftharpoons N_2O + CO \quad (2.1)$$

$$NCO + NO \rightleftharpoons N_2 + CO_2 \quad (2.2)$$

At higher temperatures prevailing in pulverized coal combustion conditions *NCO* radical oxidizes to *NO* [21],

$$NCO + O \rightleftharpoons NO + CO \quad (2.3)$$

2.3.1.2 Reactions of NH_3

Thermal $DeNO_x$ process is the combination of two overall gas phase reactions, in which NH_3 acts as a reducing agent for *NO*, reaction (2.4), and is oxidized to yield *NO,* reaction (2.5) [21, 37].

$$NO + NH_3 + 1/4O_2 \rightleftharpoons N_2 + 3/2H_2O \quad (2.4)$$

$$NH_3 + 5/4O_2 \rightleftharpoons NO + 3/2H_2O \quad (2.5)$$

The temperature window for Thermal $DeNO_x$ is 1100-1400 *K* [37]. At FBC temperatures NH_3 oxidation to N_2O is of minor importance [18, 21].

It is well documented in the literature that *HCN* is predominantly oxidized to N_2O, while NH_3 is the major source of *NO* [18, 21, 29, 30, 38-40]. Furthermore, the majority of N_2O is formed by volatile nitrogen through gas phase reactions. This also shows the main trade-off between formation of *NO* and N_2O from BFBCs [29, 41, 42]. In addition, conversion of *HCN* to NH_3 may also be significant in the presence of hydrogen species [22, 38]. Therefore, the contribution of volatile nitrogen compounds to homogeneous formation of *NO* can be lumped into NH_3.

2.3.2 Heterogeneous Gas-Solid and Catalytic Reactions

There are many heterogeneous reactions taking place in FBC environment owing to the availability of different type of solids like char, coal ash and limestone. The catalytic activity of solids mainly depends on particle size, carbon burnout for char, sulfation rate for limestone and presence of oxidizing gases for reduction reactions. Important reactions were reviewed briefly from the open literature [18, 22, 29] with the emphasis on the type of solid catalyst.

2.3.2.1 Oxidation of Char Nitrogen

During char combustion, nitrogen retained in char is oxidized to give *NO* along with oxidation of carbon. The reaction rate is proportional to char combustion rate, and *N*/*C* ratio in the char is generally accepted as the proportionality constant. However, combustion of highly devolatilized char particles shows that the yield of char nitrogen oxidation to *NO* is between 75% and 100%. It is evident that *NO* goes into a reduction reaction with char as it is formed within the pores of the particle or with the char particles nearby [22]. The formation of N_2 is also attributed to char combustion [43]. Details of *NO*-char reaction can be found in the section 2.4.3.

There are several parameters that affect the yield of *NO*. As the particle size increases, the residence time of *NO* in the pores increase leading to a decrease in the yield. *NO* yield is known to decrease with increasing reactivity of the char. Specific surface area is a measure of reactivity, which varies from 5 to 895 m^2/g for chars from different types of coal [44]. It was reviewed recently that no direct correlation between specific surface area and reactivity is present [45]. Yet, reactivity of chars in oxidation and reduction reactions increases with decreasing pyrolysis or devolatilization temperatures. It was also confirmed by coal combustion tests that *NO* yield is increased by increasing temperature. On the whole, char nitrogen oxidation was found to be the main source of *NO* from fluidized bed combustion of coal [42, 46].

2.3.2.2 Oxidation of Volatile Nitrogen

Volatile nitrogen compounds, NH_3 and HCN, are mainly oxidized to NO or N_2 over catalytic surfaces like char, ash and limestone. NH_3 and HCN oxidation reactions to NO or N_2 are as follows,

$$NH_3 + 5/4\,O_2 \rightleftharpoons NO + 3/2\,H_2O \tag{2.6}$$

$$NH_3 + 3/4\,O_2 \rightleftharpoons 1/2\,N_2 + 3/2\,H_2O \tag{2.7}$$

$$HCN + 7/4\,O_2 \rightleftharpoons NO + CO_2 + 1/2\,H_2O \tag{2.8}$$

$$HCN + 5/4\,O_2 \rightleftharpoons 1/2\,N_2 + CO_2 + 1/2\,H_2O \tag{2.9}$$

However, N_2O formation by oxidation of volatile nitrogen compounds is in minor amounts. Catalytic oxidation of tars has not been investigated in the literature.

Char: Char is a very active catalyst for the oxidation of NH_3. The selectivity of NO was found to be 80-90% at 1123K in a fixed bed reactor [47]. HCN is also oxidized to NO over char with a selectivity of 50 %, but no intrinsic value was found due to reduction reactions.

Ash: Ashes of low rank coals are very active catalysts due to high mineral contents of *Ca*, *Fe* and *Mg*. The selectivity of NH_3 oxidation for NO was reported to be 60-70% over ash of a Japanese coal (Taiheyo). MgO and Fe_2O_3 are active catalysts for HCN oxidation, and the selectivity for NO was found to be 60-80% and 60%, respectively.

Limestone: Oxidation of NH_3 over limestone is extensively studied in the literature [48] in order to understand the influence of limestone addition. Calcined limestone is highly active for the oxidation reaction, whereas sulfated and uncalcined limestone are poor catalysts. The selectivity of NH_3 oxidation over calcined limestone for NO is 50-80%. The catalytic activity of calcined limestone decreases due to increasing sulfation in the presence of SO_2 and O_2. Calcined limestone is also a very active catalyst for HCN oxidation. NO selectivity ranges from 20 to 70% depending on temperature and concentrations of the reactant gases. Sulfated

limestone was also found to be a catalyst for *HCN* oxidation with *NO* selectivity of 50-60%.

2.3.2.3 Reduction of NO

Char: Char interaction of *NO* has been extensively studied owing to its high potential of *NO* emission reduction through gas solid or catalytic reaction in the presence of reducing agents like *CO* and H_2. The most widely adopted reaction mechanism for gas-solid interaction of *NO* with char (simply denoted as *NO*-char reaction) was proposed by Chan et al. [49], and extended by Johnsson [18], where species in parentheses, *()*, refer to solid sites:

$$NO + (-C) \longrightarrow (-CNO) \tag{2.10}$$

$$2(-CNO) \longrightarrow 2(-CO) + N_2 \tag{2.11}$$

$$(-CO) \longrightarrow CO \tag{2.12}$$

$$CO + (-CO) \longrightarrow CO_2 + (-C) \tag{2.13}$$

Later studies put forward experimental evidence for the following reaction for *NO*-char interaction [45]:

$$(-CN) + NO \longrightarrow N_2 + (-CO) \text{ or } CO \tag{2.14}$$

The catalytic activity was observed to be independent of char type [50]. *HCN* was also suggested to be the intermediate specie for char nitrogen oxidation to *NO*, but the mechanism is still not clear [51]. Direct reduction of *NO* by *CO* catalyzed by char surface is given by reaction (2.15). At fluidized bed conditions, this reaction plays a dominant role [45], and it works under oxidative environment, as well [50].

$$NO + CO \rightleftharpoons 1/2 N_2 + CO_2 \tag{2.15}$$

NO reduction over char by H_2 takes place by the reactions:

$$NO + H_2 \rightleftharpoons 1/2 N_2 + H_2O \tag{2.16}$$

$$NO + 5/2H_2 \rightleftharpoons NH_3 + H_2O \quad (2.17)$$

Char is a very active catalyst for *NO* reduction by *NH₃* through the following reactions:

$$NO + 2/3NH_3 \rightleftharpoons 5/6N_2 + H_2O \quad (2.18)$$

Ash: Bed material from burning brown coal was found to be very active catalyst for reduction of *NO* by *CO*, but the activity decreases fast under oxidative conditions [50]. The activity of ash for this reaction is related to its Fe_2O_3 content. Under reducing conditions, Fe_2O_3 is converted to *FeO* which catalyzes NO reduction, whereas under oxidative conditions, *FeO* is converted back to Fe_2O_3, the activity of the solid particle is decreased. Bed material from brown coal was also observed to be an active catalyst for *NO* reduction by *NH₃* but only under reducing conditions [47].

Limestone: Calcined limestone is an active catalyst for *NO* reduction by *CO*, but the reaction is inhibited by O_2 and no reaction takes place above stoichiometric values of CO/O_2. The catalytic activity also decreases with the degree of sulfation. *NO* reduction by H_2 takes place over calcined limestone, as well. The catalytic activities of calcined limestone for *NO* reduction by *NH₃* and *HCN* were reported to be less than other calcined limestone catalyzed reactions mentioned above.

2.3.2.4 Decomposition of Volatile Nitrogen

NH_3 decomposes to give N_2 and H_2:

$$NH_3 \rightleftharpoons 1/2N_2 + 3/2H_2 \quad (2.19)$$

Char and Ash: Decomposition of *NH₃* was found not to take place over char, however ash was found to be very active catalyst. This is why, bed material from burning brown coal was observed to be more active catalyst than that from burning bituminous coal. Decomposition of *NH₃* over quartz sand was also investigated and low activity was observed.

Limestone: Calcined limestone and dolomite are active catalysts for NH_3 decomposition though the presence of H_2 inhibits the reaction over both catalysts. Uncalcined limestone was also observed to be an active catalyst for NH_3 decomposition. *HCN* was found to react with calcined limestone to produce calcium cyanide ($CaCN_2$).

$$2HCN + CaO(s) \rightleftharpoons CaCN_2(s) + CO \tag{2.20}$$

Furthermore, NH_3 and *HCN* formation was observed by decomposition of tars over calcined limestone.

2.4 NO Emissions from FBCs

In this section, a brief review on influence of coal type and some operating conditions on *NO* emissions from FBCs will be presented.

2.4.1 Influence of Coal Type

Fuel nitrogen conversion to *NO* decreases with increasing volatile matter content of coal [52, 53]. *NO* was reduced by unburned volatiles escaping to the freeboard of a bubbling fluidized bed combustor [52]. Although, higher emissions are expected to be attained at higher fuel nitrogen content, this is not confirmed by emission measurements [29, 54].

2.4.2 Influence of Temperature

NO_x emission increases sharply when the bed temperature is raised. The volatile production increases and enhances the rate of ammonia oxidation to *NO* at higher temperatures [29, 54]. In addition, char and *CO* concentration decreases due to more efficient combustion, and this leads to less *NO* reduction [29, 33]. At higher

freeboard temperatures the reduction rates of *NO* by char and gaseous components are enhanced, resulting in lower *NO* emissions [54].

2.4.3 Influence of limestone addition

The influence of limestone addition on *NO* emissions is dependent on the type of combustor. For circulating fluidized bed combustors (CFBCs), *NO* emission increases with limestone addition. However, for BFBCs, no influence of limestone addition was also reported [18]. The reason for the latter case may be due to insufficient contact between lime in the dense phase of a bubbling bed and the volatiles of the coal (owing to the rapid escape of volatiles from the bed section), which hinders the influence of lime catalyzed oxidation of volatile nitrogen [55, 56]. In addition, as limestone is fed to the combustor, the bed temperature decreases due to a cooler solid loading, and this leads to an increase in *CO* concentration. Thus, *NO* produced by lime catalyzed reaction may be reduced by *CO* over lime surface, as well [18].

2.4.4 Influence of excess air and air staging

NO emissions are increased by an increased amount of excess air in FBCs. The volatile nitrogen compounds and nitrogen remaining in the char are more likely to be oxidized to *NO* in the abundance of O_2. Besides, the concentrations of reducing agents like *CO* and H_2 decreases with increasing O_2 concentrations [18, 54].

Air staging is the most efficient way of reducing *NO* emissions. Air stream is split into two; primary and secondary air. Primary air stream is supplied from the bottom of the bed, and combustion takes place under sub-stoichiometric conditions and the secondary air stream is fed over the bed section of a BFBC or upper sections of a CFBC. As the primary air to total air ratio is decreased, a reducing atmosphere is established in the dense bed resulting in a decrease in O_2 concentration and an increase in *CO* concentration. Therefore, formation of *NO* is not favored and

reduction reactions are enhanced. Yet, severe air-staging has a negative effect on sulfur retention, leading to an increase in SO_2 concentration.

2.4.5 Influence of fly ash recycling

Lower *NO* emissions can be obtained by recycling fly ash owing to higher carbon content along the combustor and freeboard temperatures enhancing *NO* reduction reactions [21, 33, 54, 57].

2.5 Review of ABFBC models including NO emissions

In the past three decades, *NO* formation and reduction in fluidized bed combustors have been investigated by means of various modeling studies. Jensen [21] introduced an extensive review on models for bubbling fluidized bed combustors including *NO* formation and reduction. The diversity of models in the literature arises from both the difference in reactor models and the complexity of chemistry of *NO* formation and reduction. The objective of all these studies is to obtain information on *NO* formation tendency from fluidized bed combustion of coal and to bring forward strategies to reduce pollutant emissions owing to gradual introduction of increasingly restrictive legislations on emissions from combustion sources. In this section, ABFBC models including *NO* formation and reduction available in the literature are discussed with the emphasis on use of a comprehensive system model and reaction mechanism employed.

2.5.1 Existing Models

The fluidized bed reactor models including kinetic models for *NO* formation and reduction are summarized in Table 2.1, adapted from Jensen [21]. Table 2.2 describes the nomenclature used in Table 2.1. All of these modeling studies so far have attempted to predict *NO* emissions from fluidized bed combustion of high rank coals with low VM/FC ratio (0.5-1.0) and ash content. Yet, the models presented in Table 2.1 have different characteristics from each other. As can be seen from the tables, the fluidized bed has been represented in different approaches in terms of mixing of gaseous species. Furthermore, partitioning of coal nitrogen into char and volatile nitrogen, and release pattern of volatile nitrogen specie(s) diverse widely in *NO* models and sub-models. Formation and reduction reactions included in the models generally differ from each other, as well. On the whole, these differences describe the diversity of the fluidized bed models including *NO* emissions.

Table 2.1 Summary of models including NO_x formation and reduction.

Author(s)	Year	A	B	C	D	E	F	G	H	I	J
Perreira and Beer [1]	1978	2	1	1+2a	1	1a	No	1	1a+2	1	No
Rajan and Wen [2]	1980	2a*	2	3a	1	2a	Yes	2	1b+2	1	Yes
Beer et al. [3]	1981	2b	3	2b	1	2b	No	2	1a	1	No
Chaung et al. [4]	1984	2b	1+3	3b	1	2b	Yes	3	1b	1	No
Preto [21, 54]	1987	2a	1	1+2a	n.i.	n.i.	Yes	1+2	1b	1	Yes
Johnsson [5]	1989	1	1	3b	1	1b	No	1+4d	1a+2	3	No
De Souza-Santos [6]	1989	2	1	1	1	3	Yes	2	1b+2	2	Yes

n.i. : no information

Table 2.1 Summary of models including NO_x formation and reduction (continued).

Author(s)	Year	A	B	C	D	E	F	G	H	I	J
Lin et al. [7-9]	1990, 1992 & 1993	1	2	1	1	4	No	4c	2	2	No
Brem and Brouwers [10, 54]	1991	2	1	2b	1	n.i.	Yes	4c	2	2	Yes
Goel et al. [11, 12]	1995 & 1996	3	1	2b	2	1c	Yes	1*+4a	1a	1	Yes
Loeffler et al. [13, 14]	2001 & 2002	2a**	n.i.	2c	2	n.i.	Yes	1*+4b	1b	1	Yes

n.i. : no information

Table 2.2 Nomenclature for Table 2.1.

A. Fluidized Bed Model:

1. Single phase model, slow bubble regime.
2. Two phase model; bubble and emulsion phases.
    a. Compartment in series with two phases in each compartment.
        * clouded bubble phase
        ** emulsion and slug phases are present, slugs are free of solids.
    b. The lower section of the bed is in slow bubble regime.
3. Three phase model; bubble, emulsion and channeling phases.

B. Gas Flow Pattern:

1. Gases in all phases are in plug flow.
2. Gases in all phases are well mixed.
3. Emulsion phase is well mixed; bubble phase is in plug flow.

C. Devolatilization Pattern :

1. Uniform in the dense phase.
2. Instantaneous release
    a. at the feed point.
    b. at the bottom of the bed (grid section).
    c. at the middle of the bed.
3. Volatiles release is related to
    a. solids mixing rate.
    b. O_2 concentration.

D. Fuel-*N* devolatilization product:

1. NH_3.
2. NH_3 and HCN.

Table 2.2 Nomenclature for Table 2.1 (continued).

E. Fuel-*N* partitioning into volatiles:

1. Fixed value
    a. 100%
    b. 50%
    c. 33%
2. Estimated from empirical data or correlations in the literature based on
    a. Bed temperature.
    b. Char temperature.
3. Estimated from calculations performed by the model.
4. Estimated from coal properties; proportional to volatile fraction in the coal.

F. Freeboard:

Freeboard phenomena considered: Yes/No.

G. Model for NO_x Chemistry:

1. Homogeneous *NO* formation and reduction.
    * Complex reaction mechanism with ~300 elementary reaction steps and ~50 species including radicals.
2. Homogeneous *NO* formation, *NO* formation by char nitrogen oxidation and *NO* reduction by char.
3. Homogeneous *NO* formation and reduction, *NO* formation by char nitrogen oxidation and *NO* reduction by char.
4. Heterogeneous reactions including
    a. Char only.
    b. Char and ash.
    c. Char and *CaO*.
    d. Char, *CaO* and $CaSO_4$.

Table 2.2 Nomenclature for Table 2.1 (continued).

H. Predictions:

1. *NO* concentration profile**.**
    a. Along the bed
    b. Along the combustor
2. *NO* emissions.

I. Validation:

1. *NO* concentration profile validated against experimental data.
2. *NO* emissions validated against experimental data.
3. No validation.

J. Comprehensive Overall Model:

NO_x model incorporated into a comprehensive overall model: Yes/No**.**

The pioneering work in NOx modeling studies for FBCs was carried out by Perreira and Beér [1] in an attempt to verify their NOx measurements performed in bed section of a 0.3x0.3*m* AFBC test rig. *NO* formation and reduction was considered in a fluidized bed model without incorporating into an overall system model. All fuel nitrogen was assumed to be released as NH_3. Only, homogeneous reactions were utilized to represent *NO* formation and reduction, and rate expressions were taken from a previous study on premixed hydrocarbon flames at high temperature [58]. The predicted behavior of *NO* formation for bed section of the FBC was found to be in agreement with measured profile. *NO* emissions with respect to bed temperature were also predicted, but predictive accuracy of the model was found to decrease as the temperature rises above 800 ^oC.

The models developed by Beer et al. [3] and Chaung et al. [4] are further developments of the original model presented by Perreira and Beér [1]. A certain ratio of coal nitrogen was assumed to be released as volatile depending on char temperature. In addition to homogeneous reactions used by Perreira and Beér [1],

gas-solid reactions, char nitrogen oxidation and *NO*-char reaction, were also taken into account. However, the latter model includes the influence of *CO* concentration on *NO* reduction over char by adjusting the rate constant for *NO*-Char reaction. The model was extended to include freeboard phenomena by Chaung et al. [4]. Finally, reasonable agreement was obtained between the predicted concentrations of *NO* and measured data.

Incorporation of a *NO* model into a comprehensive model for fluidized bed combustion of coal was performed by Rajan and Wen [2]. Apart from homogeneous formation of *NO*, gas solid reactions like char nitrogen oxidation and *NO* reduction by char were also included in their model. Predicted concentrations of *NO* were tested against a limited number of measurements along the height of the combustor, and validation of emissions against measured data with respect to different bed temperatures was also tested. Good agreement was obtained in both validation tests. Preto [2, 38] also utilized a comprehensive model for fluidized bed combustion of coal in order to investigate *NO* emissions. The reaction mechanism employed was the same as that of Rajan and Wen [2], but rate constant for *NO* reduction by char was adjusted to fit the experimental data obtained from pilot-scale test rig. Reasonable agreement was obtained between the predicted concentration profile of *NO* and experimental data.

de Souza-Santos [6] developed another NO model which was used as a sub-model in a comprehensive system model. In his study, a detailed reaction mechanism that involves homogeneous formation reactions including thermal *NO*, heterogeneous reactions including gasification of char nitrogen and reduction of *NO* by char was taken into consideration. However, most of the reactions are hypothetical and require convergence calculations to estimate the stoichiometries and products of the reactions. In consequence, the predicted *NO* profile shows that there exist a minima and maxima of *NO* concentration in the bed section. The performance of the overall model with respect to *NO* emission was tested against a single emission data from a commercial scale FBC, where reasonable agreement was found.

A kinetic model that incorporates a large number of reactions for *NO* formation and reduction was proposed by Johnsson [5] for the first time. The reaction mechanism includes both homogeneous and heterogeneous reactions including the interaction with limestone. However, ash catalyzed reactions were not taken into consideration. The main objective of this study was to assess the relative importance of reactions, and predict the observed effects of operating conditions on the formation of *NO*. Therefore, single phase plug flow reactor was assumed to represent a fluidized bed combustor as a first approach, where simulated operating conditions such as concentration profiles of *CO* and O_2 were utilized as input parameters. As a result, reduction of *NO* over char, oxidation of NH_3 to N_2 over char and formation of *NO* by NH_3 over *CaO* were found to be the most important reactions taking place in *NO* chemistry. The predicted concentration profiles of *NO* were not compared to experimental data.

In an attempt to investigate the interaction between sulfur capture and *NO* emissions from a fluidized bed combustor, Lin et al. [7-9] extended a previously developed sulfur retention model, known as *SURE* Model, to account for *NO* formation and reduction. In order to achieve this, a single particle model for sulfation of lime and char combustion was implemented into ideally stirred tank reactor model which neglects elutriation or freeboard phenomena [8, 9]. Interaction of limestone was investigated through oxidation of NH_3 to *NO* over calcined limestone. Homogeneous reactions were not considered, but char nitrogen oxidation to *NO* and catalytic reactions over char were taken into account in the developed model. After adjusting the rate constants in the NO_x model to experimental data from bench scale test rig, the predicted ability of the model was tested against measured emissions data from pilot-scale FBC. The predicted emissions were found to be in good agreement with the measured data.

The model of Brem and Brouwers [10, 54] is a further development of the model by Preto [21, 54] in which a single particle model for char combustion and sulfur capture is incorporated into an overall system model of an AFBC. Char nitrogen oxidation to *NO* and reduction of *NO* by *CO* over char were considered in the single

particle model. However, volatile nitrogen, NH_3, was assumed to be oxidized completely and immediately to NO and N_2 over char and CaO, and the split between NO and N_2 was determined by a correlation depending on reaction kinetics, temperature, and the content of char and CaO in the bed. The rate of NO reduction was also used as a fitting parameter so that good agreement can be obtained between predicted and measured NO emissions.

Recent NO_x modeling studies have concentrated on extended reaction mechanisms for NO formation and reduction phenomena. A detailed chemical kinetic mechanism for homogeneous formation and reduction of NO and N_2O, over 300 elementary reversible reactions taking place among about 50 species, were implemented into an overall system model by Goel et al. [11, 12] and Loeffler et al. [13, 14]. Quenching of radicals over solids was also considered. Single particle model for char combustion was extended to include NO/N_2O formation from char nitrogen oxidation and reduction by char. Loeffler et al. [13, 14] conducted single particle combustion tests in an electrically heated laboratory test unit, and accordingly the system model was developed for a slugging fluidized bed. The measured data obtained from the test unit was used in order to test the predictive ability of the model and good agreement was found. Goel et al. [11, 12], on the other hand, developed their model for a bubbling fluidized bed but compared its predictions to measured data obtained from bench-scale test unit where slugging conditions prevail. Therefore, the predictions did not fit the experimental data as it was discussed in their study [12].

2.5.2 Conclusive Remarks

Incorporation of a sufficiently detailed NO formation and reduction reactions into a comprehensive overall system model for bubbling fluidized bed combustion of coal without adjusting the rate constants in the NO_x sub-model is limited in the literature. Furthermore, the modeling studies on NO_x emission performance of FBCs so far focused on good quality coals with low volatile matter and ash contents. As it is evident that NO_x formation behaviour is influenced by the type of coal according to

the discussions given in sections 2.1, 2.2, and 2.3, it is questionable whether the models published so far are capable of predicting NO_x emissions from fluidized bed combusiton of coals with high volatile matter and ash content.

Therefore, in this study, a previously developed comprehensive model will be extended to incorporate a sufficiently detailed *NO* formation and reduction reactions. Coal nitrogen split into char and volatiles, which is unique to the coal type, will be determined by pyrolysis experiments. The predictive performance of the model will be tested by comparing the model predictions with on-line concentration measurements of O_2, CO_2, CO, NO_x along the 0.3 MW_t Atmospheric Bubbling Fluidized Bed Combustor (ABFBC), where typical Turkish lignite with high volatile matter and (VM/FC ~2.0) ash content is burned in its own ash.

CHAPTER 3

STEADY-STATE ABFBC MODEL WITH *NO* FORMATION AND REDUCTION

A system model, originally proposed by Selçuk and Sivrioğlu [15] and later improved, extended and validated against experimental data by Selçuk and her colleagues [16, 17], was chosen as a basis for incorporation of *NO* formation and reduction. It is developed on the basis of first principles and used to correlate data from the Middle East Technical University (METU) 0.3 MW_t ABFBC Test Rig. The system model accounts for bed and freeboard hydrodynamics, volatiles release and combustion, char particles combustion and size distribution, heat transfer, elutriation, entrainment, char attrition, sulfur retention and *NO* formation and reduction. The assumptions involved are illustrated in Figure 3.1 and Figure 3.2 for the bed and freeboard sections, respectively.

The behavior of the fluidized bed combustor under consideration is described by a model based on conservation equations for energy and chemical species in conservative form for both bed and freeboard sections. The correlations used in estimating important parameters in the model are listed in Table 3.1. Seven chemical species, O_2, CO, CO_2, H_2O, SO_2, NH_3 and NO are considered in the model. Chemical reactions included in the model together with their rate expressions are given in Table 3.2. The components of the system model before the incorporation of *NO* formation and reduction are described in detail in the literature [16, 17]. However, for the sake of integrity, a brief summary of these sub-models will be provided in the following sections. Modifications required for the consideration of *NO* formation and reduction reactions will be explained in detail.

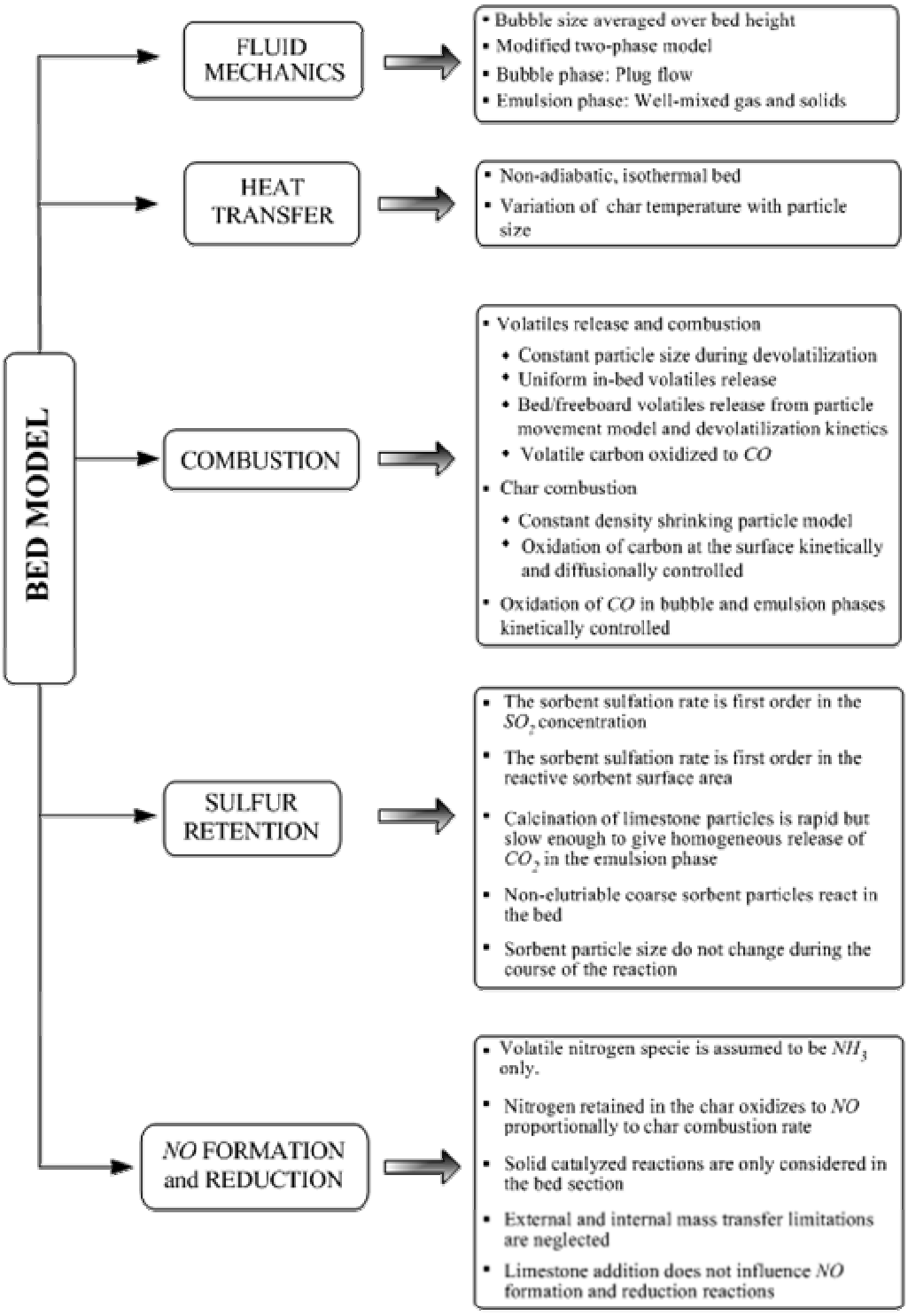

Figure 3.1 An overview of the steady state bed model assumptions.

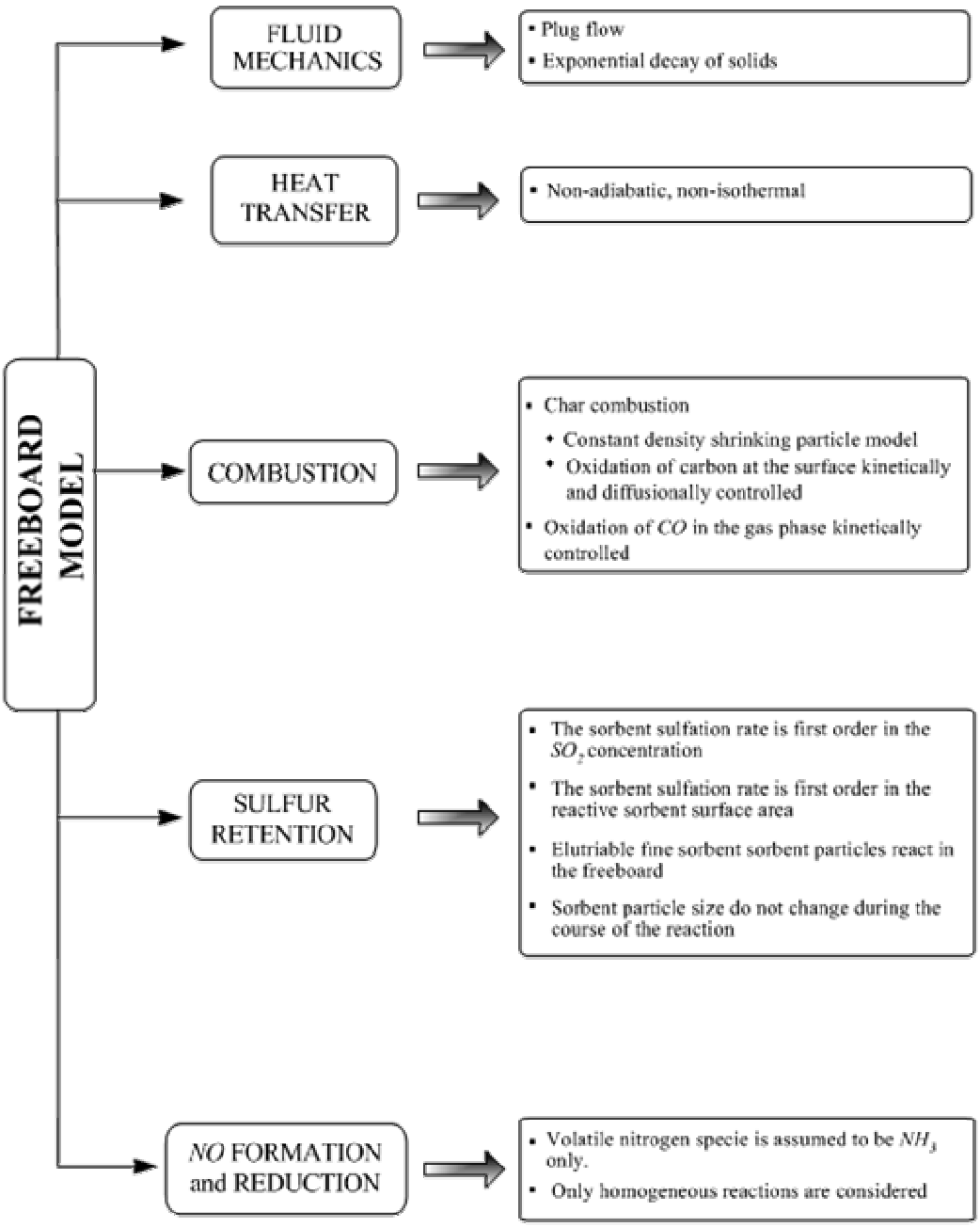

Figure 3.2 An overview of the steady state freeboard model assumptions.

Table 3.1 Correlations used in the model.

	Reference
Mass transfer to particles in the emulsion phase, k_f	[59]
Heat transfer to particles in the emulsion phase, h_p	[60]
Specific elutriation rate constant, $E(r)$	[61]
Terminal velocity of the particles, u_t	[62]
Bubble to emulsion mass transfer, K_{be}	[63]
Minimum fluidization velocity, u_{mf}	[64]
Bubble size, d_b	[65]
Emulsion phase velocity, u_e	[66]
Bubble phase volume fraction, δ	[67]
Convective heat transfer coefficient of bed wall, h_{bw}	[62]
Convective heat transfer coefficient of cooling tubes, h_{cw}	[67]
Convective heat transfer coefficient of cooling water, h_i	[68]
Exponential decay constant, a	[61]
Gas side heat transfer coefficient in freeboard, h_g	[60]

Table 3.2 Reactions and rate expressions

#	**Reaction**	**Place**	**Rate Expression**	**Unit**	**Ref.**
R1	$C_s + 1/2O_2 \rightarrow CO$	char surface	$5.95\times10^4 T_p \exp(-17967/T_p) C_{O_{2,s}}$	$mol\ cm^{-2}\ s^{-1}$	[69]
R2	$C + 1/2O_2 \rightarrow CO$	gas phase	Instantaneous		-
R3	$CO + 1/2O_2 \rightarrow CO_2$	gas phase	$3.0\times10^{10} T \exp(-8052/T_g) C_{O_2}^{0.3} C_{CO} C_{H_2O}^{0.5}$	$mol\ cm^{-3}\ s^{-1}$	[70]
R4	$H_2 + 1/2O_2 \rightarrow H_2O$	gas phase	Instantaneous		-
R5	$S + O_2 \rightarrow SO_2$	gas phase	Instantaneous		-
R6	$CaCO_3 \rightarrow CaO + CO_2$	sorbent surface	Instantaneous		-
R7	$CaO + SO_2 + 1/2O_2 \rightarrow CaSO_4$	sorbent surface	$14.9 C_{SO_2} S_o \sigma_{avg}$	$mol\ s^{-1}$	[17]
R8	$N_{vol} + 3/2H_2 \rightarrow NH_3$	gas phase	Instantaneous		-
R9	$N_s + 1/2O_2 \rightarrow NO$	char surface	proportional to the char combustion rate	$mol\ cm^{-3}\ s^{-1}$	-

Table 3.2 Reactions and rate expressions (continued)

#	Reaction	Place	Rate Expression	Unit	Ref.
R10	$NH_3 + 5/4O_2 \rightarrow NO + 3/2H_2O$	gas phase	$2.21\times10^{14}\exp(-38160/T_g)C_{NH_3}$	$mol\ cm^{-3}\ s^{-1}$	[51]
R11	$NO + 2/3NH_3 \rightarrow 5/6\ N_2 + H_2O$	gas phase	$2.45\times10^{26}\exp(-27680/T_g)C_{NO}C_{NH_3}$	$mol\ s^{-1}$	[51]
R12	$NO + Char \rightarrow 1/2\ N_2 + CO$	char surface	$3.45\times10^{6}\exp(-22200/T_d)C_{NO}^{0.52}$	$mol\ g^{-1}\ s^{-1}$	[47]
R13	$NO + CO \rightarrow CO_2 + 1/2N_2$	char surface	$3.81\times10^{9}\exp(-22800/T_d)C_{NO}^{0.39}C_{CO}^{0.53}$	$mol\ g^{-1}\ s^{-1}$	[47]
R14	$NH_3 + 5/4O_2 \rightarrow NO + 3/2H_2O$	char surface	$3.4\times10^{10}C_{NH_3}C_{O_2}$	$mol\ g^{-1}\ s^{-1}$	[47]
R15	$NH_3 + 5/4O_2 \rightarrow NO + 3/2H_2O$	ash surface	$0.4C_{NH_3}^{0.57}C_{O_2}^{0.11}$	$mol\ g^{-1}\ s^{-1}$	[47]
R16	$NH_3 + 3/4O_2 \rightarrow 1/2\ N_2 + 3/2H_2O$	char surface	$8.4\times10^{10}C_{NH_3}C_{O_2}$	$mol\ g^{-1}\ s^{-1}$	[47]
R17	$NH_3 + 3/4O_2 \rightarrow 1/2N_2 + 3/2H_2O$	ash surface	$3.92\times10^{9}C_{NH_3}^{1.8}C_{O_2}^{0.07}$	$mol\ g^{-1}\ s^{-1}$	[47]

3.1 Bed Model

Bed model can be described in terms of bed hydrodynamics, volatiles release and combustion, char combustion, particle size distribution of bed char and bed char hold-up, sulfur retention and *NO* formation and reduction.

3.1.1 Bed Hydrodynamics

Bed hydrodynamics is based on modified two-phase theory suggested by Grace and Clift [71],

$$u_o = \frac{Q_b}{A_{bed}} + u_{tf} + u_e(1-\delta) \tag{3.1}$$

where throughflow velocity, u_{tf}, can be expressed in terms of emulsion phase velocity, u_e, using modified n-type two-phase theory of Grace and Harrison [72],

$$u_{tf} = (n+1)u_e\delta \tag{3.2}$$

where $n = 2$ for three dimensional beds. Gas/solids in the emulsion phase and gas in the bubble phase are assumed to be well-stirred and in plug flow, respectively.

An integrated average mean bubble size found from bubble size expression proposed by Mori and Wen [65], in the sections unoccupied by the tube bank and from constant and uniform bubble size determined by the clearance between the tubes is utilized. Bubbles are assumed to be free of solids. The gas interchange coefficient between bubble and emulsion phases is defined as:

$$K_{be} = \frac{\left(\begin{array}{c} volume\ of\ gas\ going\ from\ bubbles \\ to\ emulsion\ or\ from\ emulsion\ to\ bubbles \end{array}\right)}{(volume\ of\ bubbles\ in\ the\ bed)(time)} \tag{3.3}$$

In this thesis study, the following relationship was used for K_{be} [63],

$$K_{be} = 4.5\frac{u_e}{d_b} \tag{3.4}$$

3.1.2 Volatiles Release and Combustion

Volatiles are assumed to be released uniformly in the emulsion phase. The amount released in bed is determined by using the volatile release model of Stubington *et al.* [73], and to describe the devolatilization kinetics the parallel independent reaction model of Anthony and Howard [74] is used. In the presence of radial temperature profile and with the assumption of evenly distributed volatile matter in the particle, total amount of volatile matter released with respect to time is given by:

$$\frac{v_{avg}}{v_\infty} = \frac{3}{R^3}\int_0^R \left[1 - \int_0^\infty exp\left(-\int_0^t k(E)dt\right) f(E)\,dE\right] r^2 dr \tag{3.5}$$

Devolatilization history of the particle yields the fraction of volatiles released in bed. The remaining volatiles are assumed to be released to freeboard while the particle is at the bed surface. With regard to combustion of volatiles released, volatile carbon and hydrogen are assumed to burn instantaneously to carbon monoxide (*CO*) and water (H_2O), respectively. The oxidation of *CO* takes place in both bubble and emulsion phases according to the rate expression of Hottel *et al.* [70]. Further details of the volatiles release model can be found in [75].

3.1.3 Char Combustion

Char particles are assumed to burn only to *CO*, as it is the major product of char combustion for typical FBC temperatures. Using the shrinking particle model and taking film mass transfer and the kinetics resistance into consideration, the rate of carbon oxidation at the particle surface can be obtained as

$$r_{C,e} = \frac{2}{1/k_f + 2/k_s}\bar{C}_{O_2,e} \tag{3.6}$$

Film mass transfer coefficient, k_f, is obtained from the equation suggested by Jung and La Nauze [59]. Kinetics of combustion of char particles is assumed to be

represented by equation of Field *et al*. [69]. Average emulsion phase oxygen (O_2) concentration is used to calculate combustion rate.

3.1.4 Char Particles Size Distribution

Since carbon consumption rate depends on the surface area provided by the burning char particles, calculation of particle size distribution and hold-up of char particles is of fundamental importance in the prediction of behavior of ABFBCs.

In order to derive a population balance based on the mass fractions for shrinking char particles the following assumptions are made:

1. Char particles enter the bed at a rate of F_o with size distribution of $P_o(r)$ which is expressed by Rosin-Rammler size distribution function.
2. As char particles are well-mixed, bed drain char size distribution represents the bed char size distribution:

$$P_{bd}(r) = P_{bed}(r) \tag{3.7}$$

3. The rate of elutriation of char particles of size r is directly proportional to their concentration in the bed, *i.e.*,

$$F_{co}P_{co}(r)dr = M_d P_{bed}(r)E(r)dr \tag{3.8}$$

   where $E(r)$ is the elutriation rate constant [61], M_d is the total mass of char in the bed and $P_b(r)$ is the size distribution of char particles in the bed.
4. Carryover char size distribution represents the recycle char size distribution, since both streams are elutriated from the bed:

$$P_{co}(r) = P_{recy} \tag{3.9}$$

5. Densities of char particles do not change during the burn-out.
6. Fragmentation of char particles is negligible since there is no noticeable fragmentation for particles having diameters less than 3 mm [76].
7. Char particles can be attrited until reaching the upper size limit of the fines,

r_f, and then becomes a fine particle itself. Fines have a size distribution of $P_f(r)$. Fines generated by attrition are not attritable themselves.

8. Char particles are considered to shrink by combustion and attrition according to shrinking particle model at a rate of

$$\left(\frac{dr}{dt}\right)=\left(\frac{dr}{dt}\right)_c+U_f\left(r_{max},r_f\right)\left(\frac{dr}{dt}\right)_a \tag{3.10}$$

where U_f is unit filter function defined to differentiate particle size ranges attained due to both combustion and attrition and due to combustion only. A detailed discussion on definition of unit filter function can be found elsewhere [76].

The working form of the population balance is given in Equation (3.11). A detailed derivation of the following equation can be found elsewhere [76, 77].

$$\frac{dW(r)}{dr}=-W(r)\left[\frac{F_{bd}}{M_d\Re(r)}+\left(1-\frac{F_{recy}}{F_{CO}}\right)\frac{E(r)}{\Re(r)}-\frac{3}{r}\right]+F_oP_o(r)+U_f\left(r_f,0\right)F_aP_f(r) \tag{3.11}$$

$W(r)$ is the dummy variable in which M_d, $P_{bed}(r)$, and shrinkage rate of char particles, $\Re(r)$, are combined.

$$W(r)=M_dP_{bed}(r)\Re(r) \tag{3.12}$$

where char particle shrinkage rate, $\Re(r)$, is expressed as

$$\Re(r)=-\frac{dr}{dt} \tag{3.13}$$

Equation (3.11) is subjected to the following boundary condition,

$$\text{at } r=r_{max} \qquad W(r)=0 \tag{3.13}$$

as the probability of having solid particles of size r_{max} in the bed, *i.e.,* P_{bed}, is practically zero, due to the shrinkage of maximum particle size in the bed. Once the solution for $W(r)$ becomes available, the bed char hold-up, M_d, bed char size distribution, $P_{bed}(r)$, carryover rate, F_{co}, carryover char size distribution, $P_{co}(r)$, can

be obtained by using the descriptions in Equations (3.8) and (3.12).

3.1.5 Desulfurization Model

It is assumed that desulfurization involves two consecutive steps, instantaneous calcination of limestone followed by sulfation reaction. The rate expression for the reaction between SO_2 and lime, reaction R7, was assumed to be first order in the SO_2 concentration and proportional to the reactive external surface area of the particles [17].

The sorbent fed has a wide particle size distribution and it is assumed that particle size of sorbent does not change during reaction. Attrition of limestone particles is not considered. Therefore, for any particle with size r, the rate equation takes the following form:

$$r_{SO_2} = kC_{SO_2}S(t) \tag{3.14}$$

Overall sulfation rate constant, k, is a combination of film mass transfer limitations and sulfation kinetics, and it was determined from fluidized bed combustion experiments.

As sulfation continues, sulfation reaction rate decreases due to pore blocking of the $CaSO_4$ product. Therefore the reactive external surface area, $S(t)$, is expressed in terms of fractional external surface area, $\sigma(t)$, and described by an exponential decay with time.

$$\frac{S(t)}{S_0} = \sigma(t) = exp\left[-\frac{6M_{CaCO_3}kC_{SO_2}}{x_{CaCO_3}\rho_{lst}d_p}t\right] \tag{3.15}$$

where total initial external surface area for spherical limestone particles, S_o, is expressed as:

$$S_0 = \frac{6M_{lst}}{\rho_s d_p} \tag{3.16}$$

In order to model sulfation reaction at steady state it is necessary to assess an average fractional external surface area, σ_{avg}, which is calculated from the solids residence time distribution function, and the fractional external surface area as a function of time $\sigma(t)$,

$$\sigma_{avg} = \frac{1}{\left[1+\frac{6M_{CaCO_3}kC_{SO_2}}{x_{CaCO_3}\rho_{lst}d_p}\tau\right]}\left[1-exp\left(-\left\{\frac{1}{\tau}+\frac{6M_{CaCO_3}kC_{SO_2}}{x_{CaCO_3}\rho_{lst}d_p}\right\}\tau_{max}\right)\right] \quad (3.17)$$

Calculation of average fractional external surface area, σ_{avg}, and determination of residence time of sorbent particles, τ, are given in detail elsewhere [77].

Finally, rate of sulfation reaction becomes:

$$r_{SO_2} = kC_{SO_2}S_0\sigma_{avg} \quad (3.18)$$

Then the total reaction rate is the summation of the rates obtained at different sizes:

$$r_{SO_2} = \sum_{i=1}^{n} r_{SO_2,i} \quad (3.19)$$

3.1.6 *NO* Formation and Reduction Model

As it was explained in Chapter 2, nitrogen in coal is split into char nitrogen and volatile nitrogen during devolatilization. Since volatile nitrogen and char bound nitrogen go into different reaction paths in the *NO* chemistry, determination of volatile nitrogen species and estimation of partitioning factor for coal nitrogen release must be the primary step for *NO* modeling studies. This factor, specific to the lignite under consideration, was found by performing pyrolysis experiments in TGA coupled with FTIR. Coal sample was heated to 900°C at a rate of 50°C/min and kept isothermal till constant weight. Pyrolysis gases were analyzed simultaneously by FTIR at a resolution of 1 cm^{-1}. After the pyrolysis, remaining char particles were subjected to elemental analysis. Consequently, 79% of coal nitrogen was found to be released as volatile nitrogen. Moreover, no *HCN* was

detected in FTIR analysis. Therefore, NH_3 was assumed to be the only intermediate specie for NO formation and reduction, and conversion of volatile nitrogen into NH_3 was considered to be instantaneous. On the other hand, amount of NH_3 was assumed to be 20% of the remaining volatiles according to the findings of pyrolysis experiments performed by Wu and Ohtsuka [19, 20]. The balance of nitrogen bearing specie was assumed to be molecular nitrogen, N_2.

It is generally accepted that nitrogen retained in char oxidizes to NO proportionally to char combustion rate. Rate of nitrogen removal from the char surface is assumed to be equal to the rate of oxidation at the particle surface, $r_{N,e}$. Therefore, for any char particle of size r,

$$\frac{d(W_N)}{dt} = -4\pi r^2 M_N r_{N,e} \tag{3.20}$$

Writing W_N in an explicit form,

$$\frac{d}{dt}\left(\frac{4}{3}\pi r^3 \rho_d \frac{x_{N,c}}{x_C + x_a}\right) = -4\pi r^2 M_N r_{N,e} \tag{3.21}$$

where $x_{N,c}$ is the fraction of nitrogen retained in the char after volatiles has released. It is not included in the denominator of the fraction as it is small compared to that of carbon and ash in the char.

Rearranging Equation (3.21) yields,

$$-\frac{dr}{dt} = \frac{1}{\rho_d}\frac{x_C + x_a}{x_{N,c}} M_N r_{N,e} \tag{3.22}$$

Substituting Equation (3.22) into Equation (3.13) and solving for $r_{N,e}$:

$$r_{N,e} = \Re(r)\frac{\rho_d}{M_N}\frac{x_{N,c}}{x_C + x_a} \tag{3.23}$$

In order to find the rate of char nitrogen oxidation for all particles of size r, $n_{N,e}$, Equation (3.24) must be multiplied with surface area of particle and number of particles of size r.

$$n_{N,e} = \frac{M_d P_b(r)}{\rho_d} \frac{1}{\frac{4}{3}\pi r^3} 4\pi r^2 r_{N,e} \tag{3.24}$$

The rate of char nitrogen oxidation in the bed section is found by rearranging Equation (3.24) and summing it up for all char particles.

$$n_{N,e} = 3M_d \left[\frac{1}{M_N} \left(\frac{x_{N,c}}{x_C + x_a} \right) \right] \int_{r_{\min}}^{r_{\max}} \frac{P_b(r)}{r} \Re(r) dr \tag{3.25}$$

Equation (3.25) is divided by gas volume in the emulsion phase in order to satisfy the unit consistency in the mass balance for emulsion phase.

$$n_{N,e} = \frac{3M_d}{V_{bed}(1-\delta)\varepsilon_{mf}} \left[\frac{1}{M_N} \left(\frac{x_{N,c}}{x_C + x_a} \right) \right] \int_{r_{\min}}^{r_{\max}} \frac{P_b(r)}{r} \Re(r) dr \tag{3.26}$$

Similarly rate of char combustion rate can be found as,

$$n_{C,e} = \frac{3M_d}{V_{bed}(1-\delta)\varepsilon_{mf}} \left[\frac{1}{M_C} \left(\frac{x_C}{x_C + x_a} \right) \right] \int_{r_{\min}}^{r_{\max}} \frac{P_b(r)}{r} \Re(r) dr \tag{3.27}$$

Equation (3.26) is divided by Equation (3.27) and rate of char nitrogen oxidation, $n_{N,e}$ is obtained in terms of $n_{C,e}$ as in Equation (3.28).

$$n_{N,e} = \frac{\left(x_{N,c} / M_N \right)}{\left(x_C / M_C \right)} n_{C,e} \tag{3.28}$$

Based on the results of pyrolysis experiments and reaction scheme proposed by Johnsson and Dam-Johansen [47] for *NO* formation and reduction mechanism, a set of reactions were selected for *NO* formation and reduction model. Among these reactions, lime catalyzed reactions were not taken into consideration due to the former findings that addition of limestone does not influence *NO* formation significantly in ABFBCs [55, 56]. Catalytic reduction of *NO* by NH_3 was also

omitted as the reaction rate expressions were reported to be valid under reducing conditions [47]. Reduction of *NO* by *CO* over ash was also discarded due to the loss of catalytic activity of ash under oxidizing conditions [50]. Since solid hold-up in the freeboard is negligible compared to that in the bed, heterogeneous reactions were only applied to the bed section. In this study, external mass transfer effects were also neglected, as Johnsson and Dam-Johansen [47] observed no external mass transfer limitation up to particles of 5 *mm* for solid catalyzed reactions and this was greater than the maximum size of particles used in this study. Table 3.2 displays reaction scheme (R10 - R17) incorporated into the overall system model. Rate expressions for heterogeneous and homogeneous reactions were taken from [51] and [47], respectively. Since it was reported that different solids have different catalytic activities [47], rate expressions of heterogeneous reactions obtained for a brown coal were used, as lignites are close to brown coals with respect to coal rank.

Reactions R12 and R13 have Arrhenius type of rate expressions including char particle temperature, T_d, so considering any char particle of size r, rate of heterogeneous reaction, r_{NO}, equals to

$$r_{N,het} = M_d P(r) r_{NO} \tag{3.29}$$

Considering wide size distribution of particles in the bed, Equation (3.29) must be summed up for all particles.

$$r_{N,het} = M_d \int_{r_{\min}}^{r_{\max}} P(r) r_{NO}\, dr \tag{3.30}$$

However, for reactions R14 and R16, rate of heterogeneous reaction, $r_{N,het}$, can be found by multiplying r_{NO} with char hold-up, M_d, directly,

$$r_{N,het} = M_d r_{NO} \tag{3.31}$$

and for reactions R15 and R17 with ash hold-up, M_i.

$$r_{N,het} = M_i r_{NO} \tag{3.32}$$

3.1.7 Mass and Energy Balance Equations

Spatial variations of species concentrations are described by the conservation equations for chemical species in bubble and emulsion phases:

$$\frac{dn_{j,b}}{dz} = A_{bed}\delta\left[\Re_{j,b} + K_{be}(C_{j,e} - C_{j,b})\right] \tag{3.33}$$

$$n_{j,e}\,|_{z=0} - n_{j,e} + V_{bed}\delta\left[\frac{1-\delta}{\delta}\varepsilon_{mf}\,\Re_{j,e} - K_{be}(C_{j,e} - \overline{C}_{j,b})\right] = 0 \tag{3.34}$$

These equations are subject to the following boundary conditions:

$$\text{at } z = 0 \qquad n_{j,b} = y_{j,b}\frac{n_a}{1 + \dfrac{u_e}{u_b}\dfrac{1-\delta}{\delta}\varepsilon_{mf}} \tag{3.35}$$

$$\text{at } z = 0 \qquad n_{j,e} = y_{j,e}\frac{n_a}{1 + \dfrac{u_b}{u_e}\dfrac{\delta}{(1-\delta)\varepsilon_{mf}}} \tag{3.36}$$

The expressions for the species generation or depletion terms appearing in Equations (3.33) and (3.34), $\Re_{j,b}$ and $\Re_{j,e}$, take the following forms for each species considered,

j=1 (O_2)

$$\Re_{1,b} = -0.5r_{CO,b} - \frac{5}{4}\left(r_{N,hom}\right)_{R10} \tag{3.37}$$

$$\begin{aligned}\Re_{1,e} = &-\frac{m_{vm}x_{vl}}{V_{bed}(1-\delta)\varepsilon_{mf}}\left\{0.5\frac{x_{C,vm}}{M_C} + 0.5\frac{x_{H,vm}}{M_{H_2}} + \frac{x_{S,vm}}{M_S} - \frac{x_{O,vm}}{M_{O_2}}\right\} \\ &- 0.5n_{C,e} - 0.5r_{CO,e} - \frac{0.5r_{SO_2,e}}{V_{bed}(1-\delta)\varepsilon_{mf}} - 0.5n_{N,e} \\ &- \frac{5}{4}\left(r_{N,hom}\right)_{R10} - \frac{1}{V_{bed}(1-\delta)\varepsilon_{mf}}\left\{\frac{5}{4}\left(r_{N,het}\right)_{R14} + \frac{5}{4}\left(r_{N,het}\right)_{R15}\right. \\ &\left. + \frac{3}{4}\left(r_{N,het}\right)_{R16} + \frac{3}{4}\left(r_{N,het}\right)_{R17}\right\}\end{aligned} \tag{3.38}$$

j=2 (CO)

$$\Re_{2,b} = -r_{CO,b} \tag{3.39}$$

$$\begin{aligned}\Re_{2,e} = {} & \frac{m_{vm}x_{vl}}{V_{bed}(1-\delta)\varepsilon_{mf}}\left\{0.5\frac{x_{C,vm}}{M_C}\right\} + n_{C,e} - r_{CO,e} \\ & + \frac{1}{V_{bed}(1-\delta)\varepsilon_{mf}}\left\{\left(r_{N,het}\right)_{R12} - \left(r_{N,het}\right)_{R13}\right\}\end{aligned} \tag{3.40}$$

j=3 (CO_2)

$$\Re_{3,b} = r_{CO,b} \tag{3.41}$$

$$\Re_{3,e} = r_{CO,e} + \frac{1}{V_{bed}(1-\delta)\varepsilon_{mf}}\left(r_{N,het}\right)_{R13} + \frac{F_{lst}x_{CaCO_3}}{M_{CaCO_3}V_{bed}(1-\delta)\varepsilon_{mf}} \tag{3.42}$$

j=4 (H_2O)

$$\Re_{4,b} = \left\{\frac{3}{2}(r_{N,hom})_{R10} + \frac{1}{V_{bed}\delta}(r_{N,hom})_{R11}\right\} \tag{3.43}$$

$$\begin{aligned}\Re_{4,e} = {} & \frac{1}{V_{bed}(1-\delta)\varepsilon_{mf}}\left\{m_{vm}x_{vl}\frac{x_{H,vm}}{M_{H_2}} + m_f\frac{x_{H_2O}}{M_{H_2O}} - \left(r_{N,hom}\right)_{R11}\right\} + \frac{3}{2}\left(r_{N,hom}\right)_{R10} \\ & + \frac{3}{2}\frac{1}{V_{bed}(1-\delta)\varepsilon_{mf}}\left\{\left(r_{N,het}\right)_{R14} + \left(r_{N,het}\right)_{R15} + \left(r_{N,het}\right)_{R16} + \left(r_{N,het}\right)_{R17}\right\}\end{aligned} \tag{3.44}$$

j=5 (SO_2)

$$\Re_{5,b} = 0 \tag{3.45}$$

$$\Re_{5,e} = \frac{1}{V_{bed}(1-\delta)\varepsilon_{mf}}\left\{\frac{m_{vm}x_{vl}x_{S,vm}}{M_S} - r_{SO_2,e}\right\} \tag{3.46}$$

j=6 (NH_3)

$$\Re_{6,b} = -\left\{ (r_{N,hom})_{R10} + \frac{2}{3}\frac{1}{V_{bed}\delta}(r_{N,hom})_{R11} \right\} \tag{3.47}$$

$$\begin{aligned}\Re_{6,e} = {} & \frac{1}{V_{bed}(1-\delta)\varepsilon_{mf}}\left\{ \frac{m_{vm}x_{vl}x_{N,vm}}{M_N} \right\} - \left(r_{N,hom}\right)_{R10} \\ & + \frac{1}{V_{bed}(1-\delta)\varepsilon_{mf}}\left\{ \left(r_{N,hom}\right)_{R11} - \left(r_{N,het}\right)_{R16} - \left(r_{N,het}\right)_{R17} \right\}\end{aligned} \tag{3.48}$$

j=7 (NO)

$$\Re_{7,b} = \left\{ (r_{N,hom})_{R10} - \frac{1}{V_{bed}\delta}(r_{N,hom})_{R11} \right\} \tag{3.49}$$

$$\begin{aligned}\Re_{7,e} = {} & n_{N,e} + \left(r_{N,hom}\right)_{R10} - \frac{1}{V_{bed}(1-\delta)\varepsilon_{mf}}\left\{ \left(r_{N,hom}\right)_{R11} + \left(r_{N,het}\right)_{R12} \right. \\ & \left. + \left(r_{N,het}\right)_{R13} - \left(r_{N,het}\right)_{R14} - \left(r_{N,het}\right)_{R15} \right\}\end{aligned} \tag{3.50}$$

On the assumption that the gas and the inert particles are at the same temperature and that the mass of combustion gases and char particles are negligible compared to the mass of inerts, a combined gas/solid phase energy balance can be written as,

$$\begin{aligned} & n_A \int_{T_r}^{T_A} c_{pA}dT - \alpha\frac{A_T}{L_T}\int_0^{L_T} U_{cw}(T_{bed} - T_{cw})dx - A_{bw}h_{bw}(T_{bed} - T_{bw,s}) \\ & - m_{recy}c_{pi}\left(T_{bed} - T_{recy}\right) - m_{co}c_{pi}(T_{bed} - T_r) - m_{bd}c_{pi}(T_{bed} - T_r) \\ & - n_g\sum_{j=1}^{8} y_j \int_{T_r}^{T_{bed}} c_{pg,j}dT - m_f x_w \lambda^0 + Q_{rxn} + Q_p = 0 \end{aligned} \tag{3.51}$$

where enthalpy generated by chemical reactions, Q_{rxn}, and energy transferred from burning char particles, Q_p, are obtained from following equations,

$$
\begin{aligned}
Q_{rxn} &= m_f x_{vm} x_{vl} \left[\frac{x_{C,vm}}{M_C} \Delta H^0_{R2} + \frac{x_{H,vm}}{M_{H_2}} \Delta H^0_{R4} + \frac{x_{S,vm}}{M_S} \Delta H^0_{R5} + \frac{x_{N,vm}}{M_N} \Delta H^0_{R8} \right] \\
&+ \left[\Delta H^0_{R3} \int_0^{H_{bed}} r_{CO,b} dz + \Delta H^0_{R10} \int_0^{H_{bed}} \left(r_{N,hom} \right)_{R10,b} dz + \frac{\Delta H^0_{R11}}{V_{bed} \delta} \int_0^{H_{bed}} \left(r_{N,hom} \right)_{R11,b} dz \right] \\
&- \frac{F_{lst} x_{CaCO_3}}{M_{CaCO_3}} \Delta H^0_{R6} + V_{bed} (1-\delta) \varepsilon_{mf} \left[\Delta H^0_{R3} r_{CO,e} + \Delta H^0_{R10} \left(r_{N,hom} \right)_{R10,e} + \Delta H^0_{R9} n_{N,e} \right] \\
&+ \left[\Delta H^0_{R11} \left(r_{N,hom} \right)_{R11,e} + \Delta H^0_{R12} \left(r_{N,het} \right)_{R12} + \Delta H^0_{R13} \left(r_{N,het} \right)_{R13} + \Delta H^0_{R14} \left(r_{N,het} \right)_{R14} \right. \\
&\left. + \Delta H^0_{R15} \left(r_{N,het} \right)_{R15} + \Delta H^0_{R16} \left(r_{N,het} \right)_{R16} + \Delta H^0_{R17} \left(r_{N,het} \right)_{R17} \right]
\end{aligned}
\tag{3.52}
$$

$$
Q_p = \frac{3 M_d}{\rho_d} \int_{r_{min}}^{r_{max}} \left[h_p (T_d - T_{bed}) + \sigma \varepsilon (T_d^4 - T_{bed}^4) \right] \frac{dr}{r} \tag{3.53}
$$

and particle temperature is calculated by solving an energy balance around the particle, which is assumed to have uniform temperature:

$$
\frac{\rho_d}{M_C} \frac{x_{fc}}{x_{fc} + x_a} \Delta H^o_{R1} \Re(r) - \left[h_p \left(T_d - T_{bed} \right) + \sigma \varepsilon \left(T_d^4 - T_{bed}^4 \right) \right] = 0 \tag{3.54}
$$

Energy loss through the bed walls is taken into account by making a one-dimensional heat transfer analysis. For a combustor with square cross-section and wall thickness of L_{bw}, the temperature profile inside the wall of variable cross section is given by the following equation:

$$
\frac{d^2 T_{bw}}{dx^2} \left(x + A_{bed}^{0.5} / 2 \right) + \frac{dT_{bw}}{dx} = 0 \tag{3.55}
$$

Equation (3.55) is subject to the following boundary conditions:

$$
\begin{aligned}
&at\ x = 0 \qquad h_{bw} \left(T_{bed} - T_{bw} \right) = -k_{bw} \frac{\partial T_{bw}}{\partial x} \\
&at\ x = L_{bw} \qquad T_{bw} = T_{bw,o}
\end{aligned}
\tag{3.56}
$$

In order to account for the energy absorbed by the in-bed heat exchanger, a separate energy balance is performed on the cooling water. Neglecting the heat transfer resistance of the tubes, the spatial variation of the temperature of the cooling water is given by the following equation:

$$\frac{4m_{cw}}{\pi}\frac{dT_{cw}}{dx}-\frac{4d_{T,o}}{c_{pcw}}h_{cw}\left(T_{bed}-T_w\right)=0 \tag{3.57}$$

The inlet temperature of the cooling water is set as boundary condition to Equation (3.57). Surface temperature of tube wall, T_w, is calculated by solving a surface energy balance:

$$h_{cw}d_{T,o}\left(T_{bed}-T_w\right)-h_i d_{T,i}\left(T_w-T_{cw}\right)=0 \tag{3.58}$$

3.2 Freeboard Model

3.2.1 Solids distribution

The hold-up of particles in the freeboard is expressed with an exponential decay function Choi et al. [61],

$$\frac{\varepsilon_s}{\varepsilon_{s,0}}=\exp\left(-az_f\right) \tag{3.59}$$

where $\varepsilon_{s,0}$ is the volume fraction of solids just above the surface of dense bubbling bed and is given by:

$$\varepsilon_{s,0}=1-\varepsilon_f \tag{3.60}$$

The volume fractions of char and inert particles of size *r* at bed surface are obtained from the following equations, respectively:

$$\varepsilon_{d,0}=\varepsilon_{s,0}\frac{M_d P_{bed}(r)\Delta r/\rho_d}{M_d/\rho_d+M_i/\rho_i} \tag{3.61}$$

$$\varepsilon_{i,0}=\varepsilon_{s,0}\frac{M_i P_{bed}(r)\Delta r/\rho_i}{M_d/\rho_d+M_i/\rho_i} \tag{3.62}$$

The entrainment flux of particles, K_i^*, is calculated by assuming that it consists of a cluster flux, K_{ih}^*, and a dispersed noncluster flux, $K_{i\infty}^*$ as suggested by Hazlett and

Bergougnou [78],

$$K_i^* = K_{ih}^* + K_{i\infty}^* \tag{3.63}$$

and are obtained from empirical correlations proposed by Choi *et al.* [61]. The elutriation rate constant, *E(r)*, defined in Equation (3.8) is then calculated from:

$$E(r) = \frac{A_{bed}}{M_d} K_{i\infty}^* \tag{3.64}$$

The elutriated particles are assumed to rise at the superficial gas velocity in the freeboard. Size distribution of entrained solid particles at any height in the freeboard is calculated by assuming that probability of finding particles of size *r* at any height is proportional to their presence in bed with proportionality constant being K_{ih}^*:

$$F_z P_z(r) = K_{ih}^* A_{bed} P_{bed}(r) \tag{3.65}$$

Multiplying both sides of Equation (3.65) by *dr* and integrating yields the flow rate of entrained particles and their size distribution as follows:

$$F_z = A_{bed} \int_{r_{\min}}^{r_{\max}} K_{ih}^* P_{bed}(r) dr \tag{3.66}$$

$$P_z(r) = A_{bed} K_{ih}^* P_{bed}(r) / F_z \tag{3.67}$$

3.2.2 Mass and Energy Balance Equations

It is assumed that the gases in the bubble and emulsion phases mix instantaneously at the top of the bed and enter freeboard. The gas flow in freeboard is assumed to be in plug flow. A shell mass balance for j^{th} gas component in the freeboard results in the following equation:

$$\frac{dn_{j,f}}{dz} = A_f (1 - \varepsilon_s) \Re_{j,f} \tag{3.68}$$

Boundary condition for Equation (3.68) is expressed as:

$$\text{at } z_f = 0 \qquad n_{j,f} = n_{j,e} + n_{j,b} \tag{3.69}$$

The expression for species generation/depletion term, $\Re_{j,f}$, appearing in Equation (3.68) takes the following forms for the species considered,

j=1 (O_2)

$$\Re_{1,f} = -\frac{m_{vm}(1-x_{vl})}{V_f(1-\varepsilon_s)}\left\{0.5\frac{x_{C,vm}}{M_C} + 0.5\frac{x_{H,vm}}{M_{H_2}} + \frac{x_{S,vm}}{M_S} - \frac{x_{O,vm}}{M_{O_2}}\right\} - \frac{0.5r_{SO_2,f}}{V_f(1-\varepsilon_s)} - 0.5n_{C,f} - 0.5r_{CO,f} - \frac{5}{4}\left(r_{N,hom}\right)_{R10} \tag{3.70}$$

j=2 (CO)

$$\Re_{2,f} = \frac{m_{vm}(1-x_{vl})}{V_f(1-\varepsilon_s)}\left\{0.5\frac{x_{C,vm}}{M_C}\right\} + n_{C,f} - r_{CO,f} \tag{3.71}$$

j=3 (CO_2)

$$\Re_{3,f} = r_{CO,f} \tag{3.72}$$

j=4 (H_2O)

$$\Re_{4,f} = \frac{1}{V_f(1-\varepsilon_s)}\left\{\frac{m_{vm}(1-x_{vl})x_{H,vm}}{M_{H_2}} + \left(r_{N,hom}\right)_{R11}\right\} + \left(r_{N,hom}\right)_{R10} \tag{3.73}$$

j=5 (SO_2)

$$\Re_{5,f} = \frac{1}{V_f(1-\varepsilon_s)}\left\{m_{vm}(1-x_{vl})\frac{x_{S,vm}}{M_S} - r_{SO_2,f}\right\} \tag{3.74}$$

j=6 (NH_3)

$$\Re_{6,f} = \frac{1}{V_f(1-\varepsilon_s)}\left\{m_{vm}(1-x_{vl})\frac{x_{N,vm}}{M_N} - \left(r_{N,hom}\right)_{R11}\right\} - \left(r_{N,hom}\right)_{R10} \tag{3.75}$$

j=7 (NO)

$$\Re_{7,f} = \left\{ \left(r_{N,hom}\right)_{R10} - \frac{1}{V_f(1-\varepsilon_s)} \left(r_{N,hom}\right)_{R11} \right\} \tag{3.76}$$

where $n_{C,f}$, the solid carbon consumption rate at any height in freeboard is the sum of carbon consumption rates for coarse and fine particles, as shown below,

$$n_{C,f} = -\frac{3\eta}{M_C} \frac{x_{fc}}{x_{fc}+x_a} \left[\rho_d \int_{r_{\max e}}^{r_{\max}} \frac{\varepsilon_{s,d} P_z(r)}{r} \Re_f(r) dr + \frac{F_{co}}{A_f} \int_{r_{\min}}^{r_{\max}} \frac{P_{co}(r)}{r \;\; u_p(r)} \Re_f(r) dr \right] \tag{3.77}$$

η in Equation (3.77) represents the contact efficiency between gas and solids in freeboard and it is calculated from the following equation proposed by Kunii and Levenspiel [79],

$$\eta = 1 - (1-\eta_0)\exp(-6.62\, z_f) \tag{3.78}$$

where,

$$\eta_0 = \frac{u_e}{u_0}(1-\delta) \tag{3.79}$$

The gas temperature profile in freeboard is obtained by solving an energy balance which considers convective transport and, generation and loss of energy:

$$\frac{dT_f}{dz} = \frac{A_f(1-\varepsilon_s)}{n_f c_{p,g}} \boldsymbol{R} \tag{3.80}$$

Equation (3.80) has the following boundary condition:

$$\text{at } z = 0 \qquad T_f = T_{bed} \tag{3.81}$$

$\boldsymbol{R}$ is the combined energy generation and loss rate per unit volume of freeboard. It is the sum of energy generated by chemical reactions, $\boldsymbol{R_{rxn}}$, energy loss from freeboard walls, $\boldsymbol{R_{fw}}$, and energy transferred from/to char and ash particles present in the freeboard, $\boldsymbol{R_p}$. These terms can be expressed as follows:

$$\boldsymbol{R_{rxn}} = \frac{m_{vm}\left(1-x_{vl}\right)}{V_f\left(1-\varepsilon_s\right)}\left[\frac{x_{C,vm}}{M_C}\Delta H^0_{R2} + \frac{x_{H,vm}}{M_{H_2}}\Delta H^0_{R4} + \frac{x_{S,vm}}{M_S}\Delta H^0_{R5} + \frac{x_{N,vm}}{M_N}\Delta H^0_{R8}\right]$$
$$+\Delta H^0_{R3} r_{CO,f} + \frac{1}{V_f\left(1-\varepsilon_s\right)}\left[\Delta H^0_{R7} r_{SO_2,f} + \Delta H^0_{R11}\left(r_{N,het}\right)_{R11,f}\right]$$
$$+\Delta H^0_{R10}\left(r_{N,het}\right)_{R10,f} \tag{3.82}$$

$$\boldsymbol{R_{fw}} = -\frac{4d_{bed}}{A_{bed}\left(1-\varepsilon_s\right)} h_{fw}\left(T_f - T_{fw}\right) \tag{3.83}$$

$$\boldsymbol{R_p} = \frac{3F_{co}}{A_{bed}\rho_d}\int_{r_{\min}}^{r_{\max e}} \frac{P_{z,d}(r)}{r\,u_p(r)}\left[h_p\left(T_d - T_f\right) + \sigma\varepsilon\left(T_d^4 - T_f^4\right)\right]dr$$
$$+3\varepsilon_d \int_{r_{\max e}}^{r_{\max}} \frac{P_{z,d}(r)}{r}\left[h_p\left(T_d - T_f\right) + \sigma\varepsilon\left(T_d^4 - T_f^4\right)\right]dr$$
$$+3\varepsilon_i \int_{r_{\max e}}^{r_{\max}} \frac{P_{z,i}(r)}{r}\left[h_p\left(T_i - T_f\right) + \sigma\varepsilon\left(T_i^4 - T_f^4\right)\right]dr \tag{3.84}$$

It is assumed that in freeboard char particles temperatures are equal to their temperatures in bed as calculated by Equation (3.54) and temperatures of inert particles remain at T_{bed}. A surface energy balance is formulated to solve for the temperature of the freeboard wall,

$$h_f\left(T_f - T_{fw}\right) - \frac{\left(T_{fw} - T_{fw,o}\right)}{R_w} = 0 \tag{3.85}$$

where h_f is calculated by using the approach of Kunii and Levenspiel [62]:

$$\frac{h_f - \left(h_r + h_g\right)}{h_{zf=0} - \left(h_r + h_g\right)} = \exp\left(-a\,z_f / 2\right) \tag{3.86}$$

3.3 Solution Procedure

The input data required by the system model are the configuration of the rig and its internals, air and coal flow rates, coal analysis, all solid and gas properties, inlet temperatures of air, cooling water and feed solids and the size distribution function of feed solids deduced from sieve analysis.

Apart from these input data, application of the model necessitates empirical and semi-empirical correlations from the literature for heat and mass transfer, combustion kinetics, elutriation and entrainment rates *etc.*, listed in Tables 3.1 and 3.2. These expressions contain empirical or semi-empirical constants which may not always comply with the experimental conditions of the system to be modeled. Therefore, it is the usual practice to adjust some of these constants until a compromise is found to reproduce the measured data as accurately as possible [80]. In this study, minimum number of fitting parameters was utilized. These were pre-exponential factor for carbon monoxide oxidation, exponential decay constant for entrained particles and elutriation rate constant.

CO concentrations predicted by using the rate expression of Hottel *et al*. [70] was found an order of magnitude lower than the measurements. To match the measured *CO* concentration at the exit of the combustor, the rate constant from Hottel et al. was multiplied by 0.3 and this value was used for model validation.

With regard to entrainment, direct use of the entrainment rate expression of Choi *et al.* [61], in the model resulted in higher char hold-up and hence lower O_2 concentrations in the freeboard compared to measurements. To match the measured O_2 concentration at the exit of the freeboard, the decay constant of the entrainment rate expression of Choi *et al.* was multiplied by 5 and used in the simulations for model validation.

Direct use of elutriation rate expression of Choi *et al.* [61] in the model yielded higher carryover flow rate at the cyclone exit. To match the measured carryover

flow rates, elutriation rate constant of Choi *et al*. was multiplied by 0.02 for Run 1, 0.05 for Run 2, 0.01 for Run 3, and 0.06 for Runs 4 and 5, and 0.07 for Run 6. Fine-tuning for the carryover flow rates at the cyclone exit was the simplest approach as the carryover flow rate was only a function of elutriation.

The solution starts with making initial guesses for T_{bed}, $\bar{y}_{O_2,e}$, M_d, F_a, $T_{bw,o}$. This is followed by computation of $\overline{T}_d$ by using estimated parameters. There are five loops of iterations to be converged for M_d, F_a, $\bar{y}_{O_2,e}$, $\overline{T}_d$, T_{bed}. For each loop, a convergence criterion, ε, is set as the absolute difference between calculated and estimated values of the parameters. Figure 3.3 shows the algorithm of the steady state model code in compact form.

The predictions reported in this study were obtained with ε values of 5×10^{-3}, 5×10^{-5}, 5×10^{-5}, 5×10^{-2} and 5×10^{-1} for iterations on M_d, F_a, $\bar{y}_{O_2,e}$, $\overline{T}_d$, T_{bed}, respectively. The integration of ODEs is carried out by Backward-Differentiation Formula (BDF) method embedded in the ODE solver LSODES [81]. Solution of the non-linear algebraic equations is performed by using the subroutine ZERO. Details of the solution procedure of steady state code can be found in [75].

The total CPU time for the complete model is about 80 seconds for SET I, and 200 seconds for SET II on 550 MHz Intel Pentium III computer.

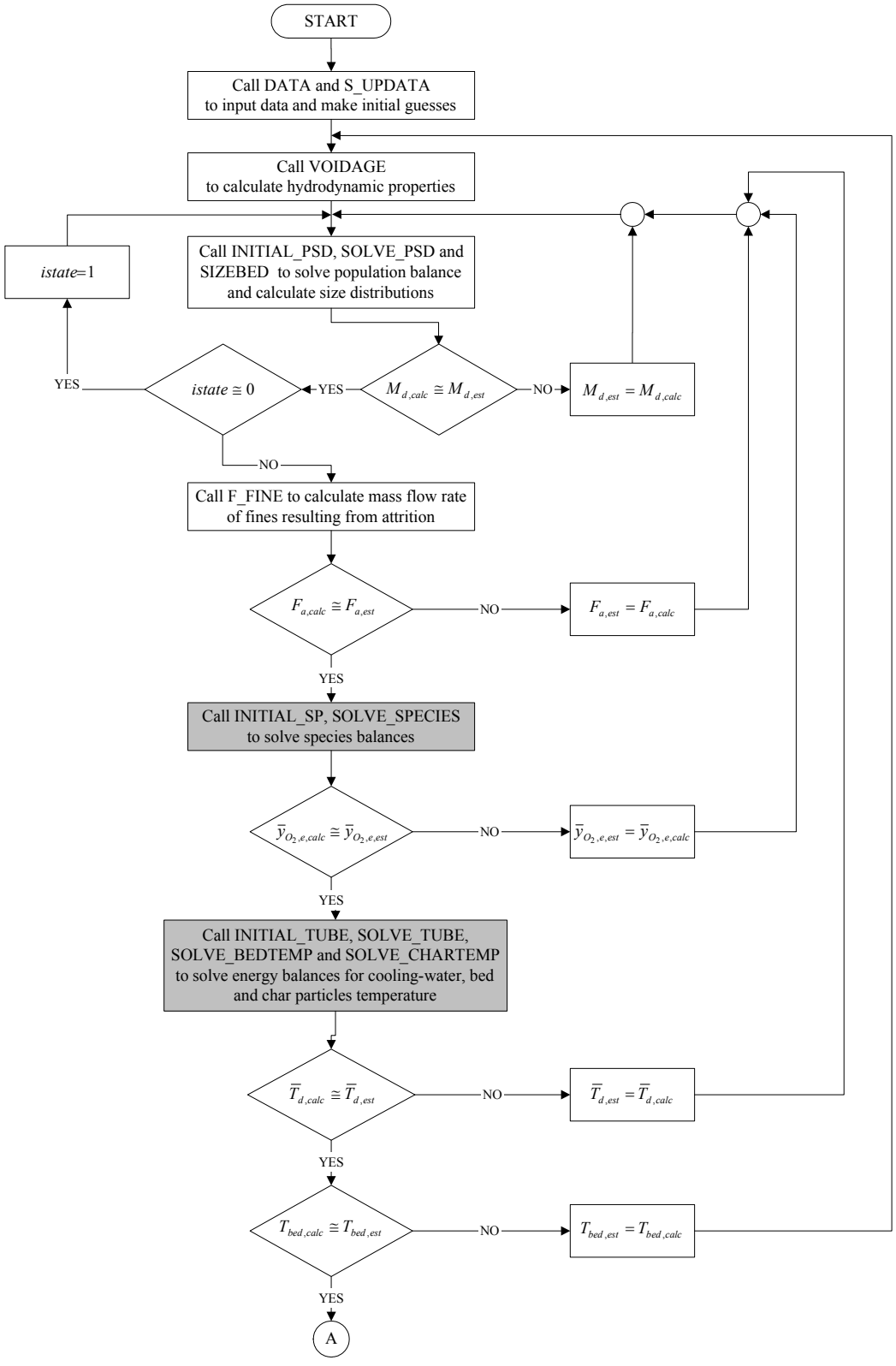

Figure 3.3 Algorithm for the steady state code (The shade area shows the modified sections this study).

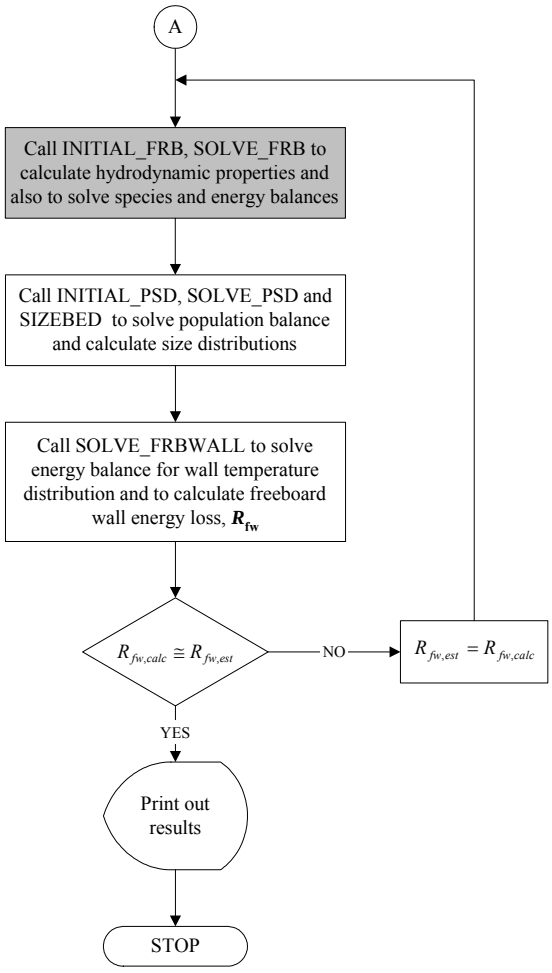

Figure 3.3 Algorithm for the steady state code (continued) (The shade area shows the modified sections this study).

CHAPTER 4

EXPERIMENTAL SET-UP AND CONDITIONS

4.1 0.3 MW_t ABFBC Test Rig

Experimental work was carried out on a 0.3 MW_t ABFBC Test Rig designed and constructed within the scope of a cooperation agreement between Middle East Technical University (METU), Babcock & Wilcox GAMA (BWG) under the auspices of Canadian Development Agency (CIDA) for the investigation of combustion and in-situ desulfurization characteristics of low quality Turkish lignites. The existing test rig was extended to incorporate a baghouse filter for capture of fine fly ash leaving with the flue gas through the stack within the scope of a recent research project, MİSAG-159, financed by The Scientific and Technical Research Council of Turkey (TÜBİTAK). The test rig in its present form is shown schematically in Figure 4.1. As can be seen from the figure, the test rig basically consists of a forced draft (FD) fan, a windbox with an ash removal system, a modular combustor, a cyclone with a recycle leg, a baghouse filter, an induced draft (ID) fan and a coal and limestone feeding system.

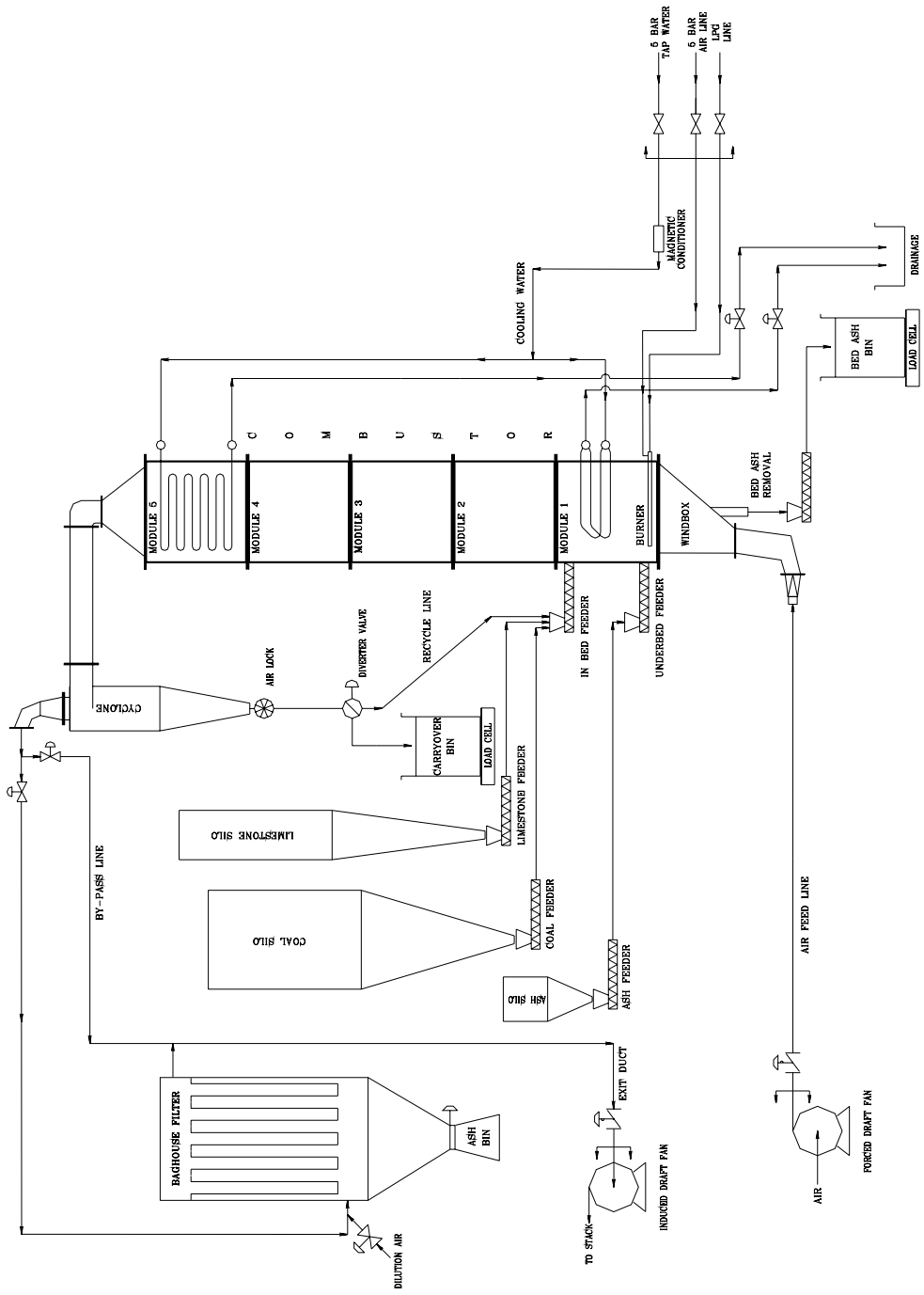

Figure 4.1 Flowsheet of 0.3 MW_t ABFBC Test Rig.

4.1.1 The Combustor

The main body of the test rig is the modular combustor formed by five modules of equal dimensions. Modular structure of the combustor is intended to provide flexibility in burning various fuels by addition or removal of heating surfaces. Each module has an internal cross-section of 0.45 × 0.45 m^2 and 1 *m* height. Inner walls of each module are refractory lined with firebricks with a thickness of 6 *cm*. Outer walls of the refractory bricks are insulated with insulation bricks with thickness of 20 *cm*. Further insulation is provided by leaving an air gap of 6 *mm* between the outer wall of insulation brick and the inner wall of the steel construction of each module.

The first and fifth modules from the bottom are referred as bed and cooler, respectively, and the ones in between are referred as freeboard modules. The bed module provides an expanded bed height of 1 *m*. It contains 6 water-cooled U-tubes (25 *mm* OD, stainless steel) for cooling purposes, 5 ports for thermocouples, 4 ports for gas sampling probes, one port for LPG distributor, one port for the ignitor and two ports for feeding coal/limestone mixture. One of the feeding ports is 22 *cm* and the other is 85 *cm* above the distributor plate. There are 6 ports for gas sampling probes and 9 ports for thermocouples in freeboard and cooler modules. There exists a water-cooled tube bundle consisting of 11 tubes (26.7 *mm* OD, carbon steel) with 14 passes installed across the cross-section of the cooler module for cooling the stack gases before leaving the combustor.

4.1.2 Air and Gas System

The fluidizing air fed by the FD fan enters the bottom of the windbox through a pipe of 6.5 *m* long and 7.8 *cm* ID on which a manual gate valve, an automatic butterfly valve and a vortex flowmeter are installed. The design of the windbox allows the installation of bed ash removal system as shown in Figure 4.1. It is a mobile windbox supported by four wheels and a distributor plate is placed on the top. Air supplied to the windbox by means of the pipe of 7.8 *cm* ID diverges to the

full cross-section of the combustor at the distributor plate located 1.4 *m* above the entrance port. Sieve type distributor plate contains 412 holes, each 4.5 *mm* in diameter, arranged in a triangular pattern. Within the bed module air mixes with lignite and limestone to affect combustion and sulfur capture.

Flue gases and elutriated fines leaving the bed surface enter the freeboard. Sufficient freeboard height is provided to permit burnout of elutriated lignite fines and combustible gases.

After leaving the freeboard, flue gases pass through the cooler module to cool the hot combustion gases. Flue gases leaving the modular combustor enter the cyclone and then the baghouse filter to leave the elutriated particles before passing through ID fan to exit from the stack. As the temperature of the flue gases entering the baghouse filter is limited by the maximum operating temperature of the bag material which is 260 °*C* for the bag material (P84-Polyimide) selected for the baghouse filter under consideration, two alternative systems were provided for the safe operation of the baghouse filter: A bypass line between the cyclone and the ID fan and an air dilution system to reduce the flue gas temperature at the inlet to the filter through a slide valve if the temperature exceeds the upper operating limit of the bag material.

The pipes carrying the flue gases before and after the baghouse filter are 14.0 and 5.3 *m* long, respectively, and have an ID of 15.3 *cm*. The pipeline between the cyclone and the ID fan of the existing test rig before the incorporation of baghouse filter was used as the bypass line. It has an ID of 12.8 *cm* and length of 14.5 *m*. The outlet of the baghouse filter joins this pipeline 4.2 *m* before the ID fan.

An orifice meter with a bore diameter of 8.05 *cm* was installed at the stack gas line before ID fan to measure the flow rate of the flue gases. The pressure drop across the orificemeter is measured by means of pressure transmitter. Knowing the temperature and pressure of the flue gases passing through the orificemeter, the

signal from the transmitter is interpreted in the control system to yield molar flow rate.

4.1.3 Solids Handling System

Crushed and sieved lignite and limestone are stored in two separate silos and conveyed into the hoppers of feeders at controlled flow rates via precalibrated volumetric feeders placed under their respective silos. The lignite/limestone mixture is continuously fed to the bed through water-cooled screw feeders. Both screw feeders are operated at controlled speed in such a way as to maintain certain amount of accumulated material in the hopper in order to prevent backflow of combustion gases from the combustor.

Bed ash is withdrawn from the bed through 5 *cm* diameter, 1.1 *m* long water-cooled ash removal pipe. Some of the bed ash is disposed and the rest is stored to provide bed inventory when required. Bed ash drain rate is adjusted from the computer to obtain the desired bed pressure drop and hence the expanded bed height. Bed ash particles are collected in a continuously weighted ash storage bin.

The majority of the elutriable fines produced from solid in the bed and those fed within the solid streams are captured by the cyclone, having dimensions of 45 *cm* OD and 2.12 *m* height. Cyclone catch particles pass through an air lock (i.e. a rotary valve) and fall onto a diverter. Depending on the position of the diverter, particles are either discharged from the system to a continuously weighted ash storage bin for experiments without recycle or flow back to the combustor for refiring. The fraction of a short time interval over which the position of the diverter remains on the recycle mode determines the recycle ratio. Continuity of flow is provided by repeating this time interval periodically. In order to provide a wider range of recycle ratio and yet not to disturb the steady state conditions within the combustor, a periodic time interval of 10 *s* was selected.

In order to catch fine particles of fly ash ($d_p \leq 40\ \mu m$) leaving the cyclone, a *pulse-jet* type baghouse filter with a 100 % collection efficiency for particles greater than 1 μm was utilized. As mentioned in the previous section, the bag material used is P84-Polyimide and it can resist temperatures up to 260 °*C*. Hence, if the inlet temperature of the flue gases exceeds 220 °*C* dilution or bypass of flue gases is employed.

Before putting the baghouse filter into service, a permanent *pre-coat* is formed on the outer surface of the bags in order to increase the collection efficiency solely provided by the porosity of the bag material itself. This is accomplished by passing the fine *CaO* particles through the filter. During the service, an additional filter cake is built up at the outer surface of the bags which in turn becomes a principal collection medium. As the filter cake gets thicker with time, a pulse of compressed air is directed into the bag from the open top, which causes a shock wave to travel down its length dislodging the filter cake from the outer surface of the bag. A unique aspect of the pulse jet system is the use of a wire cage in each bag to keep it from collapsing during normal filtration. The bag hangs from the tube sheet. A series of parallel pulse jet pipes are located above the bags with each pipe row having a solenoid valve. This allows the bags to be pulsed clean one row of five bags at a time. Filter cake cleaned off the surface fall into a hopper and is discharged to fly ash collecting container. There are two containers each having a volume of 0.13 m^3. During filtration of flue gases if one container gets full, the maximum level device gives alarm by lighting the level warning light located on control panel, and the container full of ash is replaced with the other one after closing the ash discharge opening by leak proof slide valve.

4.1.4 Cooling Water System

Cooling water required for the test rig is passed through a magnetic conditioner and is then divided into two streams, one for the in-bed tube bundles, the other for the tube bundle in the cooler module. Heat transfer areas provided by the bed and cooler modules are 0.30 m^2 and 4.3 m^2, respectively. The cooling water in bed

enters lower header and leaves the bed through the upper header. The cooling water for the cooler module enters the upper header and flows downward to provide counter-current flow to the up flowing flue gases. Water flow rates are adjusted by means of either a manual or a pneumatic control valve located at the drain of each stream to maintain maximum exit temperature of about 60 $°C$.

4.1.5 Gas Sampling System

Benefits of using advanced analytical instrumentation are negated unless a representative sample from the point of extraction can be obtained. Areas of concern in continuous gas sampling pointed out in detail by Anthony *et al*. [82] can be summarized as follows:

1. A sample must be subjected to minimum thermal chemical or fluid-mechanical disturbances by the sampling system. It is necessary to quench gas phase reactions at the point of sampling particularly when analyzing for minor constituents such as NO_x and CO.
2. The sample must be conditioned and transported to the analyzers without changing the concentration ratios of components to be measured. Conditioning is essential as the analyzers are designed to operate at near ambient temperatures and pressures and with dry, particulate free, non-corrosive, non-interfering samples. Therefore, particular care must be taken in gas sample cleanup to remove the particulates that are characteristic of Atmospheric Fluidized Bed Combustors (AFBC) and to remove the excess moisture that might otherwise condense in the sampling lines or analyzer banks.

   Another problem is that gaseous species may be partly lost along the transport line because of homogeneous or catalytic reactions or simply by absorption of gas phase species such as SO_2 in the condensate is another possible source of error, while subsequent desorption can lead to erroneously high values when sampling lower concentrations.
3. In order to accurately measure the species of interest the analyzers must also be properly calibrated and maintained.

4. The sample extraction system must be durable because of the high-temperature, corrosive atmosphere present in the combustor.

Once through the probe, the sampled combustion gas is passed through a solenoid valve and sent to the gas conditioning and analysis system of the test rig by means of sample line. The sample line itself is maintained at 150 °*C* by means of a variable DC power supply so that no water, sulfuric acid or hydrocarbons would condense along the sampling interface. In addition, all lines and fittings in contact with the gas sample are made of teflon or stainless steel to prevent interferences due to gas adsorption or heterogeneous reactions. The existing analytical system of the test rig consists of a bank of analyzers for O_2, CO, CO_2, SO_2 and NO/NO_x. The positions of the gas sampling probes and the details of gas conditioning and analysis system are given in Table 4.1 and Figure 4.2, respectively. Gas is sampled at a rate of 13 cm^3/s at STP which is small enough to cause minimal interference to the combustion system. After passing through the probe, sample gas is transported through the heated stainless steel line to a hygroscopic, ion exchange membrane type gas drier. Once through the drier, the gas is cooled, filtered and pumped to the analyzers via a teflon-coated diaphragm-type sample pump. Then, sample gas is divided into two parallel lines; one passing through O_2, CO/CO_2 and SO_2 analyzers in series, the other through NO/NO_x analyzer. After the measurement of species concentrations, sample gas is vented to the atmosphere. On-line wet analyses of O_2 and CO are also carried out at the exit of the combustor.

Table 4.1 Relative positions of gas sampling probes.

Probe No	**Distance above the distributor plate, *cm***
P10	26
P9	56
P8	69
P7	85
P6	123
P5	183
P4	291
P3	344
P2	419
P1	500

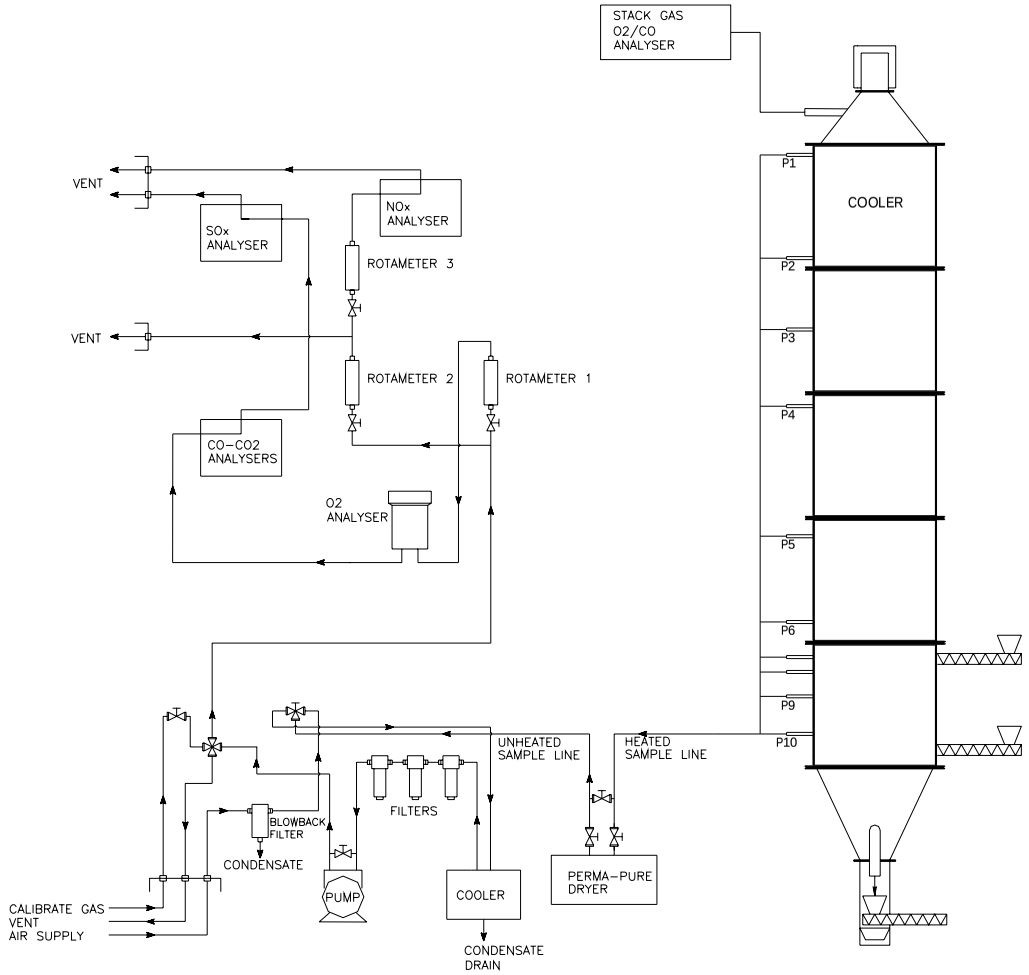

Figure 4.2 Gas conditioning and analysis system.

4.2 Instrumentation and Analytical Systems

Instrumentation and analytical systems can be divided into following categories:

- Data acquisition and control system
- Solid flow control and monitoring
- Air and gas flow control and monitoring
- Cooling-water flow control and monitoring
- On-line continuous gas analyzers
- Pressure sensors
- Temperature sensors
- Solids analyses

The test rig is equipped with a data acquisition and control system namely Bailey INFI 90. Real time process data is monitored, manipulated, collected and analyzed with the aid of a control software called Bailey LAN-90 Process Control View installed on an IBM compatible PC 486 computer running under QNX operating system. The control system scans the signals coming from all of the instruments attached to it in a fraction of a second and reports and logs their averages discretely for 30 seconds of intervals. An uninterruptible power supply is connected to Bailey INFI 90 and PC in order to enable proper shut-down in case of a electricity cut-off by preventing corruption of data logged.

Fuel and sorbent feed rates are controlled manually by adjusting the fuel feeder or sorbent feeder control dial from the computer. The flow rates of fuel and sorbent are normally set to such values that provide desired excess air and *Ca/S* molar ratio, respectively. Bed ash drain rate can also be adjusted from the computer to obtain the desired bed pressure drop and hence the expanded bed height. The interface between the controller and driving motors of fuel and sorbent feeders and bed ash drain are provided with three speed transmitters. Cyclone ash and bed ash are collected in respective bins and their flow rates are followed by load cells placed under respective bins.

The volumetric flow rate of air is measured by a vortex flow meter and adjusted with an automatic butterfly valve driven by a computer controlled pneumatic actuator. In order to achieve conversion from volumetric to molar flow, a static pressure tap and a temperature sensor is placed downstream of the vortex flow meter. The flow rate of air is normally set to a value to achieve the desired superficial velocity in the combustor. In order to achieve almost neutral pressure on the bed surface, the flow rate of exhaust gases is adjusted with an automatic butterfly valve driven by a computer controlled pneumatic actuator.

In order to measure flow rates of cooling-water flowing through bed and cooler bundles, two orifices are located up streams of their lower and upper headers, respectively. The pressure drops across the orificemeters are measured by means of pressure transmitters. The signals from the transmitters are interpreted in the control system to yield mass flow rate of the cooling-water flowing through in-bed and cooler bundles. There exist two pneumatic control valves installed on the downstream of upper and lower headers of bed and cooler bundles, respectively, to adjust the cooling-water flow in each bundle. The flow rates of cooling-water in bed and cooler bundles are normally set to a value which provide exit water temperature in the range 40-60 $^{\circ}C$.

The on-line continuous gas analyzers with which the test rig is equipped are listed in Table 4.2. Analyzers except Bailey SMA 90 are used for measuring spatial variation of species O_2, CO, CO_2, NO/NO_x and SO_2 along the combustor at the positions given in Table 4.1 on dry basis. Bailey SMA 90 uses close-coupled sampling system which does not remove water vapor from the sample. The analyzer reports CO equivalent indicating mostly CO, but also responds to other combustibles present in the flue gas. It is used for measuring temporal variation of O_2 and CO at the combustor exit.

Table 4.2 On-line gas analyzers.

Instrument	Gas species	Sensor type	Range
Leeds & Northrup	O_2	Paramagnetic	0-15 %
Anarad AR 600	CO	IR	0-5 %
	CO_2	IR	0-20 %
Siemens Ultramat 6	SO_2	NDIR	0-1 %
Servomex 1491	NO/NOx	Chemiluminescence	0-0.2 %
Bailey SMA 90	O_2	Zirconium oxide	0-25 %
	CO	Catalytic RTD	0-2 %

Pressure sensors are used for measuring differential and gauge pressures at various positions on the test rig. Measured differential pressures are the pressure drops over orificemeters, bed and distributor plate pressure drop, and gauge pressures are the pressure at the bed surface and pressure of air feed at the downstream of the vortex flow meter.

Spatial and temporal variations of gas temperatures along the height of the combustor are measured by means of thermocouples of K type (Chromel-Alumel) with grounded junction to minimize their response time. The tips of the thermocouples are on the symmetry axis of the combustor. The axial positions of thermocouples are given in Table 4.3. The temperature of air feed at the downstream of vortex flow meter and temperatures of cooling water at the exits of bed and cooler bundles are measured by resistance thermocouples of type Pt-100. Further details of the test rig and operating procedures such as procedures before cold start-up, during runs, after shut down can be found elsewhere [57].

Table 4.3 Relative positions of thermocouples.

Thermocouple No	Distance above the distributor plate, *cm*
TC1	25
TC2	44
TC3	73
TC4	73
TC5	97
TC6	133
TC7	154
TC8	226
TC9	257
TC10	285
TC11	330
TC12	361
TC13	425
TC14	500

4.3 Experimental Conditions

4.3.1 Coal and Sorbent Characteristics

Experiments were carried out with Beypazarı lignite. Beypazarı lignite supplied by Turkish Coal Enterprises (TKİ) was delivered from Çayırhan lignite mine to Çayırhan Power Station of Turkish Electricity Generation and Transmission Co. (TEAŞ) where the coal to be burned in the test rig was prepared by crushing and sieving it through –4/+1.5 mm screens twice. Crushed and sieved lignite was then transported to the laboratory in closed barrels. Representative samples from coals were then subjected to sieve analyses and proximate and ultimate analyses. The results of these analyses together with the calorific values and particle densities

determined by mercury porosimetry are summarized in Table 4.4 and Table 4.5. As can be seen from these tables, Beypazari lignite is a fuel with high VM/FC ratio (~2), high ash content (~42 %) and high total sulfur content (~4.7 %). Ash constituents of lignites are shown in Table 4.6. Very low calcium content of Beypazarı lignite ash is uncommon to the same lignite investigated previously [83].

Table 4.4 Characteristics of Beypazarı lignite used in SET I.

Sieve Analysis		**Proximate Analysis (as received)**		**Ultimate Analysis (dry)**	
Size (*mm*)	**Weight (%)**	**Component**	**Weight (%)**	**Component**	**Weight (%)**
4.000-3.350	11.5	Moisture	13.7	C	38.1
3.350-2.360	20.2	Ash	36.4	H	3.2
2.360-2.000	17.7	VM	32.7	O	12.4
2.000-1.700	16.8	FC	17.2	N	1.4
1.700-1.180	15.7	HHV: 3154 *cal/g*		S_{comb}	2.7
1.180-0.710	12.2	d_{32}: 1.26 *mm*		S_{total}	4.5
0.710-0.000	5.9	ρ_p: 1.58 g/cm^3		Ash	42.2

Table 4.5 Characteristics of Beypazarı lignite used in SET II.

Sieve Analysis		**Proximate Analysis (as received)**		**Ultimate Analysis (dry)**	
Size (*mm*)	**Weight (%)**	**Component**	**Weight (%)**	**Component**	**Weight (%)**
4.000-3.350	13.6	Moisture	14.3	C	37.2
3.350-2.360	18.5	Ash	35.2	H	2.9
2.360-2.000	15.3	VM	31.5	O	14.9
2.000-1.700	13.8	FC	19.0	N	1.3
1.700-1.180	12.0	HHV: 3030 *cal/g*		S_{comb}	2.9
1.180-0.710	13.8	d_{32}: 0.86 *mm*		S_{total}	4.8
0.710-0.000	12.0	ρ_p: 1.58 g/cm^3		Ash	41.1

Table 4.6 Ash analyses of the lignite.

Component	Weight (%)	
	SET I	SET II
SiO_2	45.0	39.2
Al_2O_3	15.9	11.3
Fe_2O_3	7.7	8.0
CaO	1.0	0.4
MgO	3.0	0.8
SO_3	16.2	12.3
Na_2O	8.0	5.1
K_2O	1.5	1.3
TiO_2	1.8	0.9

Limestone utilized in the firing tests was supplied by Park Thermic, Electric Industry and Trade, Inc. and originates from Acıbaşı limestone quarry, 10 *km* away from the Çayırhan Thermal Power Plant. Limestone delivered to the laboratory had a particle size below 6 *cm*. It was subjected to size reduction by crushing it in a jaw-crusher and a hammer mill consecutively. Crushed limestone was sieved through a 1.18 *mm* sieve and top product was crushed again by hammer mill. Particles under the sieve were utilized in the experiments. A representative sample from limestone was subjected to sieve and chemical analyses and the results are summarized in Table 4.7.

Table 4.7 Characteristics of Beypazarı limestone.

Size Distribution		**Chemical Analysis (dry)**	
Size (*mm*)	**Weight (*%*)**	**Component**	**Weight (*%*)**
1.180-1.000	11.2	$CaCO_3$	94.7
1.000-0.850	14.5	$MgCO_3$	0.7
0.850-0.710	5.8	SiO_2	4.8
0.710-0.600	6.0	Na_2O	0.1
0.600-0.500	6.5	K_2O	0.1
0.500-0.425	9.3	Al_2O_3	0.7
0.425-0.300	13.8	Fe_2O_3	0.5
0.300-0.250	19.8	LOI	40.8
0.250-0.150	6.9	d_{32} : 0.32 *mm*	
0.150-0.000	6.2	ρ_p: 2.40 g/cm^3	

4.3.2 Operating Conditions

Two sets of experiments; one without (SET I), the other with limestone addition (SET II) were carried out with fines recycle. In all the runs, the lignite was burned in its own ash due to its high ash content and without air staging. Moreover, it was necessary to burn this lignite with a sorbent addition due to its high combustible sulfur content. Table 4.8 lists the operating conditions for all experiments. Experiments without limestone addition (SET I) consist of 3 runs carried out at recycle ratios of 0.0, 0.56 and 2.37 for Runs 1, 2 and 3, respectively. Experiments with limestone addition (SET II) are also comprised of 3 runs at *Ca*/*S* molar ratios of 3.0, 3.1 and 4.0 for Runs 4, 5 and 6, respectively. Run 4 was performed without recycle whereas Runs 5 and 6 were carried out at a recycle ratios of 0.86 and 0.84, respectively. In the first set of experiments parameters other than recycle ratio were tried to be maintained constant while in the second set of experiments parameters other than *Ca*/*S* molar ratio were kept constant. Feed point location was 0.85 *m* above the distributor plate for all experiments.

Table 4.8 Operating conditions of the experiments.

	SET I			SET II		
	Run 1	**Run 2**	**Run 3**	**Run 4**	**Run 5**	**Run 6**
Coal flow rate, *kg/h*	101	101	101	102	102	102
Limestone flow rate, *kg/h*	-	-	-	25	26	33
Ca/S molar ratio	-	-	-	3.0	3.1	4.0
Bed drain flow rate, *kg/h*	7	8	11	13	14	12
Cyclone ash flow rate, *kg/h*	24	24	27	34	38	37
Baghouse filter ash flow rate, *kg/h*	1.1	1.9	3.4	1.0	2.1	6.2
Recycle ratio*	0.0	0.56	2.37	0.0	0.86	0.84
Air flow rate, *kmol/h*	22	21	21	19	19	19
Excess air, *%*	43	36	36	30	29	29
Superficial velocity, *m/s*	3.0	2.9	2.8	2.5	2.5	2.4
Average bed temperature, *°C*	875	883	846	853	830	820
Average freeboard temperature, *°C*	847	928	905	839	854	824
Bed height, *m*	0.91	0.91	0.91	0.67	0.67	0.67
Feed point location, *m*	0.85	0.85	0.85	0.85	0.85	0.85
OHTC in the bed, W/m^2-*°C*	258	239	230	255	271	268
OHTC in the freeboard, W/m^2-*°C*	41	47	52	36	40	40
Bed cooling water flowrate, *kg/h*	1867	1810	1839	1772	1784	1806
Freeboard cooling water flowrate, *kg/h*	2214	4208	4298	2307	4774	4829

* Recycle ratio = (Recycle flow rate)/(Coal flow rate)

CHAPTER 5

RESULTS AND DISCUSSION

The assessment of the accuracy of the present system model in conjunction with *NO* formation and reduction model developed in this study was carried out by predicting the behavior of the lignite-fired 0.3 MW ABFBC test rig for the lignite characteristics and operating conditions shown in Tables 4.4, 4.5, and 4.8 and comparing the predictions with measurements. Axial temperature profiles, concentration profiles of O_2, CO, CO_2 and NO throughout the combustor, gaseous emissions and sulfur retention efficiencies were used as measures of performance to test the validity of the model. Validation of the model predictions with respect to SO_2 concentration measurements was already reported by Altindag et al [17].

The input data required by the model includes the following:

- Configuration and dimensions of the test rig and its internals.
- Air and coal flow rates.
- Coal and limestone analyses.
- All solid and gas properties.
- Coal partitioning into char and volatile nitrogen
- Size distribution function of feed solids deduced from sieve analysis.
- Inlet temperatures of air, cooling water, and feed solids.

The following sections describe the comparison between measured and predicted temperature and concentration profiles, and a model sensitivity analysis on the parameters related to *NO* formation and reduction.

5.1 Temperature Profiles

Figures 5.1-5.6 illustrate comparison between the predicted and measured temperatures along the combustor for the experiments under consideration. Predicted profiles and the measured values are found to be in reasonable agreement except for Run 2 and 3 of SET I. Discrepancies between measured and predicted temperature profiles of Runs 2 and 3 may be considered to be due to insufficient physical representation of the freeboard by the hydrodynamical model employed owing to the presence of cooling tube bundle, which acts as an impact separator, and combustor hood, which acts a settling chamber, due to increase in gas flow cross-sectional area. The decrease in measured temperatures from SET I to SET II is considered to be due to the addition of limestone for sulfur capture withdrawing sensible energy from the system. Moreover, the fall in the gas temperature toward the exit is due to the presence of cooler in the final module.

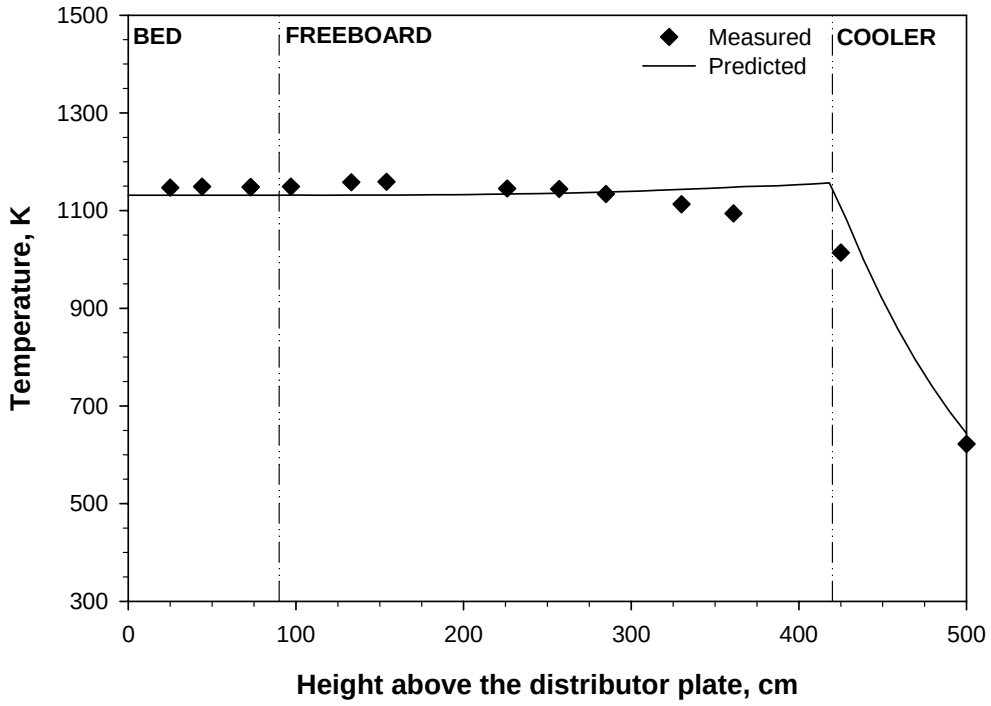

Figure 5.1 Measured and predicted temperature profiles for Run 1.

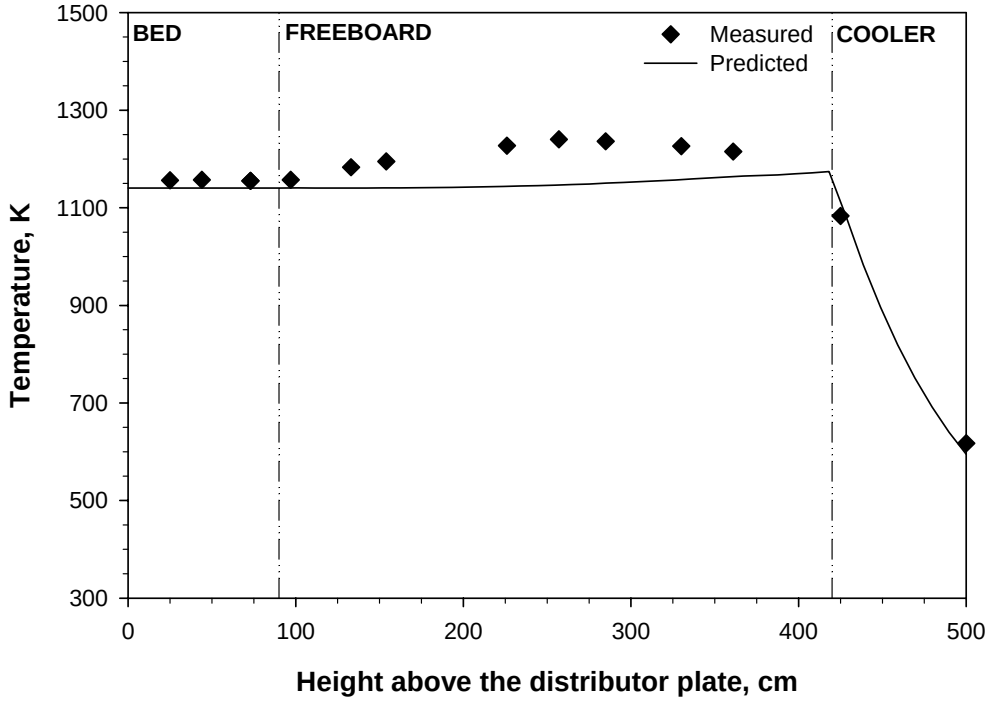

Figure 5.2 Measured and predicted temperature profiles for Run 2.

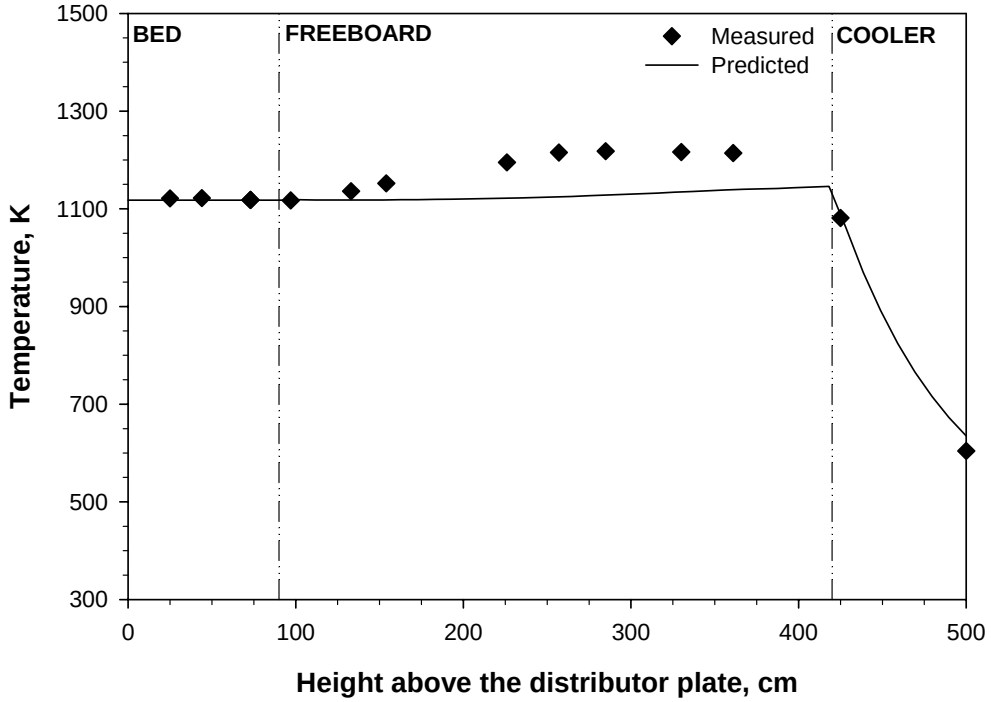

Figure 5.3 Measured and predicted temperature profiles for Run 3.

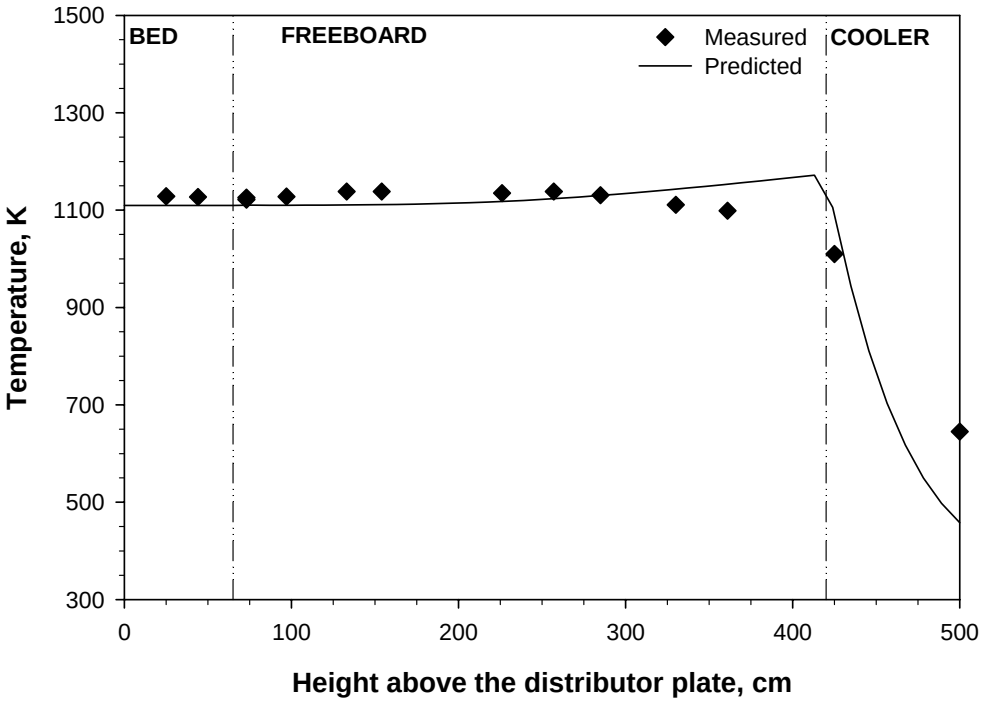

Figure 5.4 Measured and predicted temperature profiles for Run 4.

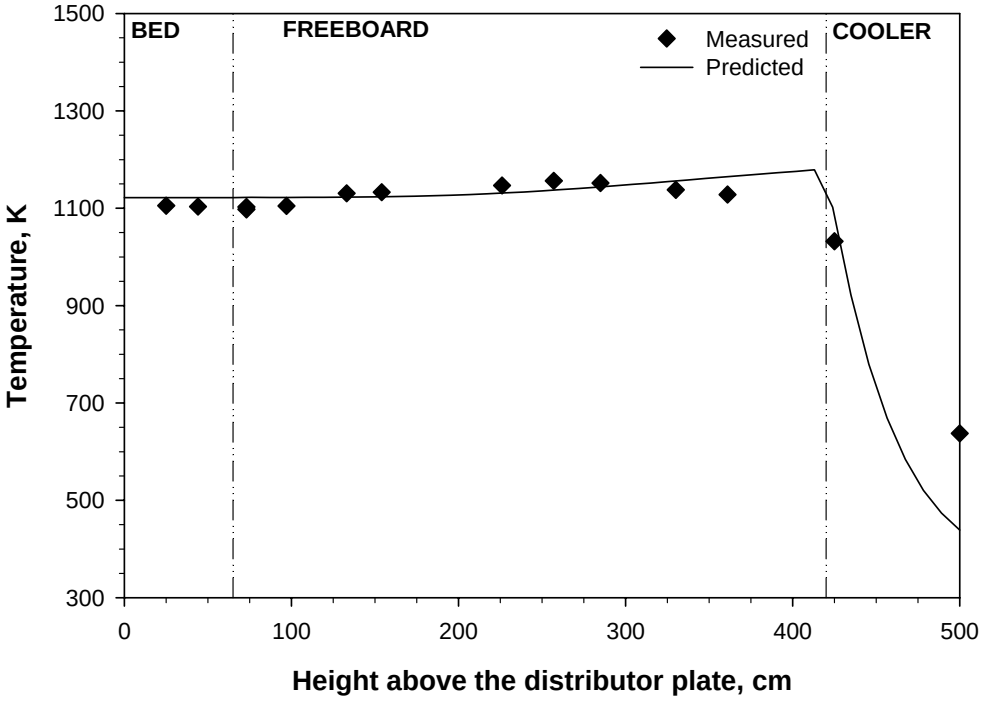

Figure 5.5 Measured and predicted temperature profiles for Run 5.

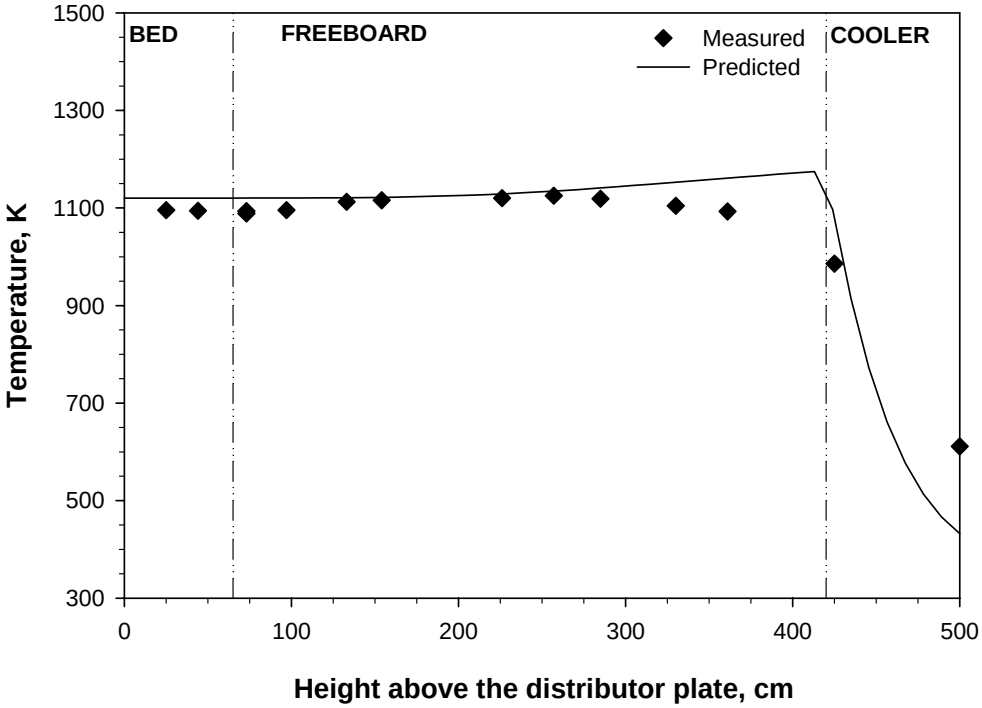

Figure 5.6 Measured and predicted temperature profiles for Run 6.

5.2 O_2, CO_2 and CO Concentration Profiles

Figures 5.7-5.12 compare the predicted and measured concentrations of O_2, CO_2 and CO along the combustor from Run 1 to Run 6. As can be seen from the figures, measured O_2 concentrations decrease until the bed surface whereas the measured CO_2 concentrations display an opposite trend in the same region. As for the freeboard section, the decrease in O_2 and increase in CO_2 concentrations keep on but with a lower slope. CO measurements, on the other hand, show maxima in the bed and decrease gradually along the freeboard with a lower slope. These profiles indicate that majority of the combustibles are burned in the bed section and that significant combustion also takes place in the freeboard. As depicted in the figures, favorable comparisons are obtained between the predicted and measured profiles.

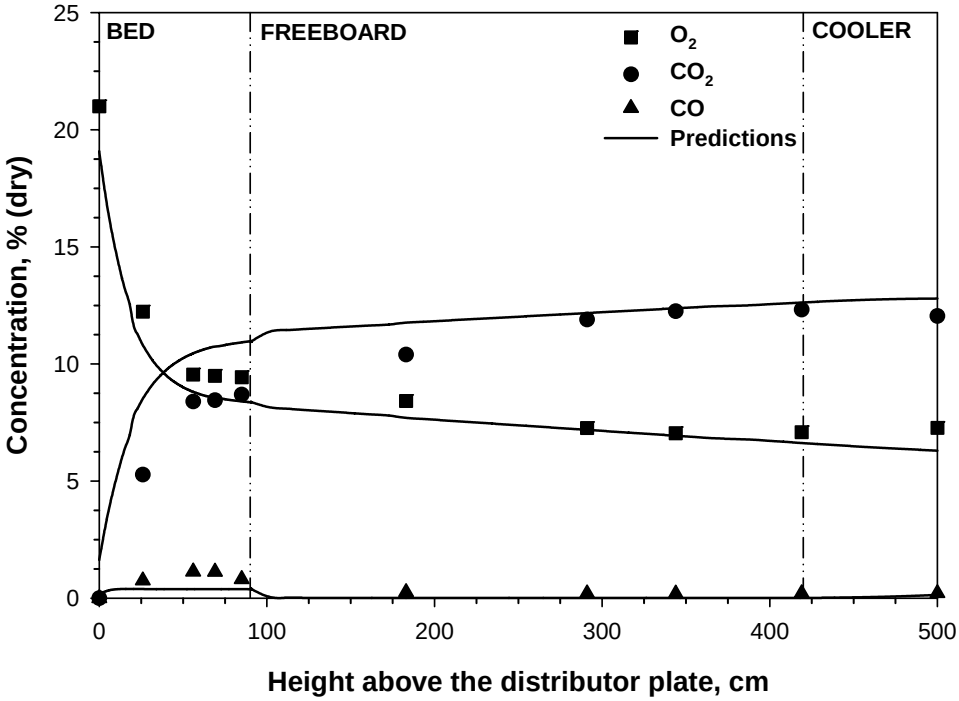

Figure 5.7 Measured and predicted O_2, CO_2, and CO concentrations for Run 1.

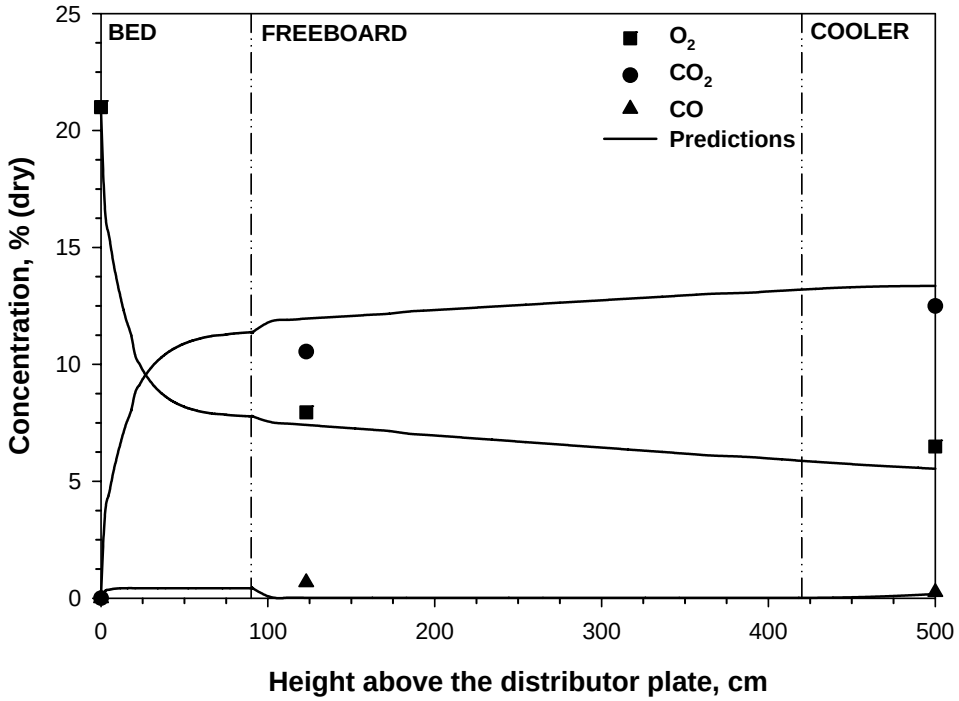

Figure 5.8 Measured and predicted O_2, CO_2, and CO concentrations Run 2.

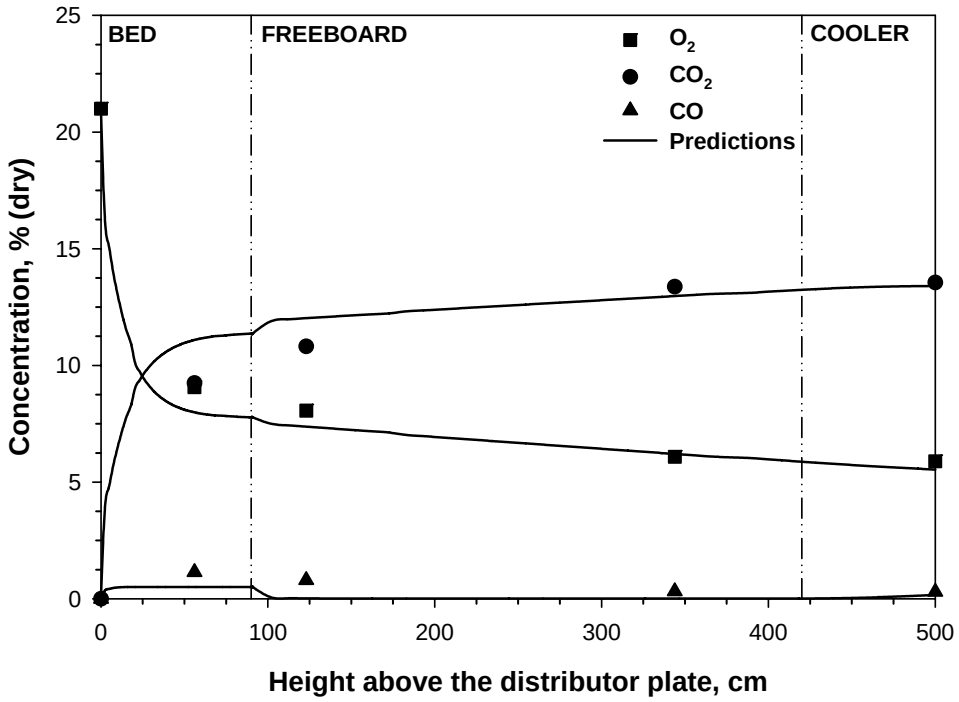

Figure 5.9 Measured and predicted O_2, CO_2, and CO concentrations Run 3.

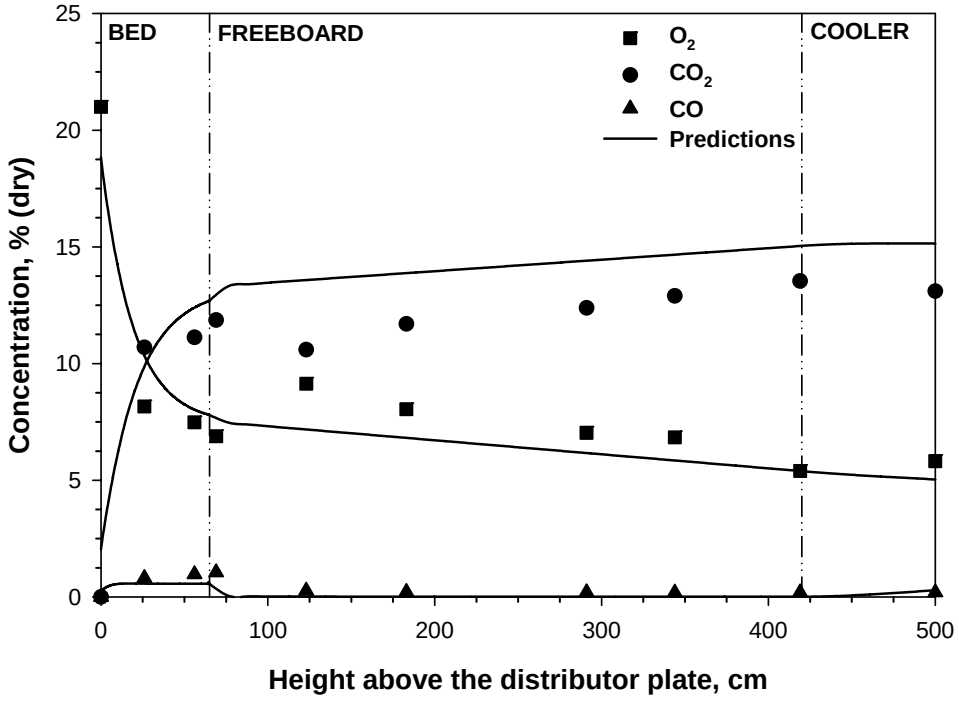

Figure 5.10 Measured and predicted O_2, CO_2, and CO concentrations Run 4.

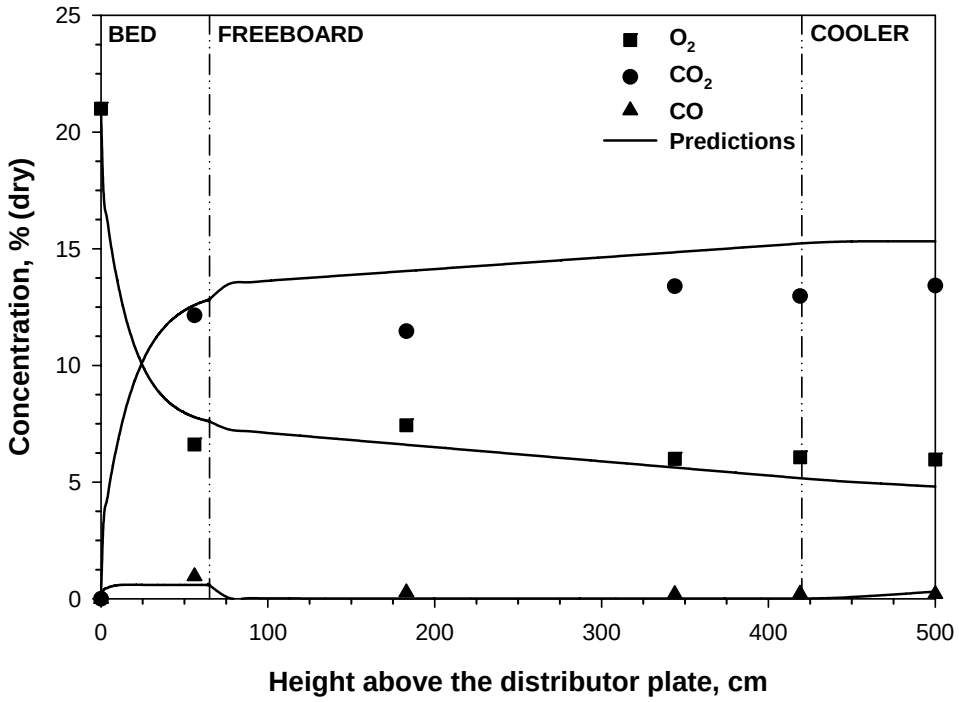

Figure 5.11 Measured and predicted O_2, CO_2, and CO concentrations Run 5.

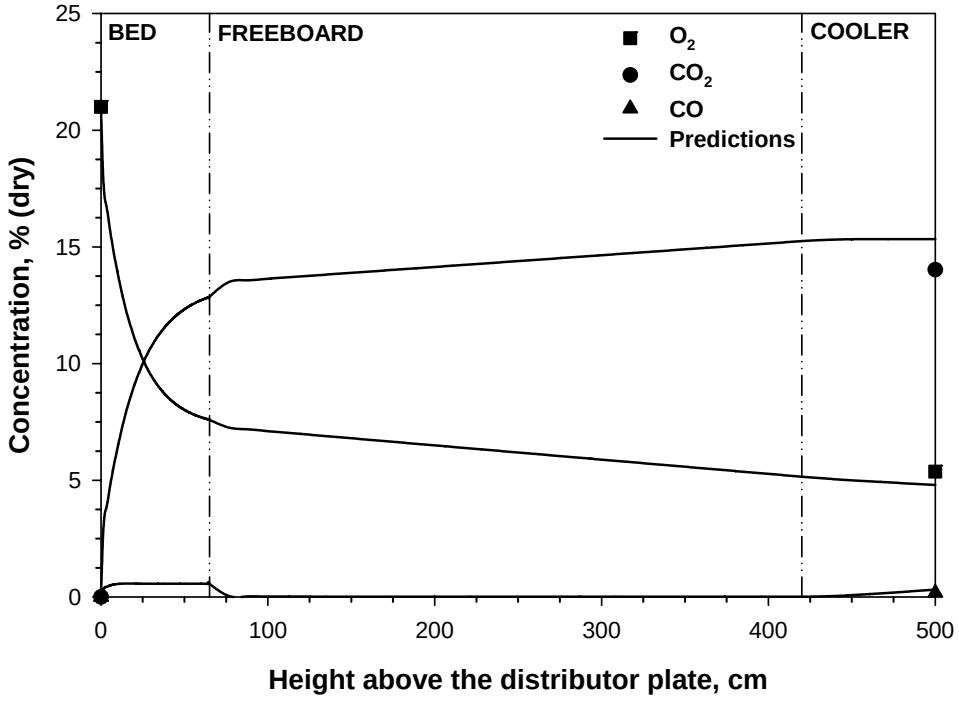

Figure 5.12 Measured and predicted O_2, CO_2, and CO concentrations Run 6.

5.3 *NO* Concentration Profiles

NO_x concentration measurements revealed that concentrations of NO_2 were negligible compared to those of *NO*. Figure 5.13-5.18 shows predicted and measured *NO* concentrations along the combustor for all runs. As can be seen from the figures, the predicted profiles follow the same trend as that of measurements, i.e. *NO* concentrations rise steeply along the bed, go through maxima and gradually decrease along the freeboard. Heterogeneous reactions gain importance in net formation of *NO* in the bed section owing to the fact that *NO* is known to form preferentially in the emulsion phase where fuel particles are devolatilized. Furthermore, *NO* reduction in the freeboard is enhanced due to high volatile matter content of the fuel [56].

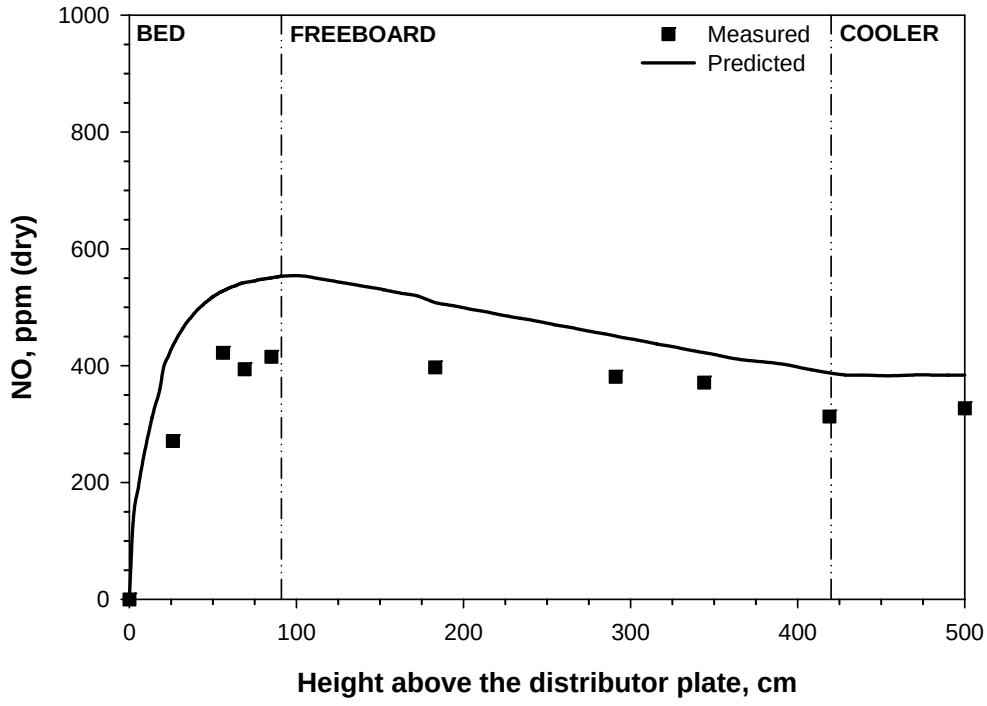

Figure 5.13 Measured and predicted *NO* concentrations for Run 1.

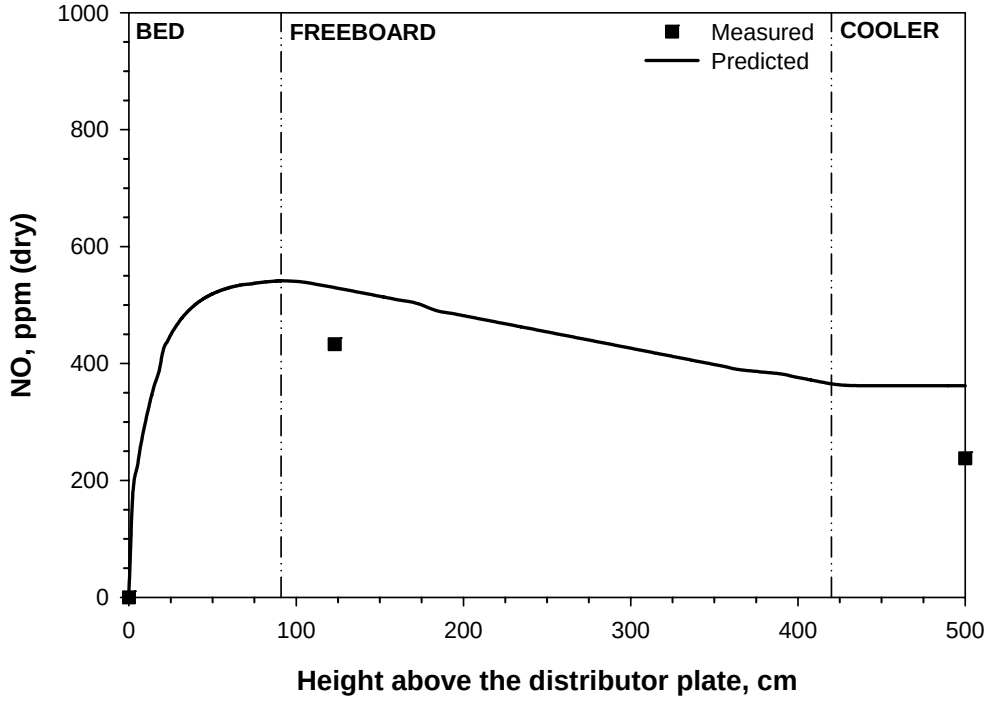

Figure 5.14 Measured and predicted *NO* concentrations for Run 2.

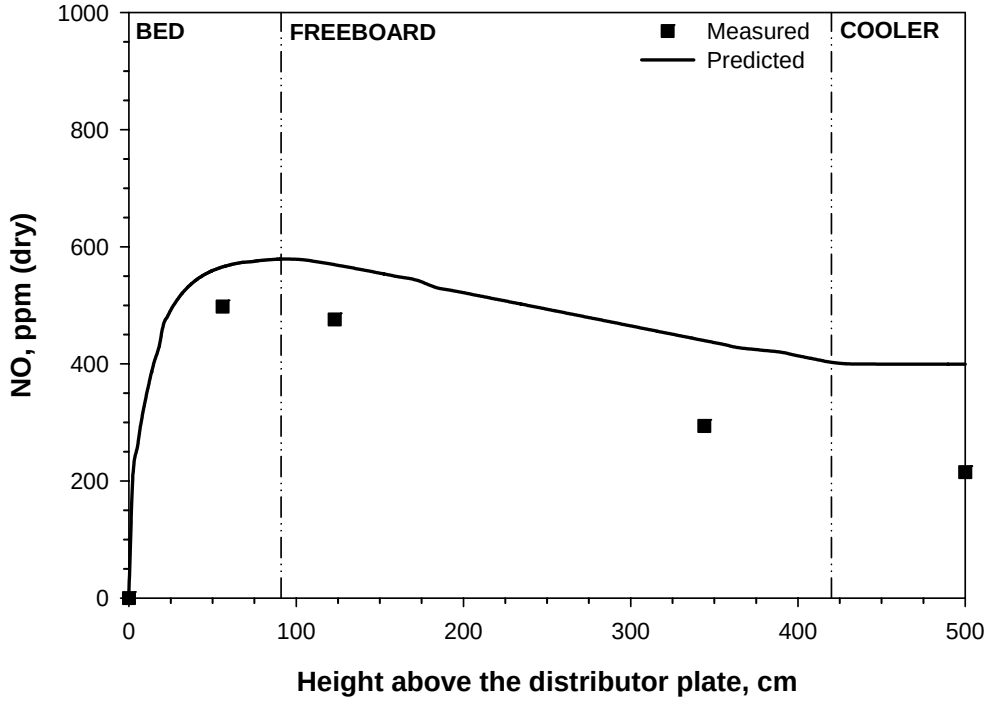

Figure 5.15 Measured and predicted *NO* concentrations for Run 3.

With regard to comparisons between measured and predicted profiles of Runs 1, 2, and 3 in Set I, agreement was found to be better in Run 1 with no recycle compared to Runs 2 and 3 with recycle. This may be attributed to the lower freeboard temperatures rather than higher char hold-up or *CO* concentration predicted by the model under recycle conditions as heterogeneous reactions are not applied to the freeboard due to very low solid hold-up. This may lead to lower *NO* reduction rates in the freeboard region.

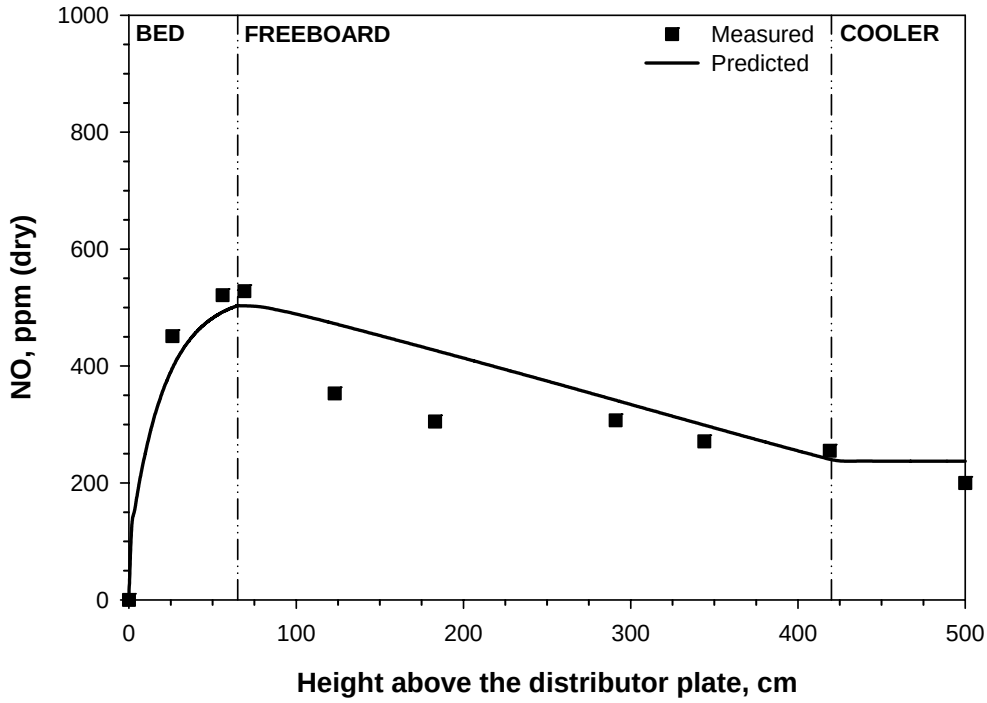

Figure 5.16 Measured and predicted *NO* concentrations for Run 4.

Regarding the experiments with limestone addition (Set II), predicted and measured *NO* concentrations were found to be in good agreement with or without recycle of fines. This may be due to better agreement between measured and predicted temperatures for this set compared to Set I. Increasing limestone addition from Run 5 to 6 was found not to affect *NO* concentration significantly, as can be seen from the comparison between Figure 5.17 and 5.18. This is in compliance with the finding of Selçuk et al. [56].

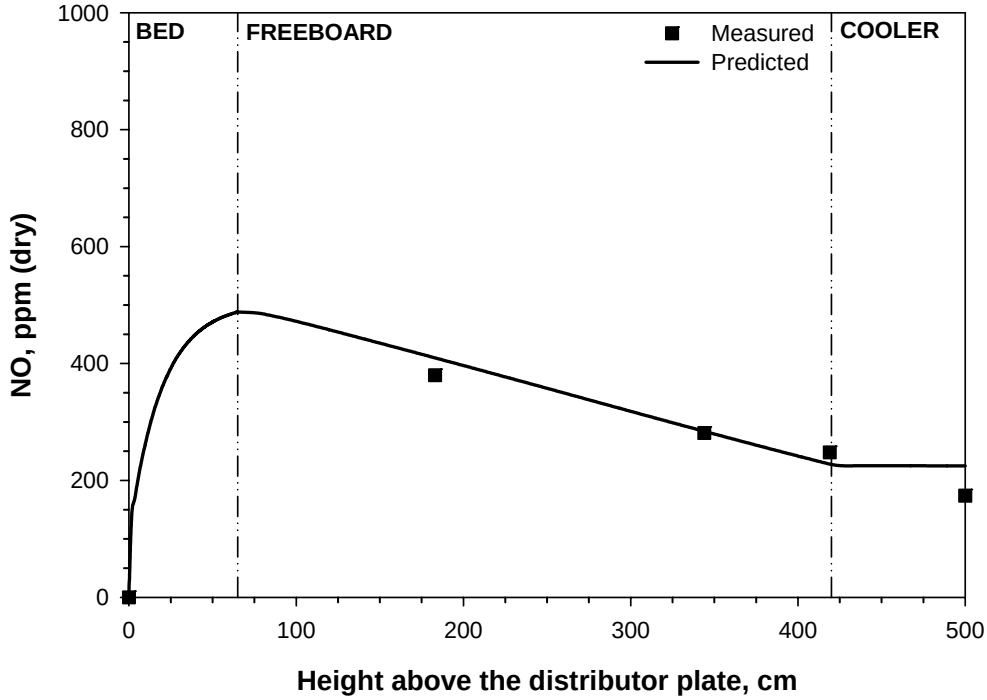

Figure 5.17 Measured and predicted *NO* concentrations for Run 5.

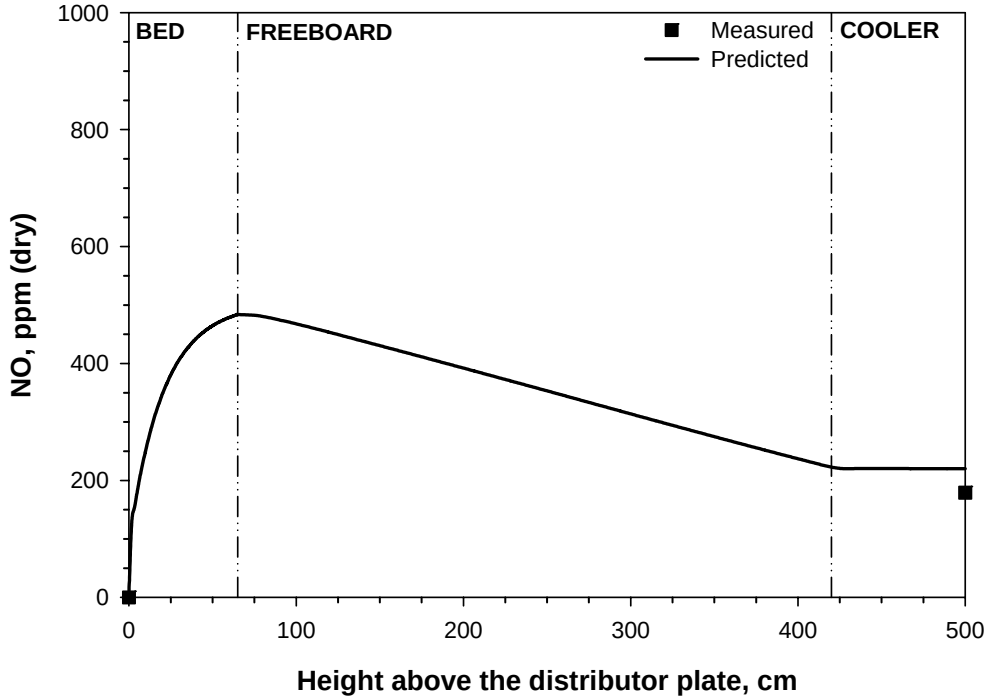

Figure 5.18 Measured and predicted *NO* concentrations for Run 6.

The influence of volatile nitrogen release along the combustor on the final *NO* emissions can be demonstrated by comparing SET I and SET II. *NO* reduction was found to increase in the freeboard for SET II compared to that in SET I due to the lower bed height which resulted in more unburned volatiles to escape to the freeboard.

The assessment of percentage contribution of reactions to net formation of *NO* in the bed section is accomplished by investigation of reaction rates. It is shown in Figure 5.19 that char nitrogen oxidation, R9, and catalytic oxidation of NH_3, R15, are the main sources of *NO*, whereas, reduction is achieved by catalytic reaction by char, R12, and by *CO* over char, R13, in the bed section. It is also illustrated in Figure 5.19 that ash catalyzed oxidation of NH_3, R15, is very important for depletion of the respective specie in the combustor especially for the cases studied, where lignite is burned in its own ash as the bed material. Homogeneous *NO* formation R10, decomposition of NH_3 over char, R16, and over ash, R17, do not produce significant rates, so these reactions are not illustrated in Figure 5.19.

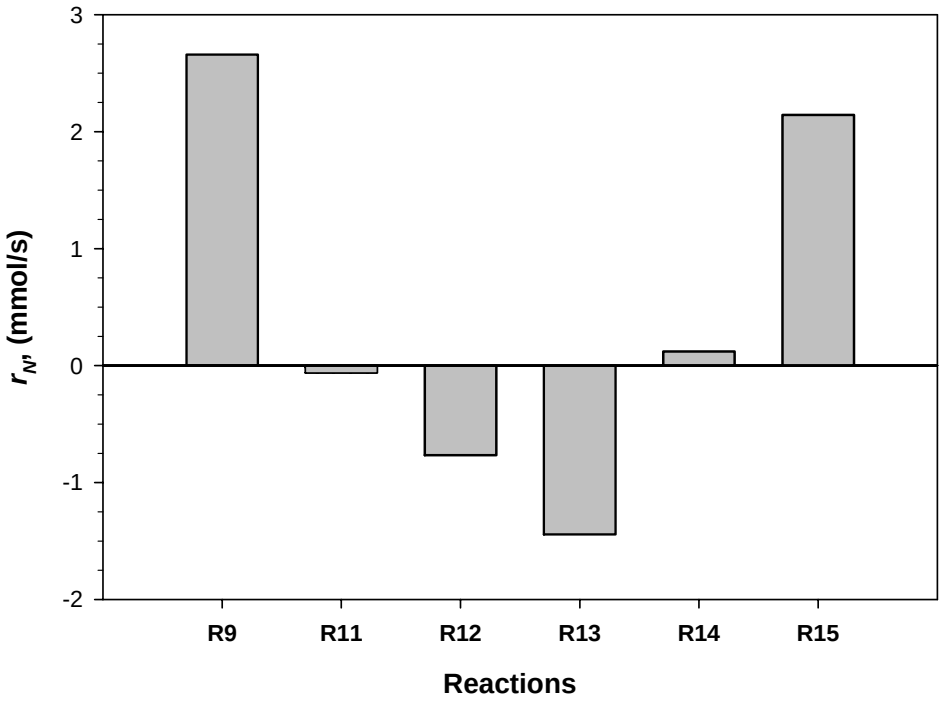

Figure 5.19 Calculated reaction rates, $r_{N,}$ in the bed section for Run 4.

Consequently, analysis of the model predictions for *NO* concentrations and comparison of the reaction rates reveal that amount of nitrogen retained in the char, char combustion rate and amount of volatile nitrogen released along the combustor are found to be the most important parameters that affect *NO* formation and reduction, which finally influences *NO* emissions in bubbling fluidized bed combustors.

5.4 Gaseous Emissions

Measured gaseous emissions together with model predictions are presented in Table 5.1. As displayed in this table, good agreement between experimental emissions and model predictions of the respective species is a consequence of the agreement between measured and predicted profile of these species.

Table 5.1 Gaseous emissions of the runs on dry basis.

	O_2, %		CO_2, %		CO, %		NO, *ppm*	
	Model	**Exp.**	**Model**	**Exp.**	**Model**	**Exp.**	**Model**	**Exp.**
Run 1	6.1	7.3	13.0	12.0	0.1	0.2	378	327
Run 2	5.3	6.5	13.6	12.5	0.2	0.3	362	238
Run 3	5.3	5.9	13.6	13.6	0.2	0.3	399	215
Run 4	4.7	6.7	15.5	13.0	0.3	0.2	237	200
Run 5	4.5	6.0	15.6	13.4	0.3	0.2	225	174
Run 6	4.5	5.4	15.7	14.0	0.3	0.2	220	179

5.5 Model Sensitivity Analysis

In NO_x modeling studies, partitioning factor for coal nitrogen release is an important input parameter, which can be estimated by either pyrolysis experiments or correlations based on coal properties and/or temperature of the system under consideration. Figure 5.20 shows the comparison between measurements of Run 4 and predictions of the model by employing different partitioning factors used in some of the NO_x models in the literature. It is obvious that the predictions of the model are not in agreement with the measurements, unless the experimentally found value for the coal under consideration is utilized. This result is an important remark for the influence of fuel type on *NO* emissions, which also exhibits how nitrogen in high volatile content lignite leads to lower emissions.

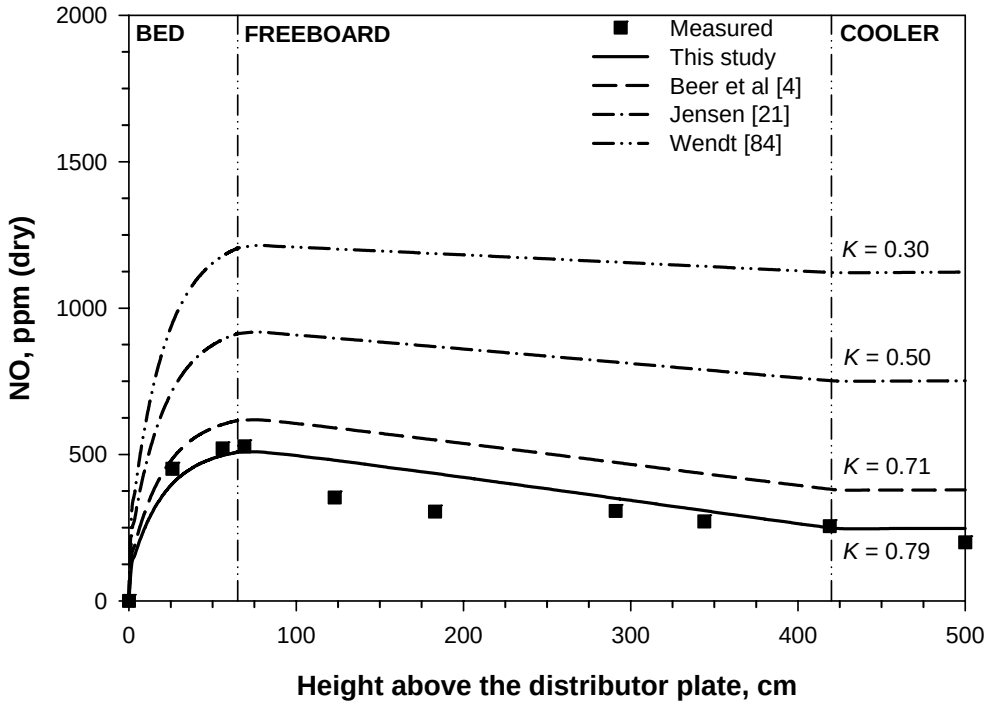

Figure 5.20 Effect of partitioning factor, *K*, on *NO* profiles

Another parametric study was performed for the effect of fraction of NH_3 in the volatile nitrogen, X_{NH_3}, on the *NO* formation and reduction reactions (Figure 5.21). As can be seen from the figure, increasing amount of NH_3 released from the coal

significantly enhances the formation and reduction of *NO* in the bed and freeboard, respectively. Agreement between measurements and the predictions of the present model based on the findings of Wu and Ohtsuka [19, 20] reflects the proximity of the assumption to the real situation.

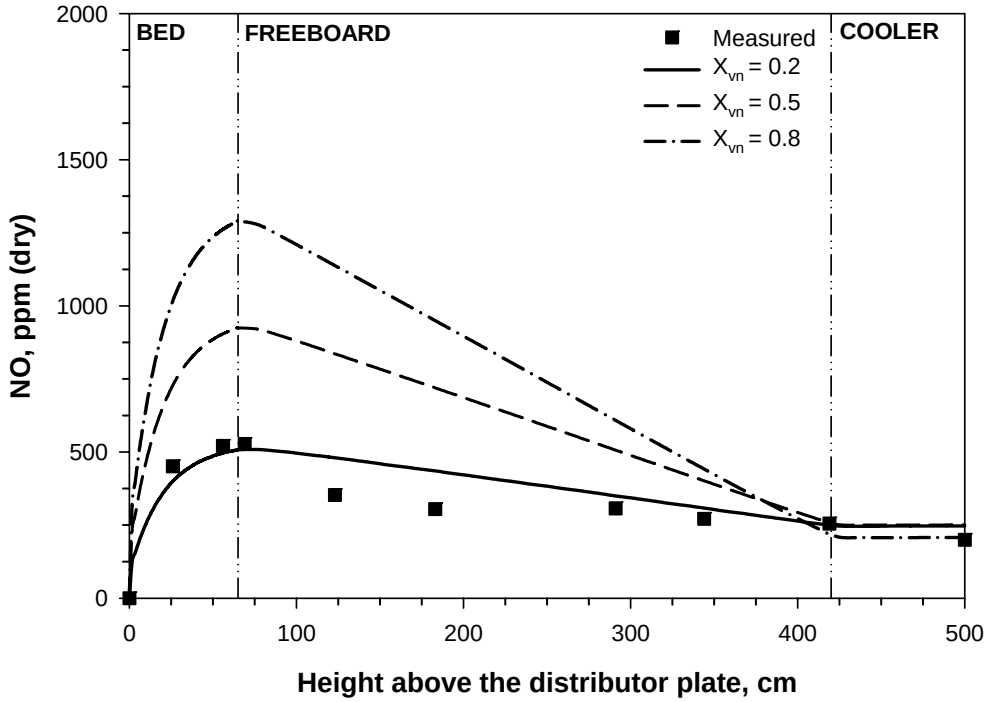

Figure 5.21 Effect of NH_3 fractions in the volatile nitrogen on *NO* profiles

As discussed in Section 2.4.4, air staging is a powerful tool for NO_x control mechanism. Most fluidized bed combustors are operated under air staging conditions to reduce NO_x emissions. Although experimental data used in this study have not been obtained under air staging conditions, its effect on NO_x emissions can be investigated by a simulation study. Figure 5.22 illustrates the effect of air staging on *NO* profiles for Run 1 where the highest *NO* emission was measured. A primary air to total air ratio of 0.7 is assumed and the secondary air is assumed to be fed just above the bed section. A more reduced atmosphere is established as compared to the case of w/o air staging owing to the deficiency of O_2 in the bed section, thus *NO* formed is reduced by char and *CO* over char leading to a significantly lower *NO* emission.

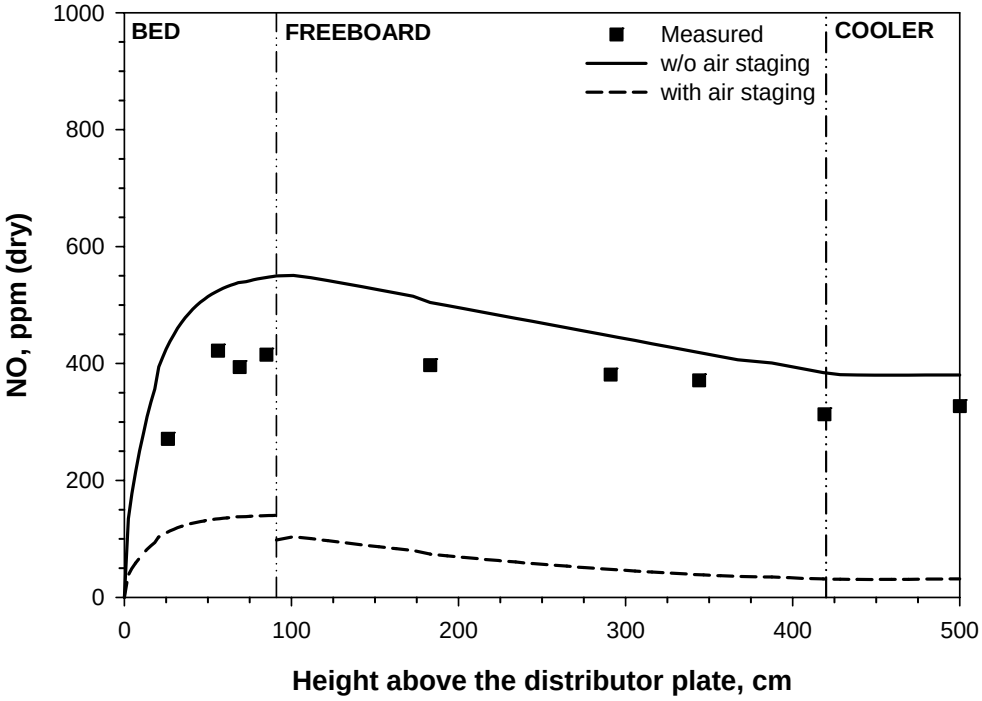

Figure 5.22 Effect of air staging on *NO* profiles

CHAPTER 6

CONCLUSIONS

NO emissions when burning lignites with high volatile and ash content was investigated by extending a previously developed model to incorporate *NO* formation and reduction. The system model accounts for hydrodynamics, volatiles release and combustion, char combustion, particle size distribution, entrainment, elutriation, sulfur retention, and *NO* formation and reduction, and is based on conservation equations for energy and chemical species. The predictive performance of the model was tested by comparing the model predictions with measurements obtained from the combustion tests carried out by burning a typical Turkish lignite, Beypazarı, in a 0.3 MW_t Atmospheric Bubbling Fluidized Bed Combustor in its own ash with and without limestone addition and fines recycle.

On the basis of the experimental observations and comparisons of the model predictions with measurements the following conclusions have been reached:

- O_2, CO, CO_2 concentration profiles and temperature profile predictions of the model are generally in good agreement with the experimental data.
- *NO* concentration profiles are in compliance with physically expected trends, and *NO* emission predictions are generally in favourable agreement with the experimental data.
- Determination of coal nitrogen partitioning into char and volatile nitrogen, and determination of volatile release along the combustor are essential for *NO* modeling purposes in fluidized bed combustors.

- *NO* formation and reduction mechanism employed in this study sufficiently represents *NO* chemistry for high volatile and ash content coals.
- Oxidation of char nitrogen and volatile nitrogen over ash in the emulsion phase dominates the formation of *NO* in the combustor.
- For fuels rich in volatile matter, *NO* reduction in the freeboard is enhanced significantly as volatile nitrogen release to freeboard is significant, which finally leads to lower *NO* emissions from bubbling fluidized bed combustors.

In consequence, the complexity of the problem of predicting NO_x emissions from fluidized bed combustion of high volatile and ash content coals has been overcome by the proposed overall model with all its sub-models which proved to be a promising tool for the evaluation of performance of bubbling fluidized bed boilers.

6.1 Suggestions for Future work

Based on the experience gained in the present study, the following recommendations for future extension of the work are suggested.

- Amount of NH_3 evolved as volatile nitrogen during devolatilization and catalytic activities of solids obtained from fluidized bed combustion of high volatile lignites needs further investigation for *NO* emission predictions.
- A model for the prediction of formation and reduction of nitrous oxide should be incorporated into the system model in order to obtain a comprehensive model for the simulation of ABFBCs.
- A radiation model is required to be coupled to freeboard heat transfer model for a more a realistic approximation of the actual physical phenomena.

REFERENCES

1. Selçuk, N., Degirmenci, E., and Gogebakan, Y., "Modeling of a Bubbling AFBC with Volatiles Release", *Journal of Energy Resources Technology-Transactions of the Asme*, vol. 125, no. 1, pp. 72-81, 2003.

2. Perreira, F.J. and Beér, J.M., "A Mathematical Model of NO Formation And Destruction in Fluidized Combustion of Coal", *Proceedings of the Second Conference on Fluidization*, Engineering Foundation, vol. 401-407, 1978.

3. Rajan, R. and Wen, C. Y., "A Comprehensive Model for Fluidized Bed Combustors", *AIChE Journal*, vol. 26, no. 4, pp. 642-655, 1980.

4. Beer, J.M., Sarofim, A.F., and Lee, Y.Y., "NO Formation and Reduction in Fluidized-Bed Combustion of Coal", *Journal of the Institute of Energy*, vol. 54, no. 418, pp. 38-47, 1981.

5. Chaung, T.Z., Lee, Y.Y., Dutta, A., Walsh, P.M., Sarofim, A. F., and Beér, J.M., *Fluidized Combustion: Nitric Oxide Formation and Reduction in the Bed and Freeboard*, in *Fluidization*, D. Kunii and R. Toei (eds.), The Engineering Foundation: NY, 1984, pp. 459-466.

6. Johnsson, J.E., "Modeling of NO_x Formation in Fluidized Bed Combustion", *Fluidization VI: Proceedings of the Sixth International Conference on Fluidization*, Engineering Foundation, pp. 435-442, 1989.

7. de Souza-Santos, M.L., "Comprehensive Modeling and Simulation of Fluidized-Bed Boilers and Gasifiers", *Fuel*, vol. 68, no. 12, pp. 1507-1521, 1989.

8. Lin, W.G., Valkenburg, P.J.M., and van den Bleek, C.M., "Prediction of NO_x and SO_x Emissions in FBC of Coal Using Easy to Determine Coal and Sorbent Characteristics", *Fuel Processing Technology*, vol. 24, no. pp. 399-405, 1990.

9. Lin, W.G., Svoboda, K., and van den Bleek, C.M., "Sulfur Capture and Its Interactions with NO_x Emissions in Fluidized-Bed Combustion of Coal - General Analytical Model Based on Particle Gas-Solid Reactions", *Chemical Engineering Science*, vol. 47, no. 9-11, pp. 2425-2430, 1992.

10. Lin, W.G., Bu, J., Korbee, R., and Svoboda, K., "Modeling SO_2 and NO_x Emissions in Fluidized-Bed Combustion of Coal", *Fuel*, vol. 72, no. 3, pp. 299-304, 1993.

11. Brem, G., and Brouwers, J.J.H., "Mathematical Modeling of Staged Combustion in an AFBC", *11th International Conference on Fluidized Bed Combustion*, ASME, pp. 449-458, 1991.

12. Goel, S.K., Beér, J.M., and Sarofim, A.F., "Significance of Destruction Reactions in Determining Net Emission of Nitrogen Oxides", *13th International Conference on Fluidized Bed Combustion*, ASME, pp. 887-898, 1995.

13. Goel, S.K., Beer, J.M., and Sarofim, A.F., "An emissions model for a bubbling FBC using detailed chemical kinetics: Significance of destruction reactions", *Journal of the Institute of Energy*, vol. 69, no. 481, pp. 201-213, 1996.

14. Loeffler, G., Andahazy, D., Wartha, C., Winter, F., and Hofbauer, H., "NO_x and N_2O formation mechanisms - A detailed chemical kinetic modeling study on a single fuel particle in a laboratory-scale fluidized bed", *Journal of Energy Resources Technology-Transactions of the Asme*, vol. 123, no. 3, pp. 228-235, 2001.

15. Loeffler, G., Wartha, C., Winter, F., and Hofbauer, H., "Study on NO and N_2O formation and destruction mechanisms in a laboratory-scale fluidized bed", *Energy & Fuels*, vol. 16, no. 5, pp. 1024-1032, 2002.

16. Selçuk, N. and Sivrioglu, Ü. "Mathematical Modeling of Coal-Fired Fluidized Beds", *Journal of Thermal Sciences and Technology (in Turkish)*, vol. 3, no. 1, pp. 31-38, 1980.

17. Altindag, H., Gogebakan, Y., and Selcuk, N., "Sulfur capture for fluidized bed combustion of high sulfur content lignites", *Applied Energy*, vol. 79, no. 4, pp. 403-424, 2004.

18. Johnsson, J.E., "Formation and Reduction of Nitrogen-Oxides in Fluidized-Bed Combustion", *Fuel*, vol. 73, no. 9, pp. 1398-1415, 1994.

19. Wu, Z.H. and Ohtsuka, Y., "Remarkable formation of N_2 from a Chinese lignite during coal pyrolysis", *Energy & Fuels*, vol. 10, no. 6, pp. 1280-1281, 1996.

20. Wu, Z.H. and Ohtsuka, Y., "Key factors for formation of N_2 from low rank coals during fixed fed pyrolysis: Pyrolysis conditions and inherent minerals", *Energy & Fuels*, vol. 11, no. 4, pp. 902-908, 1997.

21. Jensen, A., *Nitrogen Chemistry in Fluidized Bed Combustion of Coal*, Ph.D., Technical University of Denmark, Lyngby, Denmark, 1996.

22. Glarborg, P., Jensen, A.D., and Johnsson, J.E., "Fuel nitrogen conversion in solid fuel fired systems", *Progress in Energy and Combustion Science*, vol. 29, no. 2, pp. 89-113, 2003.

23. Thomas, K.M., "The release of nitrogen oxides during char combustion", *Fuel*, vol. 76, no. 6, pp. 457-473, 1997.

24. Leppalahti, J. and Koljonen, T., "Nitrogen Evolution from Coal, Peat and Wood During Gasification, Literature Review", *Fuel Processing Technology*, vol. 43, no. 1, pp. 1-45, 1995.

25. Nelson, P.F., Kelly, M.D., and Wornat, M.J., "Conversion of Fuel Nitrogen in Coal Volatiles to NO_x Precursors under Rapid Heating Conditions", *Fuel*, vol. 70, no. 3, pp. 403-407, 1991.

26. Kambara, S., Takarada, T., Yamamato, Y.,and Kato, K., "Relation between Functional Forms of Coal Nitrogen and Formation of NO_x Precursors During Rapid Pyrolysis", *Energy & Fuels*, vol. 7, no. 6, pp. 1013-1020, 1993.

27. Bassilakis, R., Zhao, Y., Solomon, P.R., and Serio, M.A., "Sulfur and Nitrogen Evolution in the Argonne Coals - Experiment and Modeling", *Energy & Fuels*, vol. 7, no. 6, pp. 710-720, 1993.

28. Baumann, H. and Moller, P., "Pyrolysis of Hard Coals under Fluidized-Bed Combustor Conditions - Distribution of Nitrogen-Compounds on Volatiles and Residual Char", *Erdol & Kohle Erdgas Petrochemie*, vol. 44, no. 1, pp. 29-33, 1991.

29. Wojtowicz, M.A., Pels, J.R., and Moulijn, J.A., "Combustion of Coal as a Source of N_2O Emission", *Fuel Processing Technology*, vol. 34, no. 1, pp. 1-71, 1993.

30. Hamalainen, J.P. and Aho, M.J., "Effect of Fuel Composition on the Conversion of Volatile Solid Fuel-N to N_2O and NO", *Fuel*, vol. 74, no. 12, pp. 1922-1924, 1995.

31. Mori, H., Asami, K., and Ohtsuka, Y., "Role of iron catalyst in fate of fuel nitrogen during coal pyrolysis", *Energy & Fuels*, vol. 10, no. 4, pp. 1022-1027, 1996.

32. Tsubouchi, N., Ohshima, Y. Xu, C., and Ohtsuka, Y., "Enhancement of N_2 formation from the nitrogen in carbon and coal by calcium", *Energy & Fuels*, vol. 15, no. 1, pp. 158-162, 2001.

33. Amand, L.E. and Leckner, B., "Influence of Fuel on the Emission of Nitrogen-Oxides (NO and N_2O) from an 8 MW Fluidized-Bed Boiler", *Combustion and Flame*, vol. 84, no. 1-2, pp. 181-196, 1991.

34. Amand, L.E. and Leckner, B., "Oxidation of Volatile Nitrogen Compounds During Combustion in Circulating Fluidized-Bed Boilers", *Energy & Fuels*, vol. 5, no. 6, pp. 809-815, 1991.

35. Amand, L.E., Kassman, H., Karlsson, M., and Leckner, B., "Measurement of the concentration of ammonia and ethene in the combustion chamber of a circulating fluidised-bed boiler", *Journal of the Institute of Energy*, vol. 70, no. 482, pp. 25-30, 1997.

36. Kassman H., Karlsson, M., and Åmand, L.-E., "Influence of Air-Staging on the Concentration Profiles of NH_3 and HCN in the Combustion Chamber of a CFB Boiler", *15th International Conference on Fluidized Bed Combustion*, ASME, Paper No. 35 (CD-ROM), 1999.

37. Miller, J.A. and Bowman C.T., "Mechanism and Modeling of Nitrogen Chemistry in Combustion", *Progress in Energy and Combustion Science*, vol. 15, no. 4, pp. 287-338, 1989.

38. Leckner, B., "Fluidized bed combustion: Mixing and pollutant limitation", *Progress in Energy and Combustion Science*, vol. 24, no. 1, pp. 31-61, 1998.

39. Kilpinen, P. and Hupa M., "Homogeneous N_2O Chemistry at Fluidized-Bed Combustion Conditions - a Kinetic Modeling Study", *Combustion and Flame*, vol. 85, no. 1-2, pp. 94-104, 1991.

40. Hulgaard, T., Glarborg, P., and Dam-Johansen, K., "Homogenous and Formation and Destruction of N_2O at Fluidized Bed Combustion Conditions", *11th International Conference on Fluidized Bed Combustion*, ASME, pp. 991-998, 1991.

41. Naruse, I., Yamamato, Y., Imanari, M., Yuan, J.W., and Ohtake K., "Study on N_2O Formation/Destruction Characteristics in Coal Combustion under a Wide Temperature Range", *Twenty-Fourth Symposium (International) on Combustion*, The Combustion Institute, pp. 1415-1421, 1992.

42. Pels, J.R., Wojtowicz, M.A., and Moulijn, J.A., "Rank Dependence of N_2O Emission in Fluidized-Bed Combustion of Coal", *Fuel*, vol. 72, no. 3, pp. 373-379, 1993.

43. Pels, J.R., Wójtowicz, M.A., Kapteijn, F., and Moulijn, J.A., "Trade-Off between NO_x and N_2O in Fluidized-Bed Combustion of Coals", *Energy & Fuels*, vol. 9, no. 5, pp. 743-752, 1995.

44. Aarna, I. and Suuberg, E.M., "A review of the kinetics of the nitric oxide carbon reaction", *Fuel*, vol. 76, no. 6, pp. 475-491, 1997.

45. Molina, A., Eddings, E.G., Pershing, D.W., and Sarofim, A.F., "Char nitrogen conversion: implications to emissions from coal-fired utility boilers", *Progress in Energy and Combustion Science*, vol. 26, no. 4-6, pp. 507-531, 2000.

46. Tullin, C.J., Sarofim, A.F., and Beer, J.M., "Formation of NO and N_2O in Coal Combustion - the Relative Importance of Volatile and Char Nitrogen", *Journal of the Institute of Energy*, vol. 66, no. 469, pp. 207-215, 1993.

47. Johnsson, J.E., and Dam-Johansen, K., "Formation and Reduction of NO_x in a Fluidized Bed Combustor", *11th International Conference on Fluidized Bed Combustion*, ASME, pp. 1389-1396, 1991.

48. Kiil, S., Bhatia, S.K., and Dam-Johansen, K., "Modelling of catalytic oxidation of NH_3 and reduction of NO on limestone during sulphur capture", *Chemical Engineering Science*, vol. 51, no. 4, pp. 587-601, 1996.

49. Chan, L.K., Sarofim, A.F., and Beer, J.M., "Kinetics of the NO-Carbon Reaction at Fluidized-Bed Combustor Conditions", *Combustion and Flame*, vol. 52, no. 1, pp. 37-45, 1983.

50. Johnsson, J.E., Jensen, A., and Nielsen, J.S., "Kinetics of Heterogeneous NO and N_2O Reduction at FBC Conditions", *15th International Conference on Fluidized Bed Combustion*, ASME, Paper No. 99 (CD-ROM), 1999.

51. Duo, W., Dam-Johansen K., and Ostergaard, K., "Kinetics of the Gas-Phase Reaction between Nitric-Oxide, Ammonia and Oxygen", *Canadian Journal of Chemical Engineering*, vol. 70, no. 5, pp. 1014-1020, 1992.

52. Hampartsoumian, E. and Gibbs, B.M., "NO_x Formation and Reduction in Fluidized-Bed Combustors", *Journal of the Institute of Energy*, vol. 57, no. 433, pp. 402-410, 1984.

53. Shimizu, T., Tachiyama, Y., Souma, M., and Inagaki, M., "Emission Control of NO_x and N_2O of Bubbling Fluidized Bed Combustor", *11th International Conference on Fluidized Bed Combustion*, ASME, pp. 695-700, 1991.

54. Valk, M., *Atmospheric Fluidized Bed Coal Combustion Research Development and Application*, Elsevier, 1995.

55. Leckner, B., and Åmand, L.-E., "Emissions from a Circulating and Stationary Fluidized Bed Boiler: A Comparison", *9th International Conference on Fluidized Bed Combustion*, ASME, pp. 891-897, 1987.

56. Selçuk, N., Batu, A., and Oymak, O., "NO_x Emissions from Combustion of High Sulfur Lignite in an ABFBC Test Rig", *17th International Conference on Fluidized Bed Combustion*, ASME, Paper No. 109 (CD-ROM), 2003.

57. Harmandar, H., *Effect of Recycling on the Performance of Bubbling Fluidized Bed Combustors*, M.Sc., METU, Ankara, Turkey, 2003.

58. de Soete, G.G., "An Overall Mechanism of Nitric Oxide Formation from Ammonia and Amines Added to Premixed Hydrocarbon Flames", *Combustion Institute European Symposium*, The Combustion Institute, vol. 439-444, 1973.

59. Jung, K., and La Nauze, R. D., "Sherwood Numbers for Burning Particles in Fluidized Beds", *Proceedings of the 4th International Conference on Fluidization*, Engineering Foundation, vol. 1, pp. 427-434, 1983.

60. Incropera, F.P., De Witt, D. P., *Fundementals of Heat and Mass Transfer*, John Wiley and Sons, 3rd Ed., 1990.

61. Choi, J.H., Chang, I. Y., Shun, D. W., Yi, C. K., Son, J. E., and Kim, S. D., "Correlation on the particle entrainment rate in gas fluidized beds", *Industrial & Engineering Chemistry Research*, vol. 38, no. 6, pp. 2491-2496, 1999.

62. Kunii, D. and Levenspiel, O., *Fluidization Engineering*, Butterworth Heinemann, 2nd Ed., 1991.

63. Davidson, J.F. and Harrison, D., *Fluidised Particles*, Cambridge University Press, 1963.

64. Ergun, S., "Fluid Flow through Packed Columns", *Chemical Engineering Progress*, vol. 48, no. 2, pp. 89-94, 1952.

65. Mori, S. and Wen, C.Y., "Estimation of Bubble Diameter in Gaseous Fluidized-Beds", *Aiche Journal*, vol. 21, no. 1, pp. 109-115, 1975.

66. Gogolek, P.E.G. and Becker, H.A., "Calculation of the Expansion of a Bubbling Fluidized-Bed of Coarse Particles", *Powder Technology*, vol. 71, no. 1, pp. 107-110, 1992.

67. Denloye, A.O.O. and Botterill, J.S.M., "Bed to Surface Heat-Transfer in a Fluidized-Bed of Large Particles", *Powder Technology*, vol. 19, no. 2, pp. 197-203, 1978.

68. Sleicher, C.A. and Rouse, M.W., "Convenient Correlation for Heat-Transfer to Constant and Variable Property Fluids in Turbulent Pipe-Flow", *International Journal of Heat and Mass Transfer*, vol. 18, no. 5, pp. 677-683, 1975.

69. Field, M.A., Gill, D.W., Morgan, B.B., and Hawksley, P.G.W., *Combustion of Pulverized Coal*, British Coal Utilization Research Association, 1967.

70. Hottel, H.C., Williams, G.C., Nerheim, N.M., and Schneider, G.R., "Kinetic Studies on Stirred Reactors, Combustion of Carbon Monoxide and Propane", *Proceedings of the 10th Int. Symp. on Combustion*, The Combustion Institute, vol. 1, pp. 975-986, 1965.

71. Grace, J.R. and Clift, R., "2-Phase Theory of Fluidization", *Chemical Engineering Science*, vol. 29, no. 2, pp. 327-334, 1974.

72. Grace, J.R. and Harrison, D., "Behaviour of Freely Bubbling Fluidised Beds", *Chemical Engineering Science*, vol. 24, no. 3, pp. 497-&, 1969.

73. Stubington, J.F., Chan, S.W., and Clough, S.J., "A Model for Volatiles Release into a Bubbling Fluidized-Bed Combustor", *AICHE Journal*, vol. 36, no. 1, pp. 75-85, 1990.

74. Anthony, D.B. and Howard, J.B., "Coal Devolatilization and Hydrogasification", *AICHE Journal*, vol. 22, no. 4, pp. 625-656, 1976.

75. Degirmenci, E., *Dynamic Simulation of Fluidized Bed Combustors*, Ph.D., METU, Ankara, Turkey, 2000.

76. Gögebakan, Y., *Char Attrition in Fluidized Bed Combustors*, M.Sc., METU, Ankara, Turkey, 2000.

77. Altindag, H., *Mathematical Modeling of Sulfur Retention in Fluidized Bed Combustors*, M.Sc., METU, Ankara, Turkey, 2003.

78. Hazlett, J.D. and Bergougnou M.A., "Influence of Bubble-Size Distribution at the Bed Surface on Entrainment Profile", *Powder Technology*, vol. 70, no. 2, pp. 99-107, 1992.

79. Kunii, D. and Levenspiel, O., "Fluidized Reactor Models. 1. For Bubbling Beds of Fine, Intermediate, and Large Particles. 2. For the Lean Phase - Freeboard and Fast Fluidization", *Industrial & Engineering Chemistry Research*, vol. 29, no. 7, pp. 1226-1234, 1990.

80. Hannes, J., *Mathematical Modeling of Circulating Fluidized Bed Combustion*, Ph.D., RWTH, Aachen, Germany, 1996.

81. Radhakrishnan, K. and Hindmarsh, A. C., Description and use of LSODE, the Livermore Solver for Ordinary Differential Equations, *Lawrance Livermore National Laboratory Report No: UCRL-ID-113855*, 1993.

82. Anthony, E.J., Couturier, M. F., and Briggs, D. W., Gas Sampling at the Point Tupper AFBC Facility, *CANMET, Energy, Mines and Resources, Division Report 86-70 (TR): Canada*, 1986.

83. Degirmenci, E., Gogebakan, Y., and Selcuk, N., "Assessment of catalyst deactivation model for sulfur retention in fluidized bed combustors", *Combustion Science and Technology*, vol. 153, pp. 95-111, 2000.

84. Wendt, J.O.L., "Fundamental coal combustion mechanisms and pollutant formation in furnaces", *Progress in Energy and Combustion Science*, Vol. 6, pp. 201-222, 1980.